

8-9-2022

Developing novel optimization and machine learning frameworks to improve and assess the safety of workplaces

Amin Aghalari
Mississippi State University, aminaghalari@gmail.com

Follow this and additional works at: <https://scholarsjunction.msstate.edu/td>



Part of the [Industrial Engineering Commons](#), and the [Operational Research Commons](#)

Recommended Citation

Aghalari, Amin, "Developing novel optimization and machine learning frameworks to improve and assess the safety of workplaces" (2022). *Theses and Dissertations*. 5633.
<https://scholarsjunction.msstate.edu/td/5633>

This Dissertation - Open Access is brought to you for free and open access by the Theses and Dissertations at Scholars Junction. It has been accepted for inclusion in Theses and Dissertations by an authorized administrator of Scholars Junction. For more information, please contact scholcomm@msstate.libanswers.com.

Developing novel optimization and machine learning frameworks to improve and assess the safety
of workplaces

By

Amin Aghalari

Approved by:

Mohammad Marufuzzaman (Major Professor)

Veera Gnaneswar Gude

Junfeng Ma

Wenmeng Tian

Mohammad Marufuzzaman (Graduate Coordinator)

Jason M. Keith (Dean, Bagley College of Engineering)

A Dissertation

Submitted to the Faculty of

Mississippi State University

in Partial Fulfillment of the Requirements

for the Degree of Doctor of Philosophy

in Industrial Engineering

in the Department of Industrial and Systems Engineering

Mississippi State, Mississippi

August 2022

Copyright by
Amin Aghalari
2022

Name: Amin Aghalari

Date of Degree: August 9, 2022

Institution: Mississippi State University

Major Field: Industrial Engineering

Major Professor: Mohammad Marufuzzaman

Title of Study: Developing novel optimization and machine learning frameworks to improve and assess the safety of workplaces

Pages of Study: 115

Candidate for Degree of Doctor of Philosophy

This study proposes several decision-making tools utilizing optimization and machine learning frameworks to assess and improve the safety of the workplaces. The first chapter of this study presents a novel mathematical model to optimally locate a set of detectors to minimize the expected number of casualties in a given threat area. The problem is formulated as a nonlinear binary integer programming model and then solved as a linearized branch-and-bound algorithm. Several sensitivity analyses illustrate the model's robustness and draw key managerial insights. One of the prevailing threats in the last decades, Active Shooting (AS) violence, poses a serious threat to public safety. The second chapter proposes an innovative mathematical model which captures several essential features (e.g., the capacity of the facility and individual choices, heterogeneity of individual behavioral and choice sets, restriction on choice sets depending on the location of the shooter and facility orientation, and many others) which are essential for appropriately characterizing and analyzing the response strategy for civilians under an AS exposed environment. We demonstrate the applicability of the proposed model by implementing the effectiveness of

the RUN.HIDE.FIGHT.® (RHF) program in an academic environment. Given most of the past incidents took place in built environments (e.g., educational and commercial buildings), there is an urgent need to methodologically assess the safety of the buildings under an active shooter situation. Finally, the third chapter aims to bridge this knowledge gap by developing a learning technique that can be used to model the behavior of the shooter and the trapped civilians in an active shooter incident. Understanding how the civilians responded to different simulated environments, a number of actions could have been undertaken to bolster the safety measures of a given facility. Finally, this study provides a customized decision-making tool that adopts a tailored maximum entropy inverse reinforcement learning algorithm and utilizes safety measurement metrics, such as the percentage of civilians who can hide/exit in/from the system, to assess a workplace's safety under an active shooter incident.

Key words: Reinforcement Learning; Choice Model; Optimization; Safety; Detector Placement; Casualty Minimization; Active Shooting

DEDICATION

This dissertation work is dedicated to my best friend and wife, Sorayya, who has been a constant source of support and encouragement during the challenges of graduate school and life. I am genuinely thankful for having you in my life. This work is also dedicated to my parents, Gholamreza and Lida, who have always loved me unconditionally and whose good examples have taught me to work hard for what I aspire to achieve.

ACKNOWLEDGEMENTS

First and foremost, I am extremely grateful to my supervisor, Prof. Mohammad Marufuzzaman, for his invaluable advice, continuous support, and patience during my Ph.D. study. His immense knowledge and plentiful experience have encouraged me in all the time of my academic research and daily life. I am also extending my appreciation to the other committee members, Dr. Veera Gnaneswar Gude, Dr. Junfeng Ma, and Dr. Wenmeng Tian, for their important and valuable comments, which undoubtedly helped improve this research.

I also thank my colleagues in the Department of Industrial Systems Engineering and especially AOL lab for their help and support. Their kind help and support have made my study and life in the US a wonderful time. Finally, I would like to express my gratitude to my parents and my wife. Without their tremendous understanding and encouragement in the past few years, it would be impossible to complete my study.

TABLE OF CONTENTS

DEDICATION	ii
ACKNOWLEDGEMENTS	iii
LIST OF TABLES	vi
LIST OF FIGURES	vii
CHAPTER	
I. OPTIMAL PLACEMENT OF DETECTORS TO MINIMIZE CASUALTIES IN AN INTENTIONAL ATTACK	1
1.1 Introduction	1
1.1.1 Related literature	2
1.1.2 Research Scope and Contributions	3
1.2 Problem Description and Mathematical Model Formulation	4
1.3 Branch-and-Bound Algorithm	12
1.4 Case Study	18
1.5 Conclusions and Future Work	27
II. OPTIMIZING CIVILIAN RESPONSE STRATEGY UNDER AN ACTIVE SHOOTING INCIDENT	29
2.1 Introduction	29
2.1.1 Motivation	29
2.1.2 Related Literature	30
2.1.3 Research Contributions	32
2.2 Problem Description and Mathematical Model Formulation	33
2.3 Solution Approach	41
2.4 Experimental Results	43
2.4.1 Survey Summary	43
2.4.2 Input Parameters	45
2.4.3 Lessons Learned	47
2.5 Conclusions and Future Research Directions	55

III.	INVERSE REINFORCEMENT LEARNING TO ASSESS SAFETY OF A WORK-PLACE UNDER AN ACTIVE SHOOTER INCIDENT	57
3.1	Introduction	57
3.1.1	Motivation	57
3.1.2	Related Literature	57
3.1.3	Summary of Major Contributions	63
3.2	Problem Formulation	63
3.2.1	Markov Decision Process	64
3.2.2	Incident Modeling	65
3.2.2.1	State definition	66
3.2.2.2	State transitions	67
3.2.2.3	Value function	67
3.2.3	Maximum Entropy Inverse Reinforcement Learning (IRL)	69
3.2.3.1	Maximum Entropy	70
3.2.3.2	Inverse Reinforcement Learning (IRL): A Case in Active Shooting Incidents	75
3.3	Experimental Results	77
3.3.1	Input Parameters	77
3.3.2	Lessons Learned	79
3.4	Conclusions and Future Work	88
	REFERENCES	91
	APPENDIX	
A.	ILLUSTRATION OF INPUT DATA	101
A.1	Summary of sets, parameters, and decision variables for chapter 2	102
A.2	Proof of <i>Proposition 1</i>	103
A.3	Proof of <i>Proposition 2</i>	105
A.4	Sample Utility Calculation	106
A.5	Illustration of different hiding and entrances/exits configurations in chapter 2	107
A.6	Illustration of different hiding and entrances/exits configurations in chapter 3	109
A.7	Illustration of different civilian distribution configurations in chapter 3 . .	109
A.8	Illustration of different shooting ranges and accuracy in chapter 3	110
A.9	Performance metrics over trials in chapter 3	112
A.10	A summary of the characteristics in chapter 3	112

LIST OF TABLES

1.1	Summary of four failure scenarios in Figure 1.3	10
1.2	Base case parameter values	20
1.3	Scenario Parameter Values	24
1.4	B&B Algorithm Resulting Detector Placements	25
2.1	Summary of the survey participants	44
2.2	Initial distribution of civilians over the test region	52
3.1	The summary of performance metrics over 50 trials (in %)	80
3.2	Initial distribution of civilians over the test region	86
A.1	The detailed information of the performance metrics based upon individual trials (in %)	112

LIST OF FIGURES

1.1	Active shooter incidents in the United States from 2000 to 2017	2
1.2	Grid representation of a threat area	6
1.3	All possible events related to a threat	10
1.4	Representation of the threat area with 8×8 equal sized squares	19
1.5	Impact of detection radius on expected casualties	21
1.6	Impact of instantaneous detection rate on expected casualties	22
1.7	Impact of budget on expected casualties	23
1.8	Detector placement for two-and-one layer detection problems (instance 24)	26
2.1	Active shooting incidents in the US between 2000-2018	30
2.2	A simplified decision-making framework for assessing civilian response strategy under an active shooter incident	43
2.3	6×6 test grid facility	46
2.4	Demonstrating how the utility is changing (majority of the individuals) in different grids with respect to the shooters position and time (in seconds)	46
2.5	Base case values of V_H , V_E , and V_{RISK} over time	48
2.6	Movement of civilians over time: base case	48
2.7	Impact of V_H , V_E , and V_{RISK} under different hiding configurations	50
2.8	Impact of V_E and V_{RISK} under different entrance/exit configurations	50
2.9	Impact of V_E and V_{RISK} under different civilian distribution configurations	52
2.10	Illustration of different civilian distribution configurations	53
2.11	Impact of V_E and V_{RISK} under different decision making capabilities of the civilians	55
3.1	Agent-environment interaction	64
3.2	10×10 test grid facility	78
3.3	Impact of V_H^1 , V_E^1 , and V_{RISK}^1 under base input parameters when simulation time is 75 seconds.	81
3.4	Reward illustration for first trial when simulation time is 75 seconds	81
3.5	Impact of V_H , V_E , and V_{RISK} under different hiding configurations.	83
3.6	Impact of V_E and V_{RISK} under different entrance/exit configurations.	84

3.7	Impact of V_E , V_{RISK} , and hidden place utilization under different civilian distribution.	86
3.8	V_{RISK} vs. shooting range and accuracy. Note that V_{RISK} denotes the percentage of civilians who are still freely floating within the threat area.	88
A.1	A sample utility calculation for grid 21	107
A.2	Illustration of different exit/entrance configurations	108
A.3	Illustration of different hiding configurations	108
A.4	Illustration of different hiding configurations. $ G^h $ represents the number of the available hidden places in the threat area.	109
A.5	Illustration of different exit/entrance configurations. $ G^e $ represents the number of the exit/entrance cells in the threat area.	109
A.6	Illustration of different civilian distribution configurations	110
A.7	Illustration of different shooting accuracy	111
A.8	Illustration of different shooting ranges	111

CHAPTER I

OPTIMAL PLACEMENT OF DETECTORS TO MINIMIZE CASUALTIES IN AN INTENTIONAL ATTACK

1.1 Introduction

Over the past few decades, there has been a significant increasing trend of manmade attacks (e.g., active shooting, bomb threat) worldwide and especially within the United States. For instance, The Federal Bureau of Investigation (FBI) reports that the average number of active shooting incidents between 2000-2007 was 7.4 incidents/year, which further increased to 17.6 incidents/year between 2008-2015 before finally accelerated to 25.7 incidents/year between 2016-2017 [27] (see Figure 1.1(a)). Most importantly, the majority of such attacks are occurring in the gun-free zones (e.g., education institutes, businesses and shopping malls, hospitals), include all areas where the general public is forbidden to carry firearms. For instance, Figure 1.1(b) shows that 90% of the past active shooting incidents occur in different gun free zones, including Pre-K to 12 schools (14.8%), universities (6%), businesses and shopping malls (42%) to even in health care facilities (4%). Such violence in the gun-free zones poses serious security concerns among public safety, primarily due to the horrifying outcomes and potentially large number of casualties that typically stem from such an attack. All the above underlying statistics indicate that there is an urgent need to methodologically securing a workplace not only to minimize the expected number of casualties from a given attack but also to restrain civilians experiencing such rare but dreadful events.

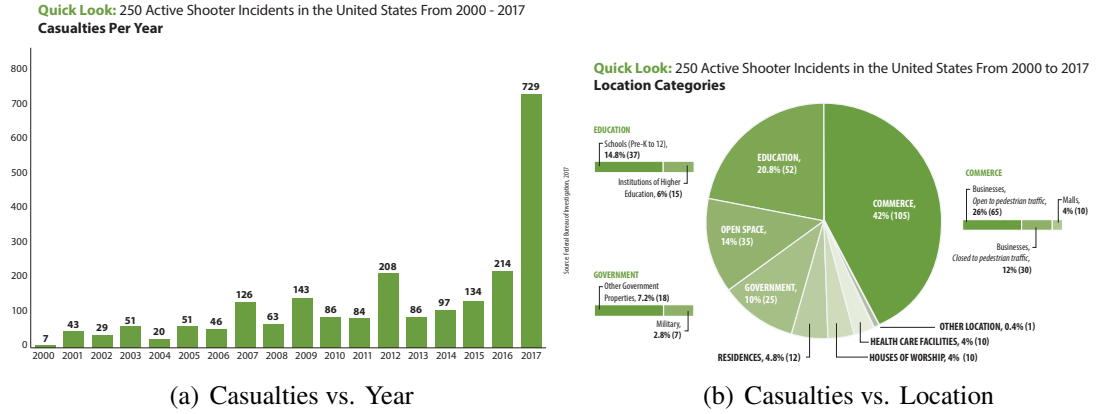


Figure 1.1

Active shooter incidents in the United States from 2000 to 2017

1.1.1 Related literature

Knowledge on how to secure potential threat areas is still very limited despite knowing about the outcomes of such events. A majority of the design decisions (e.g., sensor placement for detecting threat objects (guns, bombs)) to secure these areas are primarily made based on intuition rather than adopting a methodological framework. Though not directly related, it is worth mentioning a few past studies that attempted to locate detectors under different real-life applications. For instance, in [108], the authors proposed a method to efficiently determine the location of visual fire detectors with a dual view from a process plant. Yang et al. [107] proposed an image processing technique to optimally locate and map detectors for the oil and gas industry. Pirani et al. [75] adopted a game-theoretic approach to optimally locate a set of security-aware sensors under an attacker and a detector situation. Bard et al. [12] designed a two-phase methodology to help decision-makers selecting the right technology for a critical system. Finally, Lakats and Pate-Cornell [45] provided an analytical framework that designed and optimized a warning system from

a management perspective. The authors used an airport inspection and maintenance system as a testbed to validate the modeling results.

Unfortunately, a very limited number of articles are available in the literature that research methods to remedy this pressing problem. Kaplan and Kress [38] conducted one of the first novel initiatives along this line of research to analyze the operational effectiveness and consequences among individuals under a suicide bomber detection scheme. Given detectors with imperfect reliability, Nie et al., [70] extended this work by considering the reliability of a single type of detector. Later, Yan and Nie [105] extended this framework to consider multiple types of detectors with an application of vessel attack in a maritime port. Besides modeling approaches, a few researchers adopted the discrete event simulation approach (e.g., [40, 47, 46]) to assess the workplace safety under an active shooting situation. Note that in these studies the researchers indirectly assessed the workplace safety by examining civilian response under an active shooting situation.

1.1.2 Research Scope and Contributions

Different than the studies discussed above, especially in [70] and [105], this study assumes that a set of secondary/backup detectors are available in a workplace or any threat area in general to support the primary detectors. The purpose of these secondary/backup detectors are twofold: increasing the accuracy in detecting any threat event to minimize the (i) expected number of casualties from an attack and (ii) *false alarm* to unnecessarily confuse/shock both the civilians and the law enforcement agencies. In overall, we propose a nonlinear binary integer programming model to optimally locate a set of detectors (both primary and secondary) in such a way that

the expected number of casualties from an unexpected attack can be minimized. Because of this additional layer of detection, the complexity of the model increases significantly (i.e., a number of hard nonlinear terms are introduced) which mandates developing an efficient customized solution approach to solve them efficiently in a reasonable timeframe. To alleviate these challenges, we first attempt to linearize the proposed mathematical model, which is followed by solving via a linearized branch-and-bound algorithm. A number of sensitivity analyses are performed on a few sensitive parameters (e.g., detection radius, instantaneous detection rate, and budget availability) to illustrate the robustness of the model and to draw important managerial insights. To summarize, the major contributions of this study to the existing literature are as follows: (i) extend the framework proposed by [70] and [105] (primarily, the secondary detectors and associated considerations) to develop a novel mathematical model; (ii) develop a highly customized solution approach to efficiently solve the proposed mathematical model; and (iii) cast a number of insights by changing different key input parameters in the proposed mathematical model (e.g., detection radius, instantaneous detection rate, and budget availability) to increase our understanding on the impact of such parameters on minimizing the casualties from an intentional attack.

1.2 Problem Description and Mathematical Model Formulation

The purpose of this chapter is to optimally deploy a set of primary and secondary detectors on a threat area in such a way that the expected number of casualties from a sudden intentional attack can be minimized. We assume that both the primary and secondary detectors are stationary and perfectly concealed. We further assume that the interdiction team will start preparing for the mission after receiving an alarm from the primary detectors, while the purpose of the secondary

detectors is to check any *false detection* before the mission initiates. The goal would be to locate the detectors (both primary and secondary) in such a way that both the attacker(s) and threat element(s) (e.g., bomb, gun) are appropriately detected and the interdiction team will receive a *minimum response time* to baffle the attacker's intention.

To formulate this problem, we first assume that the threat area is rectangular with equal-sized grids. Figure 1.2 shows the threat area which has been divided into $m \times n$ grids and is denoted by set $\mathcal{G} = \{j : j = 1, 2, \dots, mn\}$. An attacker can enter into this threat area through a set of possible entrances which is denoted by $\mathcal{E} = \{1, 2, \dots, E\}$. To model physical obstructions, we categorize grids into two major types: (i) blocked grids and (ii) unblocked grids. *Blocked grids* represent the set of grids, denoted by set $\mathcal{B} \subset \mathcal{G}$, where an attacker cannot travel or no threatened individuals are present. In contrary, *unblocked grids* represent the set of grids, denoted by $\mathcal{U} = \mathcal{G} \setminus \mathcal{B}$, where an attacker can travel or threatened individuals are present. It is assumed that some level of knowledge about the attacker's potential targets are known in advance. Let $\mathcal{A} \subset \mathcal{U}$ be the set of threat grids where any attack may potentially occur. We further let γ_{ej} to be the probability associated with using an entrance $e \in \mathcal{E}$ to attack threat grid $j \in \mathcal{A}$ in a given time period. Hence, $\gamma_{ej} \geq 0; \forall e = 1, 2, \dots, E; j \in \mathcal{A}$ and $\sum_{e=1}^E \sum_{j \in \mathcal{A}} \gamma_{ej} = 1$. It is reasonable to assume that an attacker will enter into the threat area from an entrance $e \in \mathcal{E}$ and then use a shortest path, denoted by d_{ej} , to reach a threat grid $j \in \mathcal{A}$, if not obstructed by any of the blocked grids $j \in \mathcal{B}$. To find d_{ej} , we apply Dijkstra's algorithm [25], a widely used shortest path algorithm available in the literature, and we assume that the attacker will walk at a consistent pace, with a speed of κ m/sec, from one grid center to the next till she/he reaches to a threat grid $j \in \mathcal{A}$.

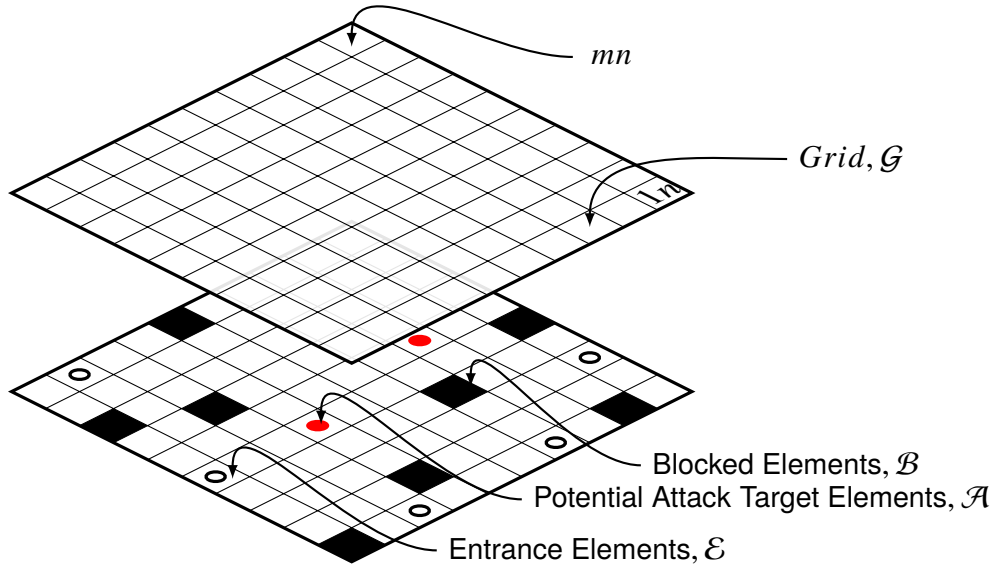


Figure 1.2

Grid representation of a threat area

In this study we consider two types of detectors: *primary* and *secondary* detectors. We assume that the grid centers are potential locations to place both the primary and secondary detectors. We further assume that the purpose of the primary detectors is to perform only a Level 1 threat detection (e.g., radar detection)¹. Let α^p , β^p , and ψ^p be the effective detection radius, instantaneous detection rate, and unit purchasing cost for primary detectors. To increase the detection probability and to minimize the false detection rate, we assume that an additional layer of protection, in the form of secondary/backup detectors (e.g., radar and video together, thermal imagery, terahertz radar), can be placed in selected critical grids. Let α^s , β^s , and ψ^s be the effective detection radius, instantaneous detection rate, and unit purchasing cost for secondary detectors. Since an additional layer of protection will be provided to the secondary detectors, it is reasonable to assume that

¹Details about different threat detection levels can be found from [28]

$\alpha^s > \alpha^p$ and $\beta^s > \beta^p$. Resultantly, the purchasing cost of a secondary detector will be significantly higher than a primary detector, i.e., $\psi^s > \psi^p$. We let M^p and M^s to denote the availability of budget to procure primary and secondary detectors, respectively.

Preventing any threat event usually consists of three main steps: (i) detection, (ii) response, and (iii) neutralization. The placement of the detectors should be made in such a way that the interdiction team receives at least χ^* seconds to neutralize the threat. Let $N_e^p(j)$ be the set of all non-blocked grids on which a primary detector can be located and timely detect the attacker while traveling on path d_{ej}^2 . We assume that as soon as the primary detector is able to detect any threat, the interdiction team will start preparing for the neutralization process, i.e., the response step starts. However, the actual neutralization process will only start after receiving a confirmation alarm (i.e., no false detection) from the secondary detectors. Let N_e^s be the set of all non-blocked grids on which a secondary detector can be located and confirm any threat event, along with the attacker, while the attacker may travel on path d_{ej} . It shall be noted that the construction of set $N_e^s(j)$ is made in such a way that the secondary detectors are still placed at least χ^* seconds away to allow the interdiction team to neutralize the threat. Given the walking speed of the attacker be κ m/sec, this converts the threat detection to be made at least $\kappa\chi^*$ meter away (e.g., 10 m as defined by Kaplan and Kress [38]).

We assume that the detectors (both primary and secondary detectors) are not perfectly reliable. There is always a probability that the detectors are unable to detect any threat which is essentially a function of the duration an attacker stay within the effective detection radius of the detectors. For every $i \in N_e^p(j)$, let ρ_{iej} be the probability associated with detecting any threat event by the

²A procedure to geometrically construct $N_e^p(j)$ can be found in [70] and [105]

primary detector which has been carried out by the attacker while traveling on path d_{ej} . Likewise, for every $i' \in N_e^s(j); \forall (i, i') \in \mathcal{U}, i \neq i'$, let $\rho_{i'ej}$ be the probability associated with detecting any threat event by the secondary detector which has been carried out by the attacker while traveling on path d_{ej} . Based on Przemieniecki [77], we calculate ρ_{iej} and $\rho_{i'ej}$ as follows: $\rho_{iej} = 1 - e^{-\beta^p l_{iej}^p}$ and $\rho_{i'ej} = 1 - e^{-\beta^s l_{i'ej}^s}$ where β^p and β^s , respectively, denote the instantaneous detection rate for the primary and secondary detectors. Further, parameters l_{iej}^p and $l_{i'ej}^s$, respectively, denote the portion of the travel length on path d_{ej} while the attacker is within the effective detection radius of the primary and secondary detectors. A procedure to geometrically calculate l_{iej}^p can be found in [70] and [105].

We are now ready to introduce the following two detector placement decisions for our proposed mathematical model. First, we define sets $\mathcal{P} = \bigcup_{e,j} N_e^p(j)$ and $\mathcal{S} = \bigcup_{e,j} N_e^s(j)$ which will realistically restrict the detectors (primary and secondary) placement decisions in our tested threat region. Let $\mathbf{X} := \{X_j\}_{\forall j \in \mathcal{P}}$ and $\mathbf{Y} := \{Y_j\}_{\forall j \in \mathcal{S}}$ to denote binary decision variables if a detector (primary or secondary) is placed on grid $j \in \mathcal{P} \cup \mathcal{S}$. More specifically, we define the variables as follows:

$$X_j = \begin{cases} 1 & \text{if a primary detector is placed in the center of grid } j \in \mathcal{P} \\ 0 & \text{otherwise;} \end{cases}$$

$$Y_j = \begin{cases} 1 & \text{if a secondary detector is placed in the center of grid } j \in \mathcal{S} \\ 0 & \text{otherwise;} \end{cases}$$

Let us now introduce all possible events that may essentially incur to any threat event (see Figure 1.3). We assume that the two detectors are independently correlated with each other. Figure 1.3 clearly depicts that there are four possible scenarios where an attack via path d_{ej} may turn out

to be successful (nodes 3, 5, 7, and 9 in Figure 1.3). One scenario is that neither the primary nor the secondary detector are capable of detecting any threat event with a probability of $\prod_{i \in N_e^p(j)} (1 - \rho_{iej})^{X_i} \prod_{i' \in N_e^s(j)} (1 - \rho_{i'ej})^{Y_{i'}}$ (node 3). Another possible scenario may arise when the primary detector is able to detect the threat but the secondary detector is not or pass this threat as a false detection (node 5). This scenario may occur with a probability of $\left[1 - \prod_{i \in N_e^p(j)} (1 - \rho_{iej})^{X_i}\right] \prod_{i' \in N_e^s(j)} (1 - \rho_{i'ej})^{Y_{i'}}$. Another possible scenario would be the case when the primary detector is unable to detect any threat but can be later detected by the secondary detector. However, even though detected, the interdiction team fails to foil this threat (node 7) which may occur with a probability of $\prod_{i \in N_e^p(j)} (1 - \rho_{iej})^{X_i} \left[1 - \prod_{i' \in N_e^s(j)} (1 - \rho_{i'ej})^{Y_{i'}}\right] (1 - \theta_2)$ where θ_2 is the probability of success of any neutralization event. The last possible scenario may occur when both primary and secondary detectors are capable of detecting the threat but the interdiction team fails to foil the threat (node 9). This scenario may occur with a probability of $\left[1 - \prod_{i \in N_e^p(j)} (1 - \rho_{iej})^{X_i}\right] \left[1 - \prod_{i' \in N_e^s(j)} (1 - \rho_{i'ej})^{Y_{i'}}\right] (1 - \theta_1)$ where θ_1 is the probability of success of any neutralization event. It is worth mentioning that the interdiction team receives less time to prepare and perform any neutralization event under the scenario defined in node 7 compared to the scenario defined in node 9. Therefore, it is reasonable to assume that $\theta_1 > \theta_2$. Table 1.1 summarizes the probabilities associated with four possible failure scenarios in Figure 1.3.

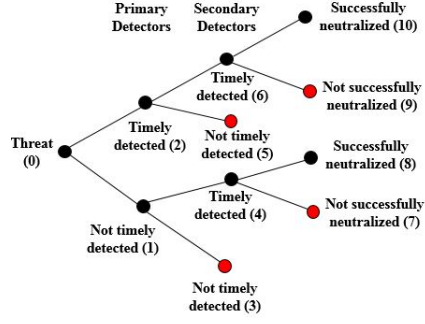


Figure 1.3

All possible events related to a threat

Table 1.1

Summary of four failure scenarios in Figure 1.3

Node	Action			Scenario Probability	Status
	P	S	N		
3	×	×		$\prod_{i \in N_e^P(j)} (1 - \rho_{ie_j})^{X_i} \prod_{i' \in N_e^S(j)} (1 - \rho_{i'e_j})^{Y_{i'}}$	Fail
5		×		$\left[1 - \prod_{i \in N_e^P(j)} (1 - \rho_{ie_j})^{X_i}\right] \prod_{i' \in N_e^S(j)} (1 - \rho_{i'e_j})^{Y_{i'}}$	Fail
7	×		×	$\prod_{i \in N_e^P(j)} (1 - \rho_{ie_j})^{X_i} \left[1 - \prod_{i' \in N_e^S(j)} (1 - \rho_{i'e_j})^{Y_{i'}}\right] (1 - \theta_2)$	Fail
9			×	$\left[1 - \prod_{i \in N_e^P(j)} (1 - \rho_{ie_j})^{X_i}\right] \left[1 - \prod_{i' \in N_e^S(j)} (1 - \rho_{i'e_j})^{Y_{i'}}\right] (1 - \theta_1)$	Fail

P: Primary detector; S: Secondary detector; N: Neutralization

Let ζ_j to denote the expected number of casualties at attack grid $j \in \mathcal{A}$. Given that an attacker utilizes path d_{ej} with probability γ_{ej} , we get the total expected number of casualties as follows:

$$\begin{aligned}
& \sum_{e=1}^E \sum_{j \in \mathcal{A}} \left\{ \prod_{i \in N_e^P(j)} (1 - \rho_{ie_j})^{X_i} \prod_{i' \in N_e^S(j)} (1 - \rho_{i'e_j})^{Y_{i'}} \zeta_j \gamma_{ej} + \left[1 - \prod_{i \in N_e^P(j)} (1 - \rho_{ie_j})^{X_i}\right] \right. \\
& \left. \prod_{i' \in N_e^S(j)} (1 - \rho_{i'e_j})^{Y_{i'}} \zeta_j \gamma_{ej} + \prod_{i \in N_e^P(j)} (1 - \rho_{ie_j})^{X_i} \left[1 - \prod_{i' \in N_e^S(j)} (1 - \rho_{i'e_j})^{Y_{i'}}\right] (1 - \theta_2) \zeta_j \gamma_{ej} + \right. \\
& \left. \left[1 - \prod_{i \in N_e^P(j)} (1 - \rho_{ie_j})^{X_i}\right] \left[1 - \prod_{i' \in N_e^S(j)} (1 - \rho_{i'e_j})^{Y_{i'}}\right] (1 - \theta_1) \zeta_j \gamma_{ej} \right\} \quad (1.1)
\end{aligned}$$

Rearranging (1.1), we obtain the following expression:

$$\sum_{e=1}^E \sum_{j \in \mathcal{A}} \left[(1 - \theta_1) \zeta_j \gamma_{ej} + (\theta_1 - \theta_2) \prod_{i \in N_e^p(j)} (1 - \rho_{iej})^{X_i} \zeta_j \gamma_{ej} + \theta_1 \prod_{i' \in N_e^s(j)} (1 - \rho_{i'ej})^{Y_{i'}} \zeta_j \gamma_{ej} - \right. \\ \left. (\theta_1 - \theta_2) \prod_{i \in N_e^p(j)} (1 - \rho_{iej})^{X_i} \prod_{i' \in N_e^s(j)} (1 - \rho_{i'ej})^{Y_{i'}} \zeta_j \gamma_{ej} \right] \quad (1.2)$$

Note that the first term in (1.2) i.e., $(1 - \theta_1) \zeta_j \gamma_{ej}$, is a constant. Therefore, we can drop this term from the objective function without sacrificing the optimality of the model. With this, we are now ready to introduce the following nonlinear binary integer program for our optimal detector placement problem.

$$\begin{aligned} \text{[DP]} \quad \underset{\mathbf{X}, \mathbf{Y}}{\text{Minimize}} \quad & \sum_{e=1}^E \sum_{j \in \mathcal{A}} \left[(\theta_1 - \theta_2) \prod_{i \in N_e^p(j)} (1 - \rho_{iej})^{X_i} \zeta_j \gamma_{ej} + \theta_1 \prod_{i' \in N_e^s(j)} (1 - \rho_{i'ej})^{Y_{i'}} \zeta_j \gamma_{ej} \right. \\ & \left. - (\theta_1 - \theta_2) \prod_{i \in N_e^p(j)} (1 - \rho_{iej})^{X_i} \prod_{i' \in N_e^s(j)} (1 - \rho_{i'ej})^{Y_{i'}} \zeta_j \gamma_{ej} \right] \end{aligned}$$

subject to

$$\sum_{j \in \mathcal{P}} \psi^p X_j \leq M^p \quad (1.3)$$

$$\sum_{j \in \mathcal{S}} \psi^s Y_j \leq M^s \quad (1.4)$$

$$X_j + Y_j \leq 1 \quad \forall j \in \mathcal{P} \bigcap \mathcal{S} \quad (1.5)$$

$$Y_j \leq \sum_{j' \in \mathcal{P}} X_{j'} \quad \forall j \in \mathcal{S} \quad (1.6)$$

$$X_j \in \{0, 1\} \quad \forall j \in \mathcal{P} \quad (1.7)$$

$$Y_j \in \{0, 1\} \quad \forall j \in \mathcal{S} \quad (1.8)$$

The objective of model **[DP]** is to minimize the expected number of casualties due to a sudden man-made attack. Constraints (1.3) and (1.4) ensure that the cost of placing detectors (primary and secondary) is restricted to their budget availability. Constraints (1.5) ensure that at most one detector, either primary or secondary, can be placed in a given grid $j \in \mathcal{P} \cap \mathcal{S}$. Constraints (1.6) ensure that a secondary detector may support multiple primary detectors. Finally, constraints (1.7) and (1.8) set binary restrictions for the detectors placement decisions.

1.3 Branch-and-Bound Algorithm

Model **[DP]** is nonlinear due to containing several nonlinear terms in the objective function. To linearize model **[DP]** and to provide quality solutions in a reasonable time, we use the linearized branch and bound (B&B) algorithm proposed by Yan and Nie [105] which is extended over the study from Sherali et al. [88] to solve a nonconvex continuous optimization model. For each (e, j) pair, we first introduce a set of decision variables, namely,

$$\mathbf{A} := \{A_{ej}\}_{\forall e=1,2,\dots,E; j \in \mathcal{A}} \quad \text{where} \quad A_{ej} = \prod_{i \in N_e(j)} (1 - \rho_{iej})^{X_i}$$

$$\mathbf{Z} := \{Z_{ej}\}_{\forall e=1,2,\dots,E; j \in \mathcal{A}} \quad \text{where} \quad Z_{ej} = \ln(A_{ej}) = \sum_{i \in N_e(j)} \ln(1 - \rho_{iej}) X_i$$

$$\mathbf{B} := \{B_{ej}\}_{\forall e=1,2,\dots,E; j \in \mathcal{A}} \quad \text{where} \quad B_{ej} = \prod_{i' \in N_e(j)} (1 - \rho_{i'ej})^{Y_{i'}}$$

$$\mathbf{F} := \{F_{ej}\}_{\forall e=1,2,\dots,E; j \in \mathcal{A}} \quad \text{where} \quad F_{ej} = \ln(B_{ej}) = \sum_{i' \in N_e(j)} \ln(1 - \rho_{i'ej}) Y_{i'}$$

Note that both A_{ej} and B_{ej} variables will be bounded by a lower and an upper bound such that $L_{ej}^A \leq A_{ej} \leq U_{ej}^A$ and $L_{ej}^B \leq B_{ej} \leq U_{ej}^B$. Let vectors \mathbf{L} and \mathbf{U} contain both lower (i.e., L_{ej}^A and L_{ej}^B) and upper (i.e., U_{ej}^A and U_{ej}^B) bounds for variables A_{ej} and B_{ej} , respectively. The initial bounds for A_{ej} and B_{ej} variables can be obtained as follows:

$$L_{ej}^{A,0} = \prod_{i \in N_e(j)} (1 - \rho_{iej}) \quad \text{and} \quad U_{ej}^{A,0} = 1 \quad \forall e = 1, 2, \dots, E; j \in \mathcal{A} \quad (1.9)$$

$$L_{ej}^{B,0} = \prod_{i' \in N_e(j)} (1 - \rho_{i'ej}) \quad \text{and} \quad U_{ej}^{B,0} = 1 \quad \forall e = 1, 2, \dots, E; j \in \mathcal{A} \quad (1.10)$$

With this, an equivalent formulation of **[DP]** can be formulated as follows:

$$[\mathbf{DPN2}(\mathbf{L}, \mathbf{U})] \underset{\mathbf{X}, \mathbf{Y}, \mathbf{A}, \mathbf{B}, \mathbf{Z}, \mathbf{F}}{\text{Minimize}} \sum_{e=1}^E \sum_{j \in \mathcal{A}} \zeta_j \gamma_{ej} \left[(\theta_1 - \theta_2) A_{ej} + \theta_1 B_{ej} - (\theta_1 - \theta_2) A_{ej} B_{ej} \right]$$

subject to (1.3)-(1.8), and

$$Z_{ej} = \sum_{i \in N_e(j)} \ln(1 - \rho_{iej}) X_i \quad \forall e = 1, 2, \dots, E; j \in \mathcal{A} \quad (1.11)$$

$$F_{ej} = \sum_{i' \in N_e(j)} \ln(1 - \rho_{i'ej}) Y_{i'} \quad \forall e = 1, 2, \dots, E; j \in \mathcal{A} \quad (1.12)$$

$$Z_{ej} = \ln(A_{ej}) \quad \forall e = 1, 2, \dots, E; j \in \mathcal{A} \quad (1.13)$$

$$F_{ej} = \ln(B_{ej}) \quad \forall e = 1, 2, \dots, E; j \in \mathcal{A} \quad (1.14)$$

$$L_{ej}^A \leq A_{ej} \leq U_{ej}^A \quad \forall e = 1, 2, \dots, E; j \in \mathcal{A} \quad (1.15)$$

$$L_{ej}^B \leq B_{ej} \leq U_{ej}^B \quad \forall e = 1, 2, \dots, E; j \in \mathcal{A} \quad (1.16)$$

Notice that model **[DPN2(L,U)]** contains two nonlinear terms: (i) multiplication of two variables ($A_{ej}B_{ej}$) in the objective function and (ii) natural logarithms in constraints (1.13) and (1.14). Yet, **[DPN2(L,U)]** is still a mixed-integer nonlinear programming model. We first attempt to linearize the natural logarithms which are present in constraints (1.13) and (1.14) in **[DPN2(L,U)]**. To linearize the natural logarithms in constraints (1.13) and (1.14), we construct a polyhedral outer approximation, as inspired by Sherali et al. [88], for each (e, j) pair which consists of a convex envelope with three tangential support points, namely, $L_{ej}^A, \bar{A}_{ej} = \frac{U_{ej}^A - L_{ej}^A}{\ln(U_{ej}^A) - \ln(L_{ej}^A)}, U_{ej}^A$ for A_{ej} variables and $L_{ej}^B, \bar{B}_{ej} = \frac{U_{ej}^B - L_{ej}^B}{\ln(U_{ej}^B) - \ln(L_{ej}^B)}, U_{ej}^B$ for B_{ej} variables. Note that the middle points, namely, \bar{A}_{ej} and \bar{B}_{ej} for the A_{ej} and B_{ej} variables, are the one that minimize the maximum approximation error. With this, **[DPN2(L,U)]** reduces to the following relaxed problem:

$$\mathbf{[DPN1(L,U)]} \underset{\mathbf{X,Y,A,B,Z,F}}{\text{Minimize}} \sum_{e=1}^E \sum_{j \in \mathcal{A}} \zeta_j \gamma_{ej} \left[(\theta_1 - \theta_2) A_{ej} + \theta_1 B_{ej} - (\theta_1 - \theta_2) A_{ej} B_{ej} \right]$$

subject to (1.3)-(1.8), (1.11), (1.12), (1.15), (1.16), and

$$Z_{ej} \geq \ln(L_{ej}^A) + \frac{\ln(U_{ej}^A) - \ln(L_{ej}^A)}{U_{ej}^A - L_{ej}^A} (A_{ej} - L_{ej}^A) \quad \forall e = 1, 2, \dots, E; j \in \mathcal{A} \quad (1.17)$$

$$Z_{ej} \leq \ln(L_{ej}^A) + \frac{A_{ej} - L_{ej}^A}{L_{ej}^A} \quad \forall e = 1, 2, \dots, E; j \in \mathcal{A} \quad (1.18)$$

$$Z_{ej} \leq \ln(\bar{A}_{ej}) + \frac{A_{ej} - \bar{A}_{ej}}{\bar{A}_{ej}} \quad \forall e = 1, 2, \dots, E; j \in \mathcal{A} \quad (1.19)$$

$$Z_{ej} \leq \ln(U_{ej}^A) + \frac{A_{ej} - U_{ej}^A}{U_{ej}^A} \quad \forall e = 1, 2, \dots, E; j \in \mathcal{A} \quad (1.20)$$

$$F_{ej} \geq \ln(L_{ej}^B) + \frac{\ln(U_{ej}^B) - \ln(L_{ej}^B)}{U_{ej}^B - L_{ej}^B} (B_{ej} - L_{ej}^B) \quad \forall e = 1, 2, \dots, E; j \in \mathcal{A} \quad (1.21)$$

$$F_{ej} \leq \ln(L_{ej}^B) + \frac{B_{ej} - L_{ej}^B}{L_{ej}^B} \quad \forall e = 1, 2, \dots, E; j \in \mathcal{A} \quad (1.22)$$

$$F_{ej} \leq \ln(\bar{B}_{ej}) + \frac{B_{ej} - \bar{B}_{ej}}{\bar{B}_{ej}} \quad \forall e = 1, 2, \dots, E; j \in \mathcal{A} \quad (1.23)$$

$$F_{ej} \leq \ln(U_{ej}^B) + \frac{B_{ej} - U_{ej}^B}{U_{ej}^B} \quad \forall e = 1, 2, \dots, E; j \in \mathcal{A} \quad (1.24)$$

Note that model **[DPN1(L,U)]** is still nonlinear due to the presence of two continuous variables in the objective function, namely, $A_{ej}B_{ej}$. To linearize this bilinear term, we employ a tighter piecewise McCormick relaxation technique as proposed by Castillo et al. [21]. Let us first introduce variables $\{V_{ej}\}_{\forall e=1,2,\dots,E; j \in \mathcal{A}}$ to substitute the bilinear term from the objective function of **[DPN1(L,U)]**, i.e., $V_{ej} = A_{ej}B_{ej}; \forall e = 1, 2, \dots, E; j \in \mathcal{A}$. The values of V_{ej} can be determined by a set of linear constraints as introduced below. To employ piecewise McCormick relaxation technique, it is assumed that the feasible region of **[DPN1(L,U)]** is divided into **P** partitions where the optimality will lie in one of the partition, as determined by binary variables

$\{H_{ejp}\}_{\forall e=1,2,\dots,E; j \in \mathcal{A}; p \in \{1,\dots,\mathbf{P}\}}$. Further, continuous variables $\{\hat{A}_{ejp}\}_{\forall e=1,2,\dots,E; j \in \mathcal{A}; p \in \{1,\dots,\mathbf{P}\}}$ and $\{\hat{B}_{ejp}\}_{\forall e=1,2,\dots,E; j \in \mathcal{A}; p \in \{1,\dots,\mathbf{P}\}}$ are used to determine the bounds of the partitions.

$$V_{ej} \geq \sum_{p=1}^{\mathbf{P}} (\hat{A}_{ejp} B_{ejp}^L + \hat{B}_{ejp} L_{ej}^A - H_{ejp} L_{ej}^A B_{ejp}^L) \quad \forall e = 1, 2, \dots, E; j \in \mathcal{A} \quad (1.25)$$

$$V_{ej} \geq \sum_{p=1}^{\mathbf{P}} (\hat{A}_{ejp} B_{ejp}^U + \hat{B}_{ejp} U_{ej}^A - H_{ejp} U_{ej}^A B_{ejp}^U) \quad \forall e = 1, 2, \dots, E; j \in \mathcal{A} \quad (1.26)$$

$$V_{ej} \leq \sum_{p=1}^{\mathbf{P}} (\hat{A}_{ejp} B_{ejp}^L + \hat{B}_{ejp} U_{ej}^A - H_{ejp} U_{ej}^A B_{ejp}^L) \quad \forall e = 1, 2, \dots, E; j \in \mathcal{A} \quad (1.27)$$

$$V_{ej} \leq \sum_{p=1}^{\mathbf{P}} (\hat{A}_{ejp} B_{ejp}^U + \hat{B}_{ejp} L_{ej}^A - H_{ejp} L_{ej}^A B_{ejp}^U) \quad \forall e = 1, 2, \dots, E; j \in \mathcal{A} \quad (1.28)$$

$$A_{ej} = \sum_{p=1}^{\mathbf{P}} \hat{A}_{ejp} \quad \forall e = 1, 2, \dots, E; j \in \mathcal{A} \quad (1.29)$$

$$B_{ej} = \sum_{p=1}^{\mathbf{P}} \hat{B}_{ejp} \quad \forall e = 1, 2, \dots, E; j \in \mathcal{A} \quad (1.30)$$

$$\sum_{p=1}^{\mathbf{P}} H_{ejp} = 1 \quad \forall e = 1, 2, \dots, E; j \in \mathcal{A} \quad (1.31)$$

$$L_{ej}^A H_{ejp} \leq \hat{A}_{ejp} \leq U_{ej}^A H_{ejp} \quad \forall e = 1, 2, \dots, E; j \in \mathcal{A}; p \in \{1, \dots, \mathbf{P}\} \quad (1.32)$$

$$B_{ejp}^L H_{ejp} \leq \hat{B}_{ejp} \leq B_{ejp}^U H_{ejp} \quad \forall e = 1, 2, \dots, E; j \in \mathcal{A}; p \in \{1, \dots, \mathbf{P}\} \quad (1.33)$$

Note that the lower and upper bounds for the discretized variables $\{B_{ej}\}_{\forall e=1,2,\dots,E; j \in \mathcal{A}}$, namely, B_{ejp}^L and B_{ejp}^U , are computed prior to solving **[DPN1(L,U)]** with the following two equations:

$$B_{ejp}^L = L_{ej}^B + \frac{(U_{ej}^B - L_{ej}^B)(p-1)}{\mathbf{P}} \quad \forall e = 1, 2, \dots, E; j \in \mathcal{A}; p \in \{1, \dots, \mathbf{P}\} \quad (1.34)$$

$$B_{ejp}^U = L_{ej}^B + \frac{(U_{ej}^B - L_{ej}^B)p}{\mathbf{P}} \quad \forall e = 1, 2, \dots, E; j \in \mathcal{A}; p \in \{1, \dots, \mathbf{P}\} \quad (1.35)$$

With this, model **[DPN1(L,U)]** now can be reduced to the following mixed-integer linear programming model, referred to as **[DPL(L,U)]**:

$$\mathbf{[DPL(L,U)]} \underset{\mathbf{X,Y,A,B,Z,F,V,H}}{\text{Minimize}} \sum_{e=1}^E \sum_{j \in \mathcal{A}} \zeta_j \gamma_{ej} \left[(\theta_1 - \theta_2) A_{ej} + \theta_1 B_{ej} - (\theta_1 - \theta_2) V_{ej} \right]$$

subject to (1.3)-(1.8), (1.11), (1.12), and (1.15)-(1.33). We are now ready to introduce the steps undertaken to solve **[DPL(L,U)]** using a linearized branch-and-bound algorithm. Note that the bounds for **L** and **U** will be updated during the continuation of the branch-and-bound algorithm. Below, we outline the procedure of the branch-and-bound algorithm.

Algorithm 1: Linearized Branch-and-Bound (B&B) algorithm:

Step 0. Set stage $s = 0$, current node $n(s) = 0$, and active node set $O_s = \{0\}$. Let $(L_{ej}^{A,0}, L_{ej}^{B,0})$ and $(U_{ej}^{A,0}, U_{ej}^{B,0})$ to be the lower and upper bounds of variables A_{ej} and B_{ej} , respectively. The initial bounds for **L**⁰ and **U**⁰ can be obtained from equations (1.9) and (1.10). With these initial bounds, solve **[DPL(L,U)]** and obtain the corresponding optimal solution (**X,Y,A,B,Z,F,V**, and **H**) and objective function $\nu[\mathbf{DPL(L,U)}]$. Since **[DPL(L,U)]** is a relaxed problem of the original model **[DP]**, $\nu[\mathbf{DPL(L,U)}]$ provides a valid lower bound of the original problem. With the feasible solution (**X,Y**) obtained via solving **[DPL(L,U)]**, solve **[DP]** to obtain a valid upper bound for the original problem. Let UB , LB , and ϵ to be the upper and lower bound and the optimality gap of the B&B algorithm. The algorithm terminates if the optimality gap (i.e., $\epsilon = |UB - LB|/UB$) falls below a threshold value (e.g., $\epsilon = 1.0\%$); otherwise, go to **Step 1**.

Step 1. In this step, we employ a branching rule to split the current node $n(s)$ into two child nodes, namely, $n + 1$ and $n + 2$. From the optimal solution of the current node, we determine

indices e' and j' in $|Z_{e'j'} - \ln(A_{e'j'})|$ and $|F_{e'j'} - \ln(B_{e'j'})|$ such that we obtain the maximum value from $\max_{e=1,2,\dots,E; j \in \mathcal{A}} \left\{ |Z_{ej}^{n(s)} - \ln(A_{ej}^{n(s)})|, |F_{ej}^{n(s)} - \ln(B_{ej}^{n(s)})| \right\}$. We then split the bound interval $[L_{e'j'}^{n(s)}, U_{e'j'}^{n(s)}]$ into two subinterval based on the maximum value obtained from the branching rule. For instance, if $|Z_{ej}^{n(s)} - \ln(A_{ej}^{n(s)})| \geq |F_{ej}^{n(s)} - \ln(B_{ej}^{n(s)})|$, two subintervals can be updated as follows: $[L_{e'j'}^{n(s)}, A_{e'j'}^{n(s)}]$ and $[A_{e'j'}^{n(s)}, U_{e'j'}^{n(s)}]$. We then update the active node set O_s by $O_s = O_s \cup \{n+1, n+2\} \setminus \{n(s)\}$ and bounds of two child nodes as $(\mathbf{L}^{n+1}, \mathbf{U}^{n+1})$ and $(\mathbf{L}^{n+2}, \mathbf{U}^{n+2})$, respectively.

Step 2. Solve the two relaxation subproblems: $[\mathbf{DPL}(\mathbf{L}^{n+1}, \mathbf{U}^{n+1})]$ and $[\mathbf{DPL}(\mathbf{L}^{n+2}, \mathbf{U}^{n+2})]$. By utilizing the variables \mathbf{X} and \mathbf{Y} which are obtained from these subproblems, solve $[\mathbf{DP}]$ to update the incumbent solution and its objective function value as UB . If the relaxed problem turns out to be infeasible or the exceeds the best known UB , we fathom that node and update O_s .

Step 3. If O_s is empty, *terminate* the B&B algorithm and report the best incumbent. Otherwise, select a node $n(s)$ from O_s with the smallest relaxation objective function value and go to **Step 1**. Set $n \leftarrow n+1$ and $s \leftarrow s+1$.

1.4 Case Study

In this section, we first introduce the problem parameters which are considered to validate the performance of the B&B algorithm in solving model $[\mathbf{DP}]$. We then perform multiple sensitivity analyses to understand the robustness of model $[\mathbf{DP}]$ and to draw important managerial insights. Both the model and B&B algorithm are coded in python 2.7 on a desktop computer with Intel Core i7 3.6 GHz processor and 32.0 GB RAM and optimized in Gurobi Optimizer 6.5³ solver.

³Available from: <http://www.gurobi.com/>

We assume that the threat area is divided into 8×8 equal sized squares of $10m \times 10m$ (see Figure 1.4). For the base case, the set of entrances, \mathcal{E} , targets, \mathcal{A} , and blocked grids, \mathcal{B} , are set as $\mathcal{E} = \{3, 6, 17, 24, 41, 48, 59, 62\}$, $\mathcal{A} = \{28, 46\}$, and $\mathcal{B} = \{13, 26, 31, 40, 43, 50\}$, respectively. We set expected number of casualties $\{\zeta_j\}_{j \in \mathcal{A}} = 100$ persons. We set unit purchasing price, ψ^p , effective detection radius, α^p , and instantaneous detection rate, β^p , for primary detectors to be $\psi^p = \$25$ thousand, $\alpha^p = 10$ m, and $\beta^p = 0.05$, respectively. Likewise, ψ^s , α^s , and β^s are set to be $\psi^s = \$35$ thousand, $\alpha^s = 15$ m, and $\beta^s = 0.08$, respectively, for the secondary detectors. Since the interdiction team will receive less time to prepare and respond to any neutralization event if any threat could not be detected by a primary detector but by a secondary detector, we logically set $\theta_1 = 0.8$ and $\theta_2 = 0.6$. Table 1.2 summarizes the values of the parameters used for the base case [38, 70, 105].

• 57	• 58	• 59	• 60	• 61	• 62	• 63	• 64
• 49	• 50	• 51	• 52	• 53	• 54	• 55	• 56
• 41	• 42	• 43	• 44	• 45	• 46	• 47	• 48
• 33	• 34	• 35	• 36	• 37	• 38	• 39	• 40
• 25	• 26	• 27	• 28	• 29	• 30	• 31	• 32
• 17	• 18	• 19	• 20	• 21	• 22	• 23	• 24
• 9	• 10	• 11	• 12	• 13	• 14	• 15	• 16
• 1	• 2	• 3	• 4	• 5	• 6	• 7	• 8

Figure 1.4

Representation of the threat area with 8×8 equal sized squares

Table 1.2

Base case parameter values

Parameter	Description	Value
\mathcal{E}	Set of entrances	{3, 6, 17, 24, 41, 48, 59, 62}
\mathcal{A}	Set of targets	{28, 46}
\mathcal{B}	Set of blocked grids	{13, 26, 31, 40, 43, 50}
γ_{ej}	Probability of choosing each path	0.0625
ζ_j	Expected casualties at target	100 person
θ_1	Probability of successful intervention	0.8
θ_2	Probability of successful intervention	0.6
k	Speed of terrorist	1 m/s
M^t	Total budget	\$320,000
M^P	Budget availability to procure primary detectors	60% M^t
M^S	Budget availability to procure secondary detectors	40% M^t
ψ^P	Unit purchasing price for primary detectors	\$25,000
ψ^S	Unit purchasing price for secondary detectors	\$35,000
α^P	Effective detection radius for primary detectors	10 m
α^S	Effective detection radius for secondary detectors	15 m
β^P	Instantaneous detection rate for primary detectors	0.05
β^S	Instantaneous detection rate for secondary detectors	0.08

The first set of experiments study the impact of detection radius for the primary (α^P) and secondary (α^S) detectors on the expected number of casualties. As evidenced from Figure 1.5 that as α^P and α^S increases, the expected number of casualties decreases. Further, the results clearly demonstrate an additional benefit of utilizing a *two-layer detection* over a *one-layer detection* mechanism. Note that by setting $\{Y_j\}_{\forall j \in \mathcal{S}} = 0$ and ignoring constraints (1.4)-(1.6) and (1.8), problem [DP] can be deduced to a *one-layer detection* problem, as introduced by Nie et al. [70]. Results indicate that casualties can be reduced by an additional 21.9% in a two-layer detection over a one-layer detection problem if the detection radius (α^P , α^S) can be increased by 50% from the base case. The results clearly signify the impact of the increase in detection radius on the expected number of casualties as well as the two layer detection method in a threat area.

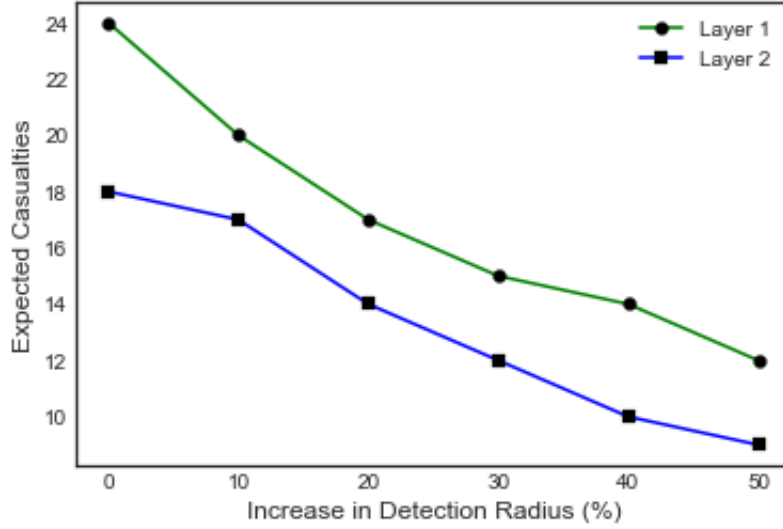


Figure 1.5

Impact of detection radius on expected casualties

The next set of experiments study the impact of instantaneous detection rate for primary (β^p) and secondary (β^s) detectors and how it affects the resulting number of casualties. To run these experiments, we first set base β^p and β^s values to $\beta^p = 0.05$ and $\beta^s = 0.08$. Figure 1.6 illustrates the relationship between instantaneous detection rates and the expected number of casualties in a given threat area. The results clearly indicate that as the values of β^p and β^s increase, the number of expected casualties decreases. This trend is expected since improving in instantaneous detection rates correlates to earlier threat detection, which is expected to reduce the number of casualties in a given threat area. Furthermore, Figure 1.6 compares the results of a one-layer and two-layer detection mechanism; a two-layer system reduces casualties by an average of 15.6% more than a one-layer system. In conclusion, the number of casualties is highly sensitive to β^p and β^s for a given threat area.

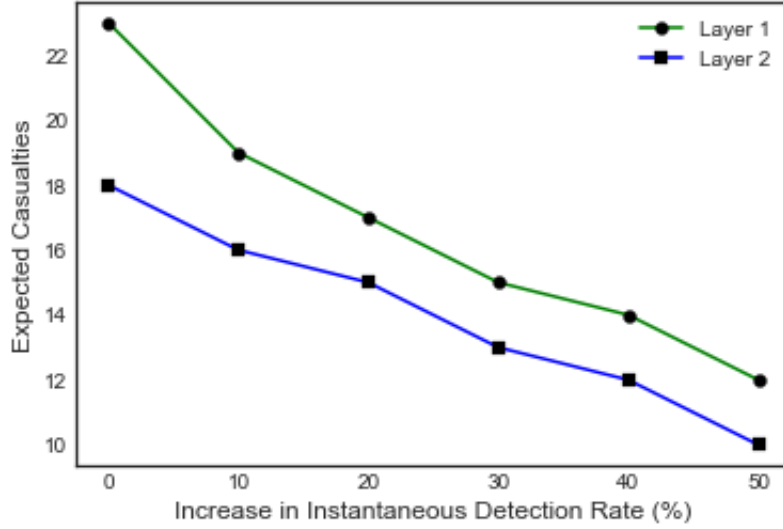


Figure 1.6

Impact of instantaneous detection rate on expected casualties

We now experiment on the impact of budget (M^p and M^s) on the expected number of casualties in a 8×8 grid threat area. As more budget is available to purchase primary and secondary detectors, this shall have an impact on reducing the expected number of casualties in a given threat area. This relationship is illustrated in Figure 1.7, where it can be shown that if the availability of budget is increased by 50%, the expected number of casualties can be dropped by approximately 53% to any threat event. Further, it is observed that if a two-layer detection plan is employed over a one-layer detection plan, then the average number of expected casualties in a given threat area can be dropped by approximately 18.1%. In overall, we observe that if an additional budget is allocated to purchase more detectors to secure a given threat area, then the optimal assignment of the detectors, provided by solving model **[DP]**, may reduce the expected number of casualties from any potential threat event.

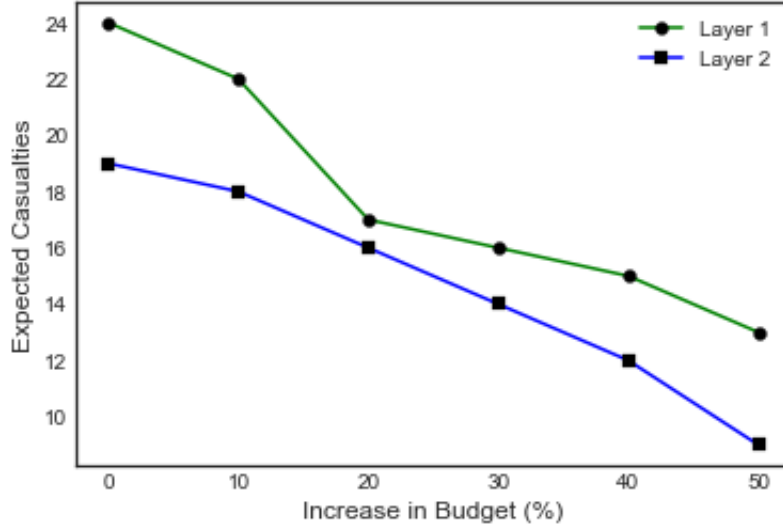


Figure 1.7

Impact of budget on expected casualties

The last set of experiments study the impact of the robustness of the B&B algorithm in solving the proposed mathematical model $[\mathbf{DLP}(\mathbf{L}, \mathbf{U})]$. To do this, we generate 27 problem instances by randomly generating different entrances, \mathcal{E} , attack, \mathcal{A} , and blocked, \mathcal{B} , grids, respectively. The respectively description of the sets for \mathcal{E} , \mathcal{A} , and \mathcal{B} in constructing these 27 problem instances are provided in Table 1.3. Table 1.4 shows the robustness of the B&B algorithm in solving the proposed mathematical model $[\mathbf{DLP}(\mathbf{L}, \mathbf{U})]$, referred to as *two-layer detection* problem, and the *one-layer detection* problem as introduced earlier. To run the experiments with the B&B algorithm, we set a 0.0% optimality gap and a 3,600 CPU time. Table 1.4 reports the location of the primary, X_j , and secondary, Y_j , detectors for the two-layer detection problem and only primary detectors, X_j , for the one-layer detection problem (second and fifth columns in Table 1.4). Note that these

locations are represented for a threat area consisting of 8×8 grids. Additionally, in Table 1.4, we report the optimal solution, V^* , and running time, T^* (in seconds), for the two detection problems.

Table 1.3

Scenario Parameter Values

Scenario	Parameter
1	$\mathcal{E}=\{20, 35, 56\}; \mathcal{A}=\{31\}; \mathcal{B}=\{6, 55\}$
2	$\mathcal{E}=\{4, 15, 50\}; \mathcal{A}=\{35\}; \mathcal{B}=\{1, 12, 16, 56\}$
3	$\mathcal{E}=\{20, 31, 42\}; \mathcal{A}=\{7\}; \mathcal{B}=\{23, 26, 36, 48, 61, 64\}$
4	$\mathcal{E}=\{14, 30, 53\}; \mathcal{A}=\{20, 42\}; \mathcal{B}=\{34, 44\}$
5	$\mathcal{E}=\{1, 41, 58\}; \mathcal{A}=\{7, 31\}; \mathcal{B}=\{2, 38, 42, 60\}$
6	$\mathcal{E}=\{22, 40, 51\}; \mathcal{A}=\{2, 17\}; \mathcal{B}=\{5, 11, 20, 29, 30, 48\}$
7	$\mathcal{E}=\{2, 14, 23\}; \mathcal{A}=\{34, 54, 64\}; \mathcal{B}=\{17, 42\}$
8	$\mathcal{E}=\{13, 37, 50\}; \mathcal{A}=\{8, 15, 35\}; \mathcal{B}=\{27, 28, 31, 62\}$
9	$\mathcal{E}=\{8, 44, 46\}; \mathcal{A}=\{12, 40, 60\}; \mathcal{B}=\{4, 5, 14, 16, 51, 53\}$
10	$\mathcal{E}=\{20, 26, 33, 34, 48, 53\}; \mathcal{A}=\{38\}; \mathcal{B}=\{23, 31\}$
11	$\mathcal{E}=\{11, 15, 18, 34, 38, 48\}; \mathcal{A}=\{44\}; \mathcal{B}=\{12, 19, 24, 52\}$
12	$\mathcal{E}=\{4, 16, 38, 39, 45, 46\}; \mathcal{A}=\{60\}; \mathcal{B}=\{13, 21, 25, 32, 62, 64\}$
13	$\mathcal{E}=\{20, 22, 26, 28, 42, 53\}; \mathcal{A}=\{47, 64\}; \mathcal{B}=\{1, 35\}$
14	$\mathcal{E}=\{17, 18, 32, 37, 45, 64\}; \mathcal{A}=\{47, 62\}; \mathcal{B}=\{19, 22, 41, 44\}$
15	$\mathcal{E}=\{1, 14, 17, 25, 50, 51\}; \mathcal{A}=\{11, 40\}; \mathcal{B}=\{7, 13, 24, 29, 35, 49\}$
16	$\mathcal{E}=\{1, 7, 16, 34, 45, 64\}; \mathcal{A}=\{19, 20, 57\}; \mathcal{B}=\{2, 52\}$
17	$\mathcal{E}=\{5, 21, 40, 41, 44, 57\}; \mathcal{A}=\{3, 17, 24\}; \mathcal{B}=\{11, 18, 25, 43\}$
18	$\mathcal{E}=\{14, 15, 37, 53, 54, 63\}; \mathcal{A}=\{48, 41, 59\}; \mathcal{B}=\{23, 30, 34, 45, 58, 64\}$
19	$\mathcal{E}=\{5, 6, 7, 13, 15, 21, 33, 42, 44\}; \mathcal{A}=\{1\}; \mathcal{B}=\{60, 64\}$
20	$\mathcal{E}=\{27, 28, 29, 37, 39, 42, 47, 49, 53\}; \mathcal{A}=\{59\}; \mathcal{B}=\{1, 15, 51, 57\}$
21	$\mathcal{E}=\{12, 17, 18, 29, 43, 59, 62, 63, 64\}; \mathcal{A}=\{33\}; \mathcal{B}=\{4, 8, 9, 14, 21, 25\}$
22	$\mathcal{E}=\{2, 9, 12, 15, 17, 25, 40, 47, 50\}; \mathcal{A}=\{37, 61\}; \mathcal{B}=\{8, 58\}$
23	$\mathcal{E}=\{5, 8, 10, 13, 33, 37, 48, 49, 59\}; \mathcal{A}=\{54, 63\}; \mathcal{B}=\{4, 15, 31, 46\}$
24	$\mathcal{E}=\{4, 10, 23, 26, 36, 40, 42, 59, 60\}; \mathcal{A}=\{20, 46\}; \mathcal{B}=\{18, 25, 27, 35, 38, 57\}$
25	$\mathcal{E}=\{4, 18, 28, 32, 35, 38, 44, 48, 59\}; \mathcal{A}=\{7, 33, 63\}; \mathcal{B}=\{12, 47\}$
26	$\mathcal{E}=\{3, 10, 11, 21, 34, 40, 43, 58, 62\}; \mathcal{A}=\{16, 38, 60\}; \mathcal{B}=\{2, 8, 20, 54\}$
27	$\mathcal{E}=\{6, 12, 18, 19, 37, 44, 54, 55, 59\}; \mathcal{A}=\{34, 39, 41\}; \mathcal{B}=\{13, 17, 25, 31, 40, 64\}$

Table 1.4 shows the robustness of the B&B algorithm in solving the proposed mathematical model $[\mathbf{DLP}(\mathbf{L}, \mathbf{U})]$, referred to as *two-layer detection* problem, and the *one-layer detection* problem as introduced earlier. To run the experiments with the B&B algorithm, set a 0.0% optimality gap and a 3,600 CPU time. Table 1.4 reports the location of the primary, X_j , and secondary, Y_j , detectors

for the two-layer detection problem and only primary detectors, X_j , for the one-layer detection problem (second and fifth columns in Table 1.4). Note that these locations are represented for an 8×8 element threat area. Additionally Table 1.4 includes the optimal solution, V^* , and running time, T^* (in seconds), for the two detection problems.

Table 1.4

B&B Algorithm Resulting Detector Placements

Scenario	Two-layer System			One-layer System		
	Primary and Secondary	V^*	T^* (sec)	Primary	V^*	T^* (sec)
1	$X_j = \{20, 27, 28, 29, 35, 36, 37\}$ $Y_j = \{22, 23, 30, 38\}$	0.39	0.38	$X_j = \{20, 21, 22, 27, 28, 29, 30, 35, 36, 38\}$	0.64	0.02
2	$X_j = \{14, 21, 22, 29, 50\}$ $Y_j = \{28, 34, 36, 42, 43\}$	0.92	0.33	$X_j = \{14, 21, 22, 23, 27, 28, 29, 36, 42, 43, 50, 51\}$	1.06	0.02
3	$X_j = \{12, 13, 20, 21, 22, 27, 28, 29, 35, 43\}$ $Y_j = \{6, 14\}$	0.35	0.20	$X_j = \{6, 12, 13, 14, 15, 20, 21, 28, 29, 34, 35, 43\}$	0.64	0.03
4	$X_j = \{22, 28, 36, 37, 45, 52, 53\}$ $Y_j = \{21, 29, 35, 51\}$	2.75	0.76	$X_j = \{21, 22, 28, 29, 30, 36, 37, 43, 45, 51, 52, 53\}$	3.40	0.06
5	$X_j = \{3, 4, 5, 34, 37, 43, 44\}$ $Y_j = \{6, 14, 22, 30\}$	2.45	0.77	$X_j = \{3, 4, 5, 6, 14, 28, 30, 34, 35, 37, 44, 51\}$	2.92	1.00
6	$X_j = \{12, 13, 19, 21, 22, 34, 42\}$ $Y_j = \{3, 9, 25, 26\}$	2.87	2.1	$X_j = \{3, 12, 13, 18, 19, 21, 22, 26, 34, 35, 42, 43\}$	3.99	0.17
7	$X_j = \{10, 18, 20, 22, 29, 31, 39\}$ $Y_j = \{26, 27, 45, 55\}$	4.63	3.34	$X_j = \{10, 18, 20, 22, 23, 26, 27, 28, 31, 39, 46, 47\}$	4.06	8.59
8	$X_j = \{12, 13, 14, 21, 29, 30, 51\}$ $Y_j = \{7, 22, 36, 42\}$	9.24	0.97	$X_j = \{7, 13, 14, 20, 21, 22, 23, 29, 30, 42, 43, 50\}$	12.68	0.26
9	$X_j = \{7, 8, 24, 28, 38, 44, 45, 46\}$ $Y_j = \{21, 31, 39, 52\}$	9.88	3.09	$X_j = \{7, 13, 20, 24, 28, 32, 38, 44, 45, 46, 47, 52\}$	10.58	0.26
10	$X_j = \{21, 28, 36, 40, 48, 53, 54\}$ $Y_j = \{29, 37, 46, 47\}$	3.07	0.35	$X_j = \{21, 29, 30, 34, 35, 37, 39, 45, 46, 47, 48, 53\}$	5.24	0.04
11	$X_j = \{22, 26, 27, 30, 34, 38, 42, 46\}$ $Y_j = \{35, 36, 45\}$	3.28	0.49	$X_j = \{22, 26, 27, 28, 34, 35, 36, 37, 38, 42, 45, 46\}$	4.52	0.1
12	$X_j = \{12, 23, 28, 38, 44, 45, 46, 54, 44\}$ $Y_j = \{51, 52, 53\}$	1.85	1.01	$X_j = \{12, 28, 36, 37, 38, 44, 45, 46, 52, 53, 54, 61\}$	2.97	0.07
13	$X_j = \{8, 29, 31, 37, 44, 45, 53, 54\}$ $Y_j = \{38, 46, 55\}$	16.05	1.53	$X_j = \{29, 30, 36, 38, 39, 43, 45, 46, 53, 54, 55, 63\}$	17.87	0.63
14	$X_j = \{27, 31, 36, 37, 45, 46, 64\}$ $Y_j = \{38, 53, 54, 55\}$	14.28	0.55	$X_j = \{27, 37, 38, 39, 40, 45, 46, 53, 54, 55, 63, 64\}$	11.92	0.57
15	$X_j = \{1, 9, 14, 17, 27, 38, 43\}$ $Y_j = \{10, 12, 18, 39\}$	17.29	2.35	$X_j = \{2, 9, 10, 12, 18, 19, 26, 27, 38, 39, 43, 45\}$	19.87	2.66
16	$X_j = \{9, 14, 34, 37, 44\}$ $Y_j = \{12, 18, 28, 49, 50\}$	20.1	3.01	$X_j = \{9, 13, 15, 21, 26, 27, 28, 37, 49, 50, 58, 63\}$	22.25	9.6
17	$X_j = \{27, 34, 35, 36, 44, 49, 57\}$ $Y_j = \{12, 23, 26\}$	28.94	1.11	$X_j = \{4, 5, 12, 19, 20, 23, 26, 30, 32, 33, 36, 41\}$	23.55	2.23
18	$X_j = \{31, 44, 46, 53, 63\}$ $Y_j = \{39, 42, 47, 52, 55\}$	18.89	4.39	$X_j = \{21, 22, 39, 40, 42, 44, 46, 47, 52, 55, 60, 61\}$	20.17	3.93
19	$X_j = \{3, 4, 5, 11, 12, 18, 19, 26, 27, 34\}$ $Y_j = \{2, 10\}$	2.25	0.28	$X_j = \{2, 3, 4, 5, 6, 9, 10, 11, 13, 18, 26, 34\}$	2.95	0.22
20	$X_j = \{35, 43, 44, 45, 46, 49, 53, 61\}$ $Y_j = \{50, 52, 58\}$	6.23	0.9	$X_j = \{27, 35, 42, 43, 44, 45, 46, 50, 52, 53, 58, 60\}$	7.83	0.16
21	$X_j = \{17, 18, 19, 27, 35, 43, 51, 53\}$ $Y_j = \{26, 41, 42\}$	6.51	3.1	$X_j = \{17, 18, 19, 26, 27, 34, 35, 41, 42, 43, 51, 53\}$	8.76	0.35
22	$X_j = \{20, 26, 27, 35, 44, 46, 51\}$ $Y_j = \{36, 38, 52, 54\}$	19.66	0.94	$X_j = \{20, 27, 28, 29, 36, 38, 44, 46, 51, 52, 53, 54\}$	16.21	2.35
23	$X_j = \{21, 30, 38, 39, 48, 52, 60\}$ $Y_j = \{45, 47, 56, 62\}$	17.8	0.78	$X_j = \{30, 37, 38, 39, 45, 47, 52, 53, 55, 56, 60, 62\}$	16.26	1.76
24	$X_j = \{30, 36, 43, 52\}$ $Y_j = \{11, 21, 28, 29, 39, 45\}$	22.39	0.46	$X_j = \{12, 19, 21, 22, 28, 30, 36, 37, 39, 28, 43, 44, 45\}$	26.73	1.79
25	$X_j = \{5, 22, 35, 36, 44, 46, 48\}$ $Y_j = \{14, 34, 54, 55\}$	30.77	2.72	$X_j = \{6, 14, 15, 23, 29, 34, 35, 36, 48, 54, 55, 62\}$	36.73	8.8
26	$X_j = \{11, 21, 35, 36, 40, 44, 62\}$ $Y_j = \{23, 29, 46, 52\}$	34.3	3.98	$X_j = \{11, 14, 15, 24, 29, 30, 35, 37, 39, 46, 51, 52\}$	39.03	12.9
27	$X_j = \{18, 20, 36, 37, 44, 51, 55\}$ $Y_j = \{27, 38, 42, 46\}$	30.23	4.97	$X_j = \{19, 26, 27, 30, 35, 38, 42, 43, 44, 46, 47, 51, 47\}$	36.52	5.96

Figure 1.8 shows the optimal detector placements for both the two-and-one layer detection problems in a given test instance (instance 24). Results demonstrate how the X_j and Y_j and only X_j are placed in Figures 1.8(a) and 1.8(b), respectively, to minimize the expected number of casualties in a 8×8 threat area. It can be observed that an additional 16.2% expected number of casualties can now be saved due to optimally placing the backup/secondary detectors in the threat area. Likewise, Table 1.4 provides optimal detector placements for other test instances and under both two-and-one layer detection problems.

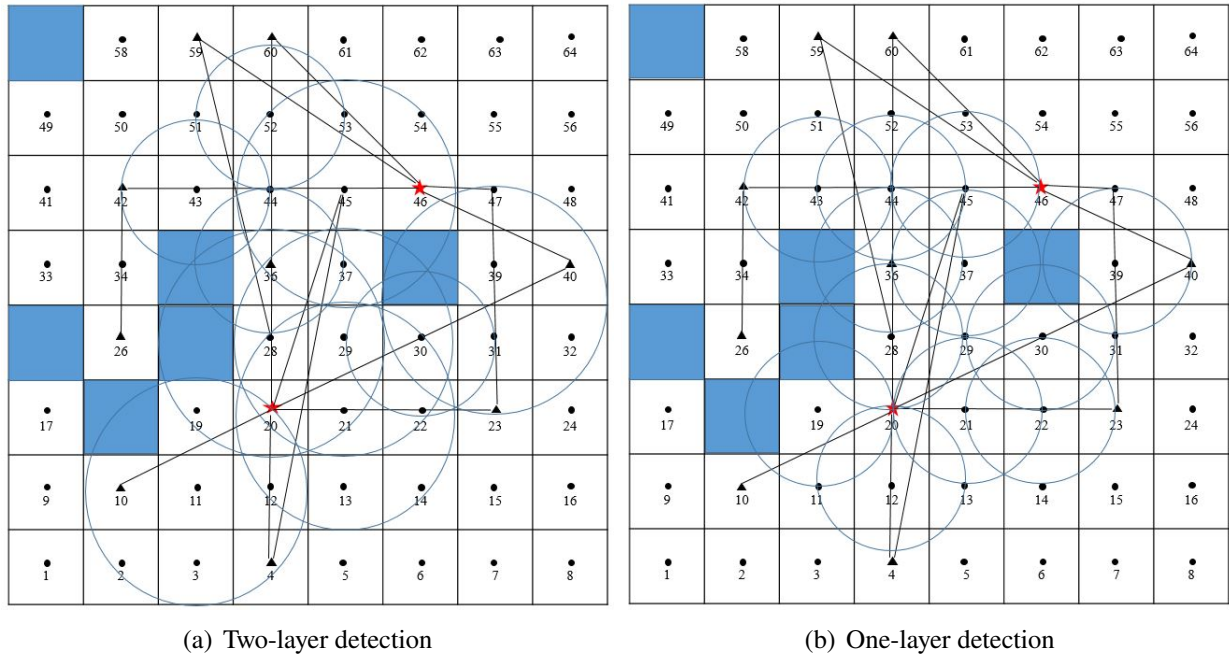


Figure 1.8

Detector placement for two-and-one layer detection problems (instance 24)

Results in Table 1.4 clearly demonstrate the efficiency of the B&B algorithm in solving both the two-and-one layer detection problems. It can be observed that the B&B algorithm is capable

of finding an optimal solution for both the two problems in a reasonable amount of time. For the two-layer detection problem, the maximum running time (T^*) is found to be 4.97 CPU seconds among all the instances. Likewise, the maximum T^* is found to be 12.9 CPU seconds for the one-layer detection problem. In summary, it can be concluded that the B&B algorithm is shown to be robust in consistently generating high-quality solutions within our test instances.

1.5 Conclusions and Future Work

This study proposes an innovative nonlinear binary integer programming model to optimally deploy a set of primary and secondary detectors on a threat area in such a way that the expected number of casualties can be minimized. We then employ a linearized branch-and-bound algorithm to solve our proposed mathematical model. To the end, a number of sensitivity analyses are performed to illustrate the robustness of the model and to draw key managerial insights. A few notable insights are given below.

- An additional 21.9% casualties can be saved in a two-layer detection over a one-layer detection problem if the detection radius (α^p , α^s) can be increased by 50% from the base case.
- Under the base instantaneous detection rates for primary (β^p) and secondary (β^s) detectors, on average an additional 15.6% casualties can be saved if a two-layer detection mechanism is employed over a one-layer detection mechanism. The percentage can be improved even further with the advancement in α^p and α^s in the near future.
- The availability of budget to purchase additional primary and secondary detectors will significantly secure an area and drop the expected number of casualties under a given threat

event. For instance, we observe an approximately 53% drop in casualties with an increment of 50% budget from the base case scenario.

- The B&B algorithm is shown to be robust in consistently generating high-quality solutions in solving our proposed mathematical model within our test instances.

This study can be extended in several research directions. First, our study assumes independent failures of the detectors (both primary and secondary and detectors). However, in reality, interdependent failures may occur. Second, our study assumes known threat areas. It might be interesting to examine how the model would behave under a dynamic threat attack. We also would like to examine how the adoption of mobile detectors minimizes the expected number of casualties in a given threat area. Finally, an extension of the cost modeling could also include expected costs due to casualties incurred by delayed response times, lack of threat detection, or untimely threat detection. Such real-world cost considerations would impact engineering management choices as to whether or not it is cost-effective for the ownership organization to invest in the additional layer of sensors as offset by increases of expected casualties and insurance costs. These issues will be addressed in future studies.

CHAPTER II

OPTIMIZING CIVILIAN RESPONSE STRATEGY UNDER AN ACTIVE SHOOTING INCIDENT

2.1 Introduction

2.1.1 Motivation

Active Shooting (AS)¹ is a common terminology that is frequently being used in the US and all over the world in the last few decades, especially after the early 2,000. Despite remarkable improvements in developing advanced training modules and civilian response strategies in the last couple of years, neither the incident rate nor the casualty rate is seeing at a decline. The Federal Bureau of Investigation (FBI) reports that the average number of AS incidents between 2000-2007 were 7.4 incidents/year, which further increased to 17.6 incidents/year between 2008-2015 before finally accelerated to 25.7 incidents/year between 2016-2018 [27] (see Fig. 2.1 for details). Most importantly, approximately 90% of the AS incidents occur in the gun-free (GF) facilities, include all areas where the general public is forbidden to carry firearms (e.g., Pre-K to 12 schools (14.8%), universities (6%), businesses and shopping malls (42%), and health care facilities (4%)) [27]. Such violence in the GF facilities poses serious security concerns among public safety, primarily due to the horrifying outcomes and potentially large number of casualties that typically stem from such an attack. Another worrisome fact is that 70% of the past AS incidents ended in less than 5 minutes

¹formally defined by The US Department of Homeland Security (DHS) as *An individual actively engaged in killing or attempting to kill people in a confined and populated area; in most cases, active shooters use firearm(s), and there is no pattern or method to their selection of victim* [101]

(11% among them ended in less than 2 minutes) [84]. With an average law enforcement response time greater than 5 minutes [91], the GF facilities must be carefully designed so that the civilians get ample time to hide/exit in/from the system and the expected number of casualties from an AS attack can be minimized.

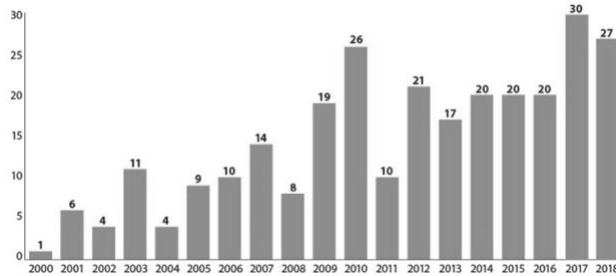


Figure 2.1

Active shooting incidents in the US between 2000-2018

2.1.2 Related Literature

AS research in GF facilities probably started on November 12, 1840, when a law professor at the University of Virginia was fatally shot (died in 3 days later) by one of his students [97]. This perhaps was the first-ever recorded AS incident that held in any school infrastructure or campus in the US. However, the 1999 Columbine school shooting can be considered as one of the most tragic incident in the US history that let the policymakers and law enforcement officers feel for the first time that such incidents can happen at any time and in any community and cannot continue to be unprepared for such situations. Following this incident, in addition to SWAT team training, specialized civilian training programs, such as the RUN.HIDE.FIGHT.® (RHF), Avoid, Deny, Defend™ (ADD) programs, are introduced. Additionally, many statistics/case-based reports

have started to publish periodically, primarily by the Department of Homeland Security (DHS), Texas State University, and Purdue Homeland Security Institute. However, very little attention has been paid to date to determine the optimal response strategy or assessing the safety of a workplace under an AS exposed environment.

Realizing that many hypothetical situations can be modeled and analyzed easily and a significant detail and fidelity can be incorporated into the model, researchers predominantly use an agent-based simulation approach to mimic an AS exposed environment (e.g., [40, 91, 47, 48, 46]). For instance, mitigation strategies, such as RHF [16, 91, 48, 46] and automatic door locking system [47], can be modeled and visualized with the help of an agent-based simulation model. Additionally, few studies attempted to simulate the past AS incidents, such as the 2012 movie theatre shooting in Aurora, Colorado [33], and the 2017 Las Vegas shooting [48], to derive useful insights. To the end, different policies, such as the effectiveness of the Senator Feinstein's bill to regulate assault weapons and magazine capacity [33], and scenarios, such as the no security/security guard/concealed carry gun scenario [9, 40]; automatic door locking system [47]; civilian evacuation time and firearm discharge rate by the shooter and police [48]; and cognitive delay [91], can be analyzed and assessed using an agent-based simulation model. Other than adopting any modeling framework, a number of studies qualitatively discuss different AS mitigation and response strategies on healthcare applications [37, 44, 67, 83, 41].

Our problem can be considered as a special case of emergency evacuation problems (e.g., hurricane [117, 53]), fire ([104, 60]), football stadium evacuation [60]), except the fact that in this specific case the threat actively chases to find the next target to maximize the number of casualties in a given AS incident. Further, such incidents are characterized by highly unpredictable, evolve

quickly, having (typically) no escape plan for the shooter(s), and with a major goal of mass murdering in a very limited timeframe. Few studies examine the impact of crowd evacuation under crowd density and various building parameters (e.g., sizes and position of doors) [78, 109, 51]. It is noteworthy to mention the study conducted by Li et al. [52], which first develops a comprehensive three-stage decision-making and behavioral model for pedestrian evacuation under different terrorist attacks (e.g., bombing, shooting, melee attack). Other closely related studies include identifying patterns and relations to understand terrorist behaviors (e.g., [99]), attack occurrences (e.g., [96, 32]), and vulnerability assessment of critical facilities in combating the terrorism (e.g., [10, 8]).

2.1.3 Research Contributions

While previous studies have done a phenomenal job in quantifying and analyzing the effects of many parameters (e.g., discharge rate, magazine capacity) in different AS situations, they just ignored modeling/optimizing individual civilian response behaviors or often made simple assumptions that may not accurately reflect the reality (e.g., setting one response strategy (move/do not move) for all civilians in a given simulation trial). Research is needed to develop advanced quantitative methods to generate and analyze different possible AS scenarios for a specific population (e.g., age group, diversity) and facility (e.g., school, shopping mall, hospital) in mind. Unfortunately, no rigorous quantitative technique has been developed to date that takes into account all these critical factors and analyzes or optimizes civilian's response strategy under an AS-exposed environment.

To the best of the authors knowledge, this study, for the first time in the literature, proposed a mathematical model formulation that specifically optimizes individual's behavioral decision

while accounting several critical features, such as capacity of the facility and individual choices, heterogeneity of individual behavioral and choice sets, restriction on choice sets depending on the location of the shooter and facility orientation, and many others, which are essential for appropriately characterizing and analyzing the response strategy for civilian's under an AS exposed environment. To realistically capture the time-space movement for both the civilians and the shooter(s), we propose a greedy heuristic that can solve our mathematical model under a rolling horizon framework.

We demonstrate the applicability of our proposed model by implementing the effectiveness of the RHF program in an academic environment. A survey is conducted among a sample of the students taking classes in that academic building to understand their responses under different AS exposed environment. The choice behavior of the *students* (hereafter *civilians* to make this generic) are collected and then appropriately incorporated into the proposed mathematical model to maximize individuals utility under an AS exposed environment. Finally, a number of numerical experiments are conducted, including varying building configurations (e.g., location and number of hiding and entrances/exits), initial distribution and cognitive delay of the civilians, which may provide significant managerial insights to the decision makers and hold promise to enhance the reliability and resiliency of various threatening GF facilities (e.g., schools, hospitals, shopping malls).

2.2 Problem Description and Mathematical Model Formulation

In this section, we present a mathematical model formulation which aims to maximize civilians utility under an AS exposed environment. To formulate this problem, we first assume that a

GF area is rectangular which has been divided into $m \times n$ equal-sized grids, denoted by set $\mathcal{G} = \{g : g = 1, 2, \dots, mn\}$. To model physical obstruction, we divide set \mathcal{G} into two major types: (i) blocked grids and (ii) unblocked grids. *Blocked grids*, denoted by set $\mathcal{G}^b \subset \mathcal{G}$, represent the set of grids where the shooter cannot travel or no civilians are present. On the other hand, *unblocked grids*, denoted by set $\mathcal{G}^u = \mathcal{G} \setminus \mathcal{G}^b$, represent the set of grids where both the shooter and the civilians can travel and $\mathcal{G} = \mathcal{G}^b \cup \mathcal{G}^u$. It is assumed that the knowledge about a shooter's potential target is known in advance. Let $\mathcal{G}^a \subset \mathcal{G}^u$ be the set of grids where a attack may potentially occur (e.g., food court, library). We further define $\mathcal{G}^e \subset \mathcal{G}^u$ to be the set of grids from which a shooter or a civilian can enter or exit the facility. It is assumed that the shooter will enter the facility from one of the entrances $g \in \mathcal{G}^e$ and reach to attack grid $g \in \mathcal{G}^a$ by utilizing a shortest path. Let $\mathcal{G}^h \subset \mathcal{G}^u$ to be the set of grids where a civilian can potentially hide (e.g., locked classroom/office). We further define set \mathcal{G}^s , which includes a cell $g \in \mathcal{G}^u$ and it's neighbouring cells. Appendix A1 summarizes the sets, parameters, and decision variables used in this section.

We assume a population of N civilians, denoted by set \mathcal{N} and indexed by n , present in the GF area. A set of alternatives, denoted by set \mathcal{I} (indexed by i), is also available for each civilian $n \in \mathcal{N}$. Since in this study we test the effectiveness of RHF program [46], we construct the set of alternatives \mathcal{I} as $\mathcal{I} = \{\text{runUp}, \text{runDown}, \text{runLeft}, \text{runRight}, \text{stay}\}$. The first four alternatives in set \mathcal{I} determine the direction of running, whereas the last alternative indicates if the civilian decides to stay in the same grid. We now introduce subset $\mathcal{G}_{g,i}$ that represents the neighbouring cells of cell $g \in \mathcal{G}^u$, given action $i \in \mathcal{I}$ is undertaken. Further, $\forall g \in \mathcal{G}^h$, we define a set of possible actions, \mathcal{I}_g , in such a way that if we undertake them, they can lead us to a respective hidden cell. Finally, we introduce set $\mathcal{G}_{g,i}$ to represent the neighbouring cells of cell $g \in \mathcal{G}^h$, given

that the action $i \in \mathcal{I}_g$ is undertaken. If a civilian decides to run towards the direction of travel of the shooter, we then infer that the civilian may fight with the shooter. On the other hand, a civilian may find it safe by staying in a hiding grid $g \in \mathcal{G}^h$. Such model rely on the assumption that each individual $n \in \mathcal{N}$ associates a score, referred to as *utility*, with each alternative $i \in \mathcal{I}$. Let us define $\mathbf{U}^1 := \{U_{ingr} | \forall i \in \mathcal{I}, n \in \mathcal{N}, g \in \mathcal{G}^u, r = 1, 2, \dots, R\}$ to denote the utility associated with choosing alternative i by civilian n located in grid g under realization r . Given the nonlinear nature of the utility functions, we use the simulation approach proposed by Bierlaire [14] to derive a linear utility function. Essentially, the probabilistic nature of the choice model is captured via generating R draws, $\xi_{ing1}, \xi_{ing2}, \dots, \xi_{ingR}$, from the distribution of the random error term of the original utility function. Note that each of these draws represents a specific behavioral scenario. Once all the draws are generated, for each realization r , we obtain the following utility associated with alternative i by civilian n located in grid g :

$$U_{ingr} = \sum_k \beta_k \hat{x}_{ingk} + f(\tilde{x}_{ing}) + \xi_{ingr}$$

$$\forall i \in \mathcal{I}, n \in \mathcal{N}, g \in \mathcal{G}^u, r = 1, 2, \dots, R \quad (2.1)$$

where \hat{x}_{ingk} and \tilde{x}_{ing} represent, respectively, the endogenous and exogenous variables of the model and β_k are the associated parameters of the endogenous variables. Note that $f(\tilde{x}_{ing})$ will be preprocessed prior to using them in the model; therefore, it does not matter if this function is linear or not.

Given an alternative may become unavailable to a civilian (e.g., hidden place), we introduce a binary variable $\mathbf{Y}^1 := \{Y_{ing} | \forall i \in \mathcal{I}, n \in \mathcal{N}, g \in \mathcal{G}^u\}$ to denote the availability of alternative i to a

civilian n located in grid g . Further, the availability of alternative i to a civilian n located in grid g under realization r is modeled by introducing another binary variable $\mathbf{Y}^2 := \{Y_{ingr} | \forall i \in \mathcal{I}, n \in \mathcal{N}, g \in \mathcal{G}^u, r = 1, 2, \dots, R\}$, and we let $\mathbf{Y} = \mathbf{Y}^1 \cup \mathbf{Y}^2$. Note that through introducing variables Y_{ing} and Y_{ingr} , heterogeneity among individuals decision can be captured. For instance, a disable or aged civilian may not be able to run to escape herself/himself in a nearby entrances/exits even though the alternative may be viable for most of the other civilians located in grid $g \in \mathcal{G}^u$. The relationship between variables Y_{ing} and Y_{ingr} can be modeled as follows:

$$Y_{ingr} \leq Y_{ing} \quad \forall i \in \mathcal{I}, n \in \mathcal{N}, g \in \mathcal{G}^u, r = 1, 2, \dots, R \quad (2.2)$$

Constraints (3.2) indicate that an alternative $i \in \mathcal{I}$ is not be available in the scenario level r if that alternative is not a feasible option for grid $g \in \mathcal{G}^u$ or not considered by the civilian $n \in \mathcal{N}$.

We now employ the concept of *discounted utility* [46] to associate an alternative with the highest utility, pending the alternative is selected by the civilian; otherwise, a low utility value is assigned to that alternative. To capture this behavior, we introduce a variable $\mathbf{X} := \{X_{ingr} | \forall i \in \mathcal{I}, n \in \mathcal{N}, g \in \mathcal{G}^u, r = 1, 2, \dots, R\}$ to represent the discounted utility associated with alternative i chosen by civilian n located in grid g under scenario r , i.e.,

$$X_{ingr} = \begin{cases} U_{ingr} & \text{if } Y_{ingr} = 1 \\ l_{ngr} & \text{if } Y_{ingr} = 0 \end{cases} \quad \forall i, n, g, r = 1, 2, \dots, R \quad (2.3)$$

where $l_{ngr} = \min_{i \in \mathcal{I}} l_{ingr}$ to represent the smallest lower bound across all alternatives. Below, $\forall i \in \mathcal{I}, n \in \mathcal{N}, g \in \mathcal{G}^u, r = 1, 2, \dots, R$, constraints (3.4)-(3.7) are provided to linearize condition

(3.3). **Proposition 1** proves that constraints (3.4)-(3.7) indeed provide an equivalent representation of condition (3.3).

$$l_{ngr} \leq X_{ngr} \quad (2.4)$$

$$X_{ngr} \leq l_{ngr} + \bar{\phi}_{ngr} Y_{ngr} \quad (2.5)$$

$$U_{ngr} - \bar{\phi}_{ngr}(1 - Y_{ngr}) \leq X_{ngr} \quad (2.6)$$

$$X_{ngr} \leq U_{ngr} \quad (2.7)$$

where parameter $\bar{\phi}_{ngr}$ can be defined as follows: $\bar{\phi}_{ngr} = (\phi_{ngr} - l_{ngr})$ and ϕ_{ngr} is the upper bound across all alternatives. Note that since \hat{x}_{ingr} are bounded and \tilde{x}_{ingr} are given; therefore, we can bound U_{ingr} as follows:

$$\begin{aligned} l_{ingr} \leq U_{ingr} &\leq \phi_{ingr} \quad \forall i \in \mathcal{I}, n \in \mathcal{N}, \\ g &\in \mathcal{G}^u, r = 1, 2, \dots, R \end{aligned} \quad (2.8)$$

Proposition 1 Constraints (3.4)-(3.7) are equivalent to (3.3).

Proof. See Appendix A2.

We now introduce a binary variable $\mathbf{Z}^1 := \{Z_{ingr} | \forall i \in \mathcal{I}, n \in \mathcal{N}, g \in \mathcal{G}^u, r = 1, 2, \dots, R\}$ to denote the choice of alternative i by civilian n located in grid g under realization r . We further introduce another binary variable $\mathbf{Z}^2 := \{Z_{ingg'r} | \forall i \in \mathcal{I}, n \in \mathcal{N}, g \in \mathcal{G}^u, g' \in \mathcal{G}_{g,i}, r = 1, 2, \dots, R\}$ to indicate that the movement of civilian n from grid g to g' by choosing alternative i under

realization r and $\mathbf{Z} := \mathbf{Z}^1 \cup \mathbf{Z}^2$. Since civilian n cannot select alternative i if that alternative is not available to that grid g , we introduce the following logical constraints:

$$Z_{ingr} \leq Y_{ingr} \quad \forall i \in \mathcal{I}, n \in \mathcal{N}, g \in \mathcal{G}^u, r = 1, 2, \dots, R \quad (2.9)$$

Each civilian $n \in \mathcal{N}$ located in grid $g \in \mathcal{G}^u$ under realization $r = 1, 2, \dots, R$ is allowed to choose only one alternative. This is enforced via constraints (3.10).

$$\sum_{g \in \mathcal{G}^u} \sum_{i \in \mathcal{I}} Z_{ingr} = 1 \quad \forall n \in \mathcal{N}, r = 1, 2, \dots, R \quad (2.10)$$

It may take time for a civilian to realize that a shooting is occurring and then to appropriately respond to such incident. This is known as *cognitive delay* [91]. This civilian-specific factor is appropriately captured via introducing parameter $\pi_n; \forall n \in \mathcal{N}$. Let $\tilde{t}_{gg'}$ to denote the standard average travel time for a civilian to run from grid $g \in \mathcal{G}^u$ to $g' \in \mathcal{G}^s \setminus \{g\}$. We further denote $t_{ngg'}$ to be the actual travel time by civilian $n \in \mathcal{N}$ to run from grid $g \in \mathcal{G}^u$ to $g' \in \mathcal{G}^s \setminus \{g\}$. Note that the civilian-specific $t_{ngg'}$ parameter will be impacted by crowd density, facility configuration, age, gender, and many other related factors. Finally, a binary parameter $\zeta_g \in \{0, 1\}$ is introduced to indicate the proximity of shooter near grid $g \in \mathcal{G}^u$. If ζ_g is equal to zero (within the shooting range of the shooter), running towards exit may not be a feasible decision.

$$\begin{aligned} (\pi_n + t_{ngg'}) Z_{ingg'r} &\leq \zeta_g \tilde{t}_{gg'} \quad \forall n \in \mathcal{N}, g \in \mathcal{G}^u, i \in \mathcal{I} \setminus \{i_5\} \\ &\quad , g' \in \mathcal{G}_{g,i}, r = 1, 2, \dots, R \end{aligned} \quad (2.11)$$

Note that if a civilian $n \in \mathcal{N}$ decides to run from grid $g \in \mathcal{G}^u$, then she/he can reach to any of the neighbouring grid $g' \in \mathcal{G}^g$. This is ensured via introducing the following constraints.

$$\begin{aligned} Z_{ingr} &= Z_{ingg'r} \quad \forall i \in \mathcal{I}, n \in \mathcal{N}, g \in \mathcal{G}^u, g' \in \mathcal{G}_{g,i}, \\ r &= 1, 2, \dots, R \end{aligned} \quad (2.12)$$

Due to capacity restrictions, civilians are not allowed to hide more than \bar{v}_g numbers in a specific grid $g \in \mathcal{G}^h$. We assume a 100% safety level for civilians upon reaching to a hidden grid $g \in \mathcal{G}^h$. Note that $\bar{v}_g \leftarrow 0$, if no hiding option is available for the civilians in a specific grid $g \in \mathcal{G}^h$ (e.g., open corridor in a building). The above restriction is enforced via constraints (2.13) as shown below.

$$\sum_{n \in \mathcal{N}} \sum_{i \in \mathcal{I}_{g'}} \sum_{g \in \mathcal{G}_{g',i}} Z_{ingg'} \leq \bar{v}_{g'} \quad \forall g' \in \mathcal{G}^h, r = 1, 2, \dots, R \quad (2.13)$$

Based on the behavioral assumption, the alternative $i \in \mathcal{I}$ picked by the civilian $n \in \mathcal{N}$ should associate with a highest discounted utility. This is ensured via introducing a continuous decision variable $\mathbf{U}^2 := \{U_{ngr} | \forall n \in \mathcal{N}, g \in \mathcal{G}^u, r = 1, 2, \dots, R\}$ and is defined as follows:

$$U_{ngr} = \max_{i \in \mathcal{I}} X_{ingr} \quad \forall n \in \mathcal{N}, g \in \mathcal{G}^u, r = 1, 2, \dots, R \quad (2.14)$$

Constraints (2.14) can be linearized as follows:

$$X_{ngr} \leq U_{ngr} \quad \forall i \in \mathcal{I}, n \in \mathcal{N}, g \in \mathcal{G}^u, \\ r = 1, 2, \dots, R \quad (2.15)$$

$$U_{ngr} \leq X_{ngr} + \bar{\phi}_{ngr}(1 - Z_{ngr}) \quad \forall i \in \mathcal{I}, n \in \mathcal{N}, \\ g \in \mathcal{G}^u, r = 1, 2, \dots, R \quad (2.16)$$

where $\bar{\phi}_{ngr} = (\phi_{ngr} - l_{ngr})$ is the difference between the largest upper bound (ϕ_{ngr}) and the smallest lower bound (l_{ngr}) and ϕ_{ngr} is defined as follows: $\phi_{ngr} = \max_{i \in \mathcal{I}} \phi_{ingr}$. **Proposition 2** proves that constraints (2.15)-(2.16) indeed provide an equivalent representation of condition (2.14).

Proposition 2 Constraints (2.15)-(2.16) are equivalent to (2.14).

Proof. See Appendix A3.

The objective of this problem, referred to as model **[AS]**, is to maximize the utility associated with each civilians under an AS incident.

$$\textbf{[AS]} \quad \text{Maximize } \frac{1}{R} \sum_{n \in \mathcal{N}} \sum_{g \in \mathcal{G}} U_{ngr}$$

subject to (3.1), (3.2), (3.4)-(2.13), and (2.15)-(2.16).

2.3 Solution Approach

Model [AS] is static. To represent a more realistic situation for an AS incident, we need to appropriately capture the time-space movement for both the civilians and the shooter(s). In this section, we propose a greedy solution approach to capture such behaviors dynamically. Additionally, a set of performance measures are introduced to quantify the impact of our proposed model to an AS situation.

Let $\chi = 1, 2, \dots, P$ to be the set of trails where in each trial it is assumed that the shooter may enter the facility from one of the entrances and reach to a threat grid. For each trial $\chi = 1, 2, \dots, P$, we capture the movement of the shooter and civilians in different discrete time periods, denoted by $t = 1, 2, \dots, T$. Since model [AS] is now solved in each time period t to obtain $\{Y_{ing}^t, Y_{ingr}^t, Z_{ingr}^t, Z_{ingg'r}^t, X_{ingr}^t, U_{ingr}^t, U_{ngr}^t\}$ decisions, we redefine model [AS] by [AS(t)]. Accordingly, parameters $\zeta_g^{t,\chi}$ and $\bar{v}_{g'}^t$ are updated in each time period $t = 1, 2, \dots, T$. At the end of each trial $\chi = 1, 2, \dots, P$, the following performance measures are evaluated:

- V_E^χ : the number of civilians *exit* the system at the end of trial χ
- V_H^χ : the number of civilians *hide* in the system at the end of trial χ
- V_{RISK}^χ : the number of civilians are in *risk* (neither exit/hide from/in the system) at the end of trial χ
- V_{sol}^χ : overall *utility* at the end of trial χ

Likewise, at the end of evaluating all possible trials, performance measures V_E , V_H , V_{RISK} , and V_{sol} are obtained. Performance metric V_{RISK} quantifies the average number of civilians who might be at risk at the end of evaluating all possible trails. We determine this number by subtracting the total number of civilians (N^χ) with the number of civilians exit (V_E)/hide (V_H) from/to the system

i.e., $V_{RISK} := \sum_{\chi=1}^P N^\chi - (V_E + V_H)$. The entire decision-making process is handled under a rolling horizon framework, which is reported in **Algorithm 1**.

```

for  $\chi = 1, 2, \dots, P$  do
  Initialize  $\zeta_g^{t,\chi}, \pi_n^\chi, V_E^\chi, V_H^\chi, V_{RISK}^\chi, V_{sol}^{t,\chi}, V_{sol}^\chi, V_E^{t,\chi}$  and the distribution of population  $N^\chi$ 
  for  $t = 1, 2, \dots, T$  do
    Solve model [AS(t)] to obtain  $\{Y_{ing}^t, Y_{ingr}^t, Z_{ingr}^t, Z_{inggr}^t, X_{ingr}^t, U_{ingr}^t, U_{ngr}^t\}$  and  $V_{sol}^{t,\chi}$ 
    Update  $\zeta_g^{t,\chi}$  and  $\bar{v}_{g'}$ 
    Calculate:  $V_E^{t,\chi} := \frac{1}{R} \sum_{n=1}^{N^\chi} \sum_{g \in (\mathcal{G}^{u'} \cup \mathcal{G}^h)} \sum_{g' \in \mathcal{G}^e} Z_{inggr}^t$ 
  end
  Calculate:  $V_E^\chi := \sum_{t=1}^T V_E^{t,\chi}$ 
            $V_H^\chi := \frac{1}{R} \sum_{n=1}^{N^\chi} \sum_{g' \in \mathcal{G}^h} (Z_{isngr}^T + \sum_{i \in I \setminus \{i_5\}} \sum_{g \in \mathcal{G}^{u'}} Z_{inggr}^T)$ 
            $V_{RISK}^\chi := N^\chi - (V_E^\chi + V_H^\chi)$ 
            $V_{sol}^\chi := \sum_{t=1}^T V_{sol}^{t,\chi}$ 
end
Calculate:  $V_E := \sum_{\chi=1}^P V_E^\chi$ 
            $V_H := \sum_{\chi=1}^P V_H^\chi$ 
            $V_{RISK} := \sum_{\chi=1}^P N^\chi - (V_E + V_H)$ 
            $V_{sol} := \sum_{\chi=1}^P V_{sol}^\chi$ 

```

Algorithm 1: Greedy Heuristic

Figure 2.2 outlined a simplified decision-making framework for assessing the civilian response strategy under an active shooter incident. From the figure, it can be seen that the successful implementation and interpretation of the model [AS(t)] is contingent upon a number of input parameters, such as individual's choice behavior, building-specific and active shooter-specific attributes, which can be obtained from participation survey, case building, or existing literature and reports (see Section 2.4 for details). Once model [AS(t)] is solved for different time periods, $t = 1, 2, \dots, T$, a number of performance metrics, namely, V_E , V_H , V_{RISK} , and V_{SOL} , are checked and are reviewed by the decision-makers (e.g., school officials, law enforcement officers). If the performance measures sound acceptable by the decision-makers, the decision-making process terminates; otherwise, different model attributes can be changed (e.g., number or position of the entrances/exits, hiding places), and the performance metrics are reevaluated.

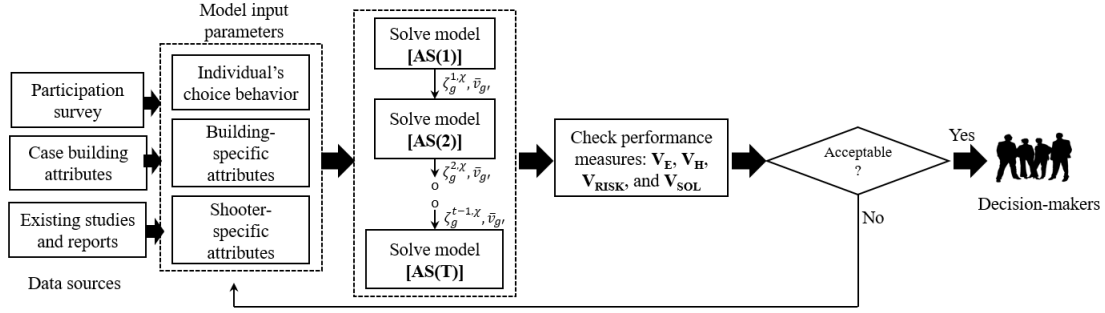


Figure 2.2

A simplified decision-making framework for assessing civilian response strategy under an active shooter incident

2.4 Experimental Results

This section first presents our survey results (Section 2.4.1), problem input parameters (Section 3.3.1), and then a series of numerical experiments to illustrate the model applications and to draw useful managerial insights (Section 2.4.3). Both the model and the solution algorithm are coded in Python 2.7 on a desktop computer with Intel Core i7 3.6 GHz processor and 32.0 GB RAM. A state-of-the-art commercial solver, Gurobi Optimizer 6.5², is used to solve the proposed greedy heuristic. We set a 1.0% optimality gap and 3,600 CPU seconds time limit to solve the model [AS(t)] using the greedy heuristic. Note that all the experiments investigated in this study are solved in less than 10 seconds.

2.4.1 Survey Summary

We surveyed among university students to get their responses under an AS incident. The students were asked the type of grid-specific alternative (e.g., run, stay) they would pick under different realistic AS situations (e.g., proximity to the shooter, hiding places, and exits). In total,

²Available from: <http://www.gurobi.com/>

175 students (31.4% female) participated this survey. Among the students, 98.9% of students fall in the age group between 16 to 30 while the remaining portion falls in the age group between 31 to 45. Majority of the participants were Caucasian (80.6%; 29.1% among them were female), followed by African-American: 8.6% (53.3% female), Asian: 6.9% (50% female), Latino-Hispanic: 2.9% (no female), and others (e.g., Native American and Native Hawaiian/Pacific Islander): 1.0% (no female). Among our participants, 5.1% had a physical or mental impairment (22.2% among them were female); 22.3% had prior online AS training experiences (28.2% among them were female), and 10.9% never played any shooting-related video games (78.9% among them were female). Finally, 72% of the participants reported that they would be able to make a decision (e.g., choosing an alternative as described before) between 2 to 6 seconds under an extremely stressful situation. A summary of the participants is provided in Table 2.1.

Table 2.1

Summary of the survey participants

Item	Description
Total samples	175 (31.4% female)
Ethnicity	Caucasian: 80.6% (29.1% female) African-American: 8.6% (53.3% female) Asian: 6.9% (50% female) Latino-Hispanic: 2.9% (no female) Others: 1.0% (no female)
Total disability	5.1% (22.2% female)
Online training experience	Yes: 22.3% (28.2% female) No: 77.7% (32.4% female)
Gaming experience	None: 10.9% (78.9% female) Basic: 17.1% (66.7% female) Average: 20.6% (25.0% female) Above average: 23.4% (22.0% female) Expert: 28.0% (4.1% female)
Decision making capability (under stress)	Very slow (>8 seconds): 2.3% (25.0% female) Slow (6–8 seconds): 3.4% (33.3% female) Average (4–6 seconds): 30.3% (45.3% female) Quick (2–4 seconds): 41.7% (32.9% female) Very quick (<2 seconds): 22.3% (10.3% female)

2.4.2 Input Parameters

Fig. 3.2 shows a 6×6 test grid facility (with an area of approximately 24,500 sq. ft) that we have considered as a test-bed to visualize and validate our modeling results. The facility has three *entrances/exits* (grid 4, 24, and 33), six *blocked* grids (grid 8, 12, 17, 21, 25, and 29), and a *hiding* grid (grid 14). Later, we test this base facility with varying entrance/exit and hidden grid configurations. We assume that the shooter will enter the facility from one of the entrances and reach to her/his destination by visiting different grids during this active shooting period. Accordingly, we asked our participants to input their feedback under different position for them and the shooter. Variables, such as proximity to nearest exits/entrances, hiding grids, shooter's position, and direction of the shooter and shooting range (binary variable), are considered to construct the utility U_{ingr} for each individual $n \in \mathcal{N}$, choosing alternative $i \in \mathcal{I}$, locating in grid $g \in \mathcal{G}^u$, and under realization $r = 1, 2, \dots, R$ (shown in equation (3.1)). We use Mixed Multinomial logit (MMNL) model [66] to derive these utilities U_{ingr} . Fig. 3.4 demonstrates how the utilities (U_{ingr}) from the majority of the individuals are changing in different grids with respect to the shooters position on different time periods. For instance, highest utility in grid 32 corresponds to action `runDown` (Fig. 2.4.2) which instantaneously changed to action `runRight` (Fig. 2.4.2) when the shooter changed her/his position from grid 33 to 27 (See Appendix A4 for a sample utility calculation). We assume that it will require 15 seconds for a shooter to run from one center grid to the center of it's neighboring grid. Grid 14 is a hidden grid; therefore, the highest utility for this grid corresponds to action `stay`. Other parameters for model [AS] are set as follows: $\{\bar{v}_g\}_{g \in \mathcal{G}^h} = 10$ civilians, $\tilde{t}_{gg'} = 20$ seconds, and $t_{ngg'} \approx t_{gg'} = 15$ seconds³; $\forall g \in \mathcal{G}^u; g' \in (\mathcal{G}^{u'} \cup \mathcal{G}^h \cup \mathcal{G}^e)$.

³We set $t_{ngg'} \approx t_{gg'}$ since 98.9% of our participants age group fall between 16 to 30 years

Finally, the cognitive delay of a civilian $\{\pi_n\}_{\forall n \in \mathcal{N}}$ is obtained from the inputs of our survey participants (see “Decision making capability (under stress)” rows in Table 2.1).

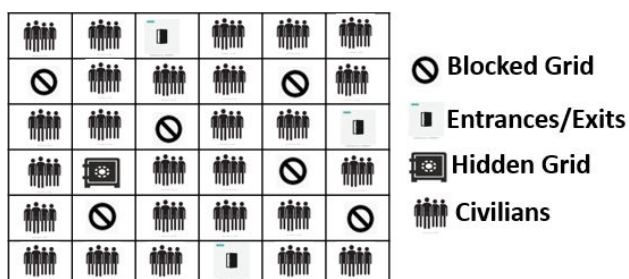


Figure 2.3

6×6 test grid facility

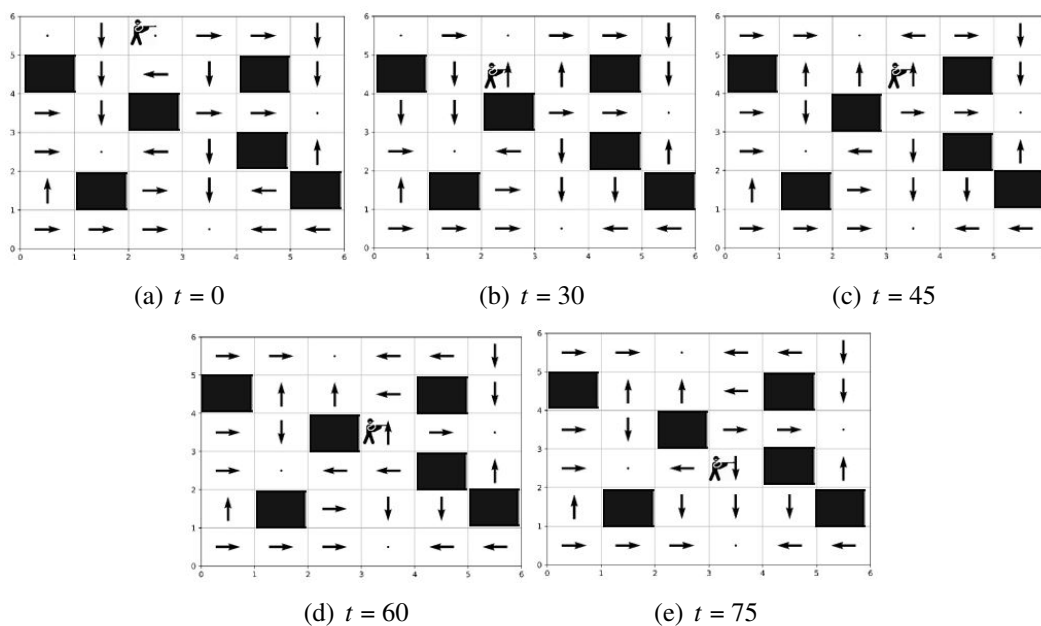


Figure 2.4

Demonstrating how the utility is changing (majority of the individuals) in different grids with respect to the shooters position and time (in seconds)

2.4.3 Lessons Learned

In this subsection, we first present the base case results to illustrate the model applications. Following to this, we vary a set of key input parameters, such as the number of hidden grids $|\mathcal{G}^h|$, entrances/exits $|\mathcal{G}^e|$, cognitive delay of a civilian $\{\pi_n\}_{n \in \mathcal{N}}$, and initial distribution of civilians in our 6×6 test grid facility (shown in Figure 3.2), to derive important lessons for the decision-makers. We believe such lessons may help the decision-makers to design a safe and reliable facility that can potentially hedge against possible AS threats. Fig. 2.5 shows the values of performance measures, V_E , V_H , and V_{RISK} , over time period $t = \{0, 15, 30, 45, 60, 75\}$ seconds and under the base input parameters as discussed in Section 3.3.1. Recall that we collected data from 175 civilians (31.4% female). Results indicate that the curve for V_H stabilizes just after 15 seconds. This is understandable given we have only one hiding place with a capacity of 10 individuals ($\{\bar{v}_g\}_{g \in \mathcal{G}^h} = 10$) in our base case configuration. Interestingly, we notice that the values for performance measures V_E and V_{RISK} increases and decreases, respectively, till time $t = 45$ seconds and then remain flat till the end of this tested incident period. This might be due to the availability of either one hiding grid ($|\mathcal{G}^h| = 1$), the current entrance/exit configurations ($|\mathcal{G}^e| = 3$), the initial and updated position of the civilians and shooter, and the cognitive delay of the civilians, or a combination thereof.

Fig. 2.6 shows the movement of civilians over time under the base case setup. At time $t = 0$ second, civilians are uniformly distributed in our test facility. As soon as the shooter becomes available (at grid 33) at time $t = 15$ seconds, the movement of the civilians' changes and is continued to be changing till the end of the incident period ($t = 75$ seconds). Notice that the intensity of the two entrances/exits (grid 4 and 24) are getting darker over time. This is again

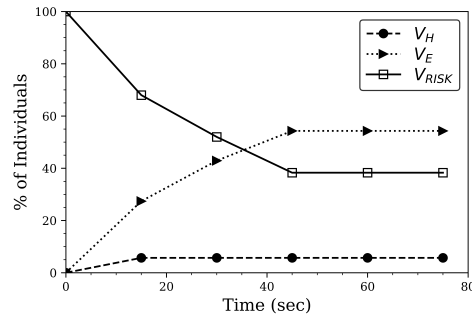


Figure 2.5

Base case values of V_H , V_E , and V_{RISK} over time

understandable since the locations of this two entrances/exits are farther away from the shooter's position. It is important to highlight that approximately 38% of the civilians (V_{RISK}) are still at risk even after 75 seconds. Rigorous system design and safety planning are required to drop the percentage of V_{RISK} under an active shooting incident.

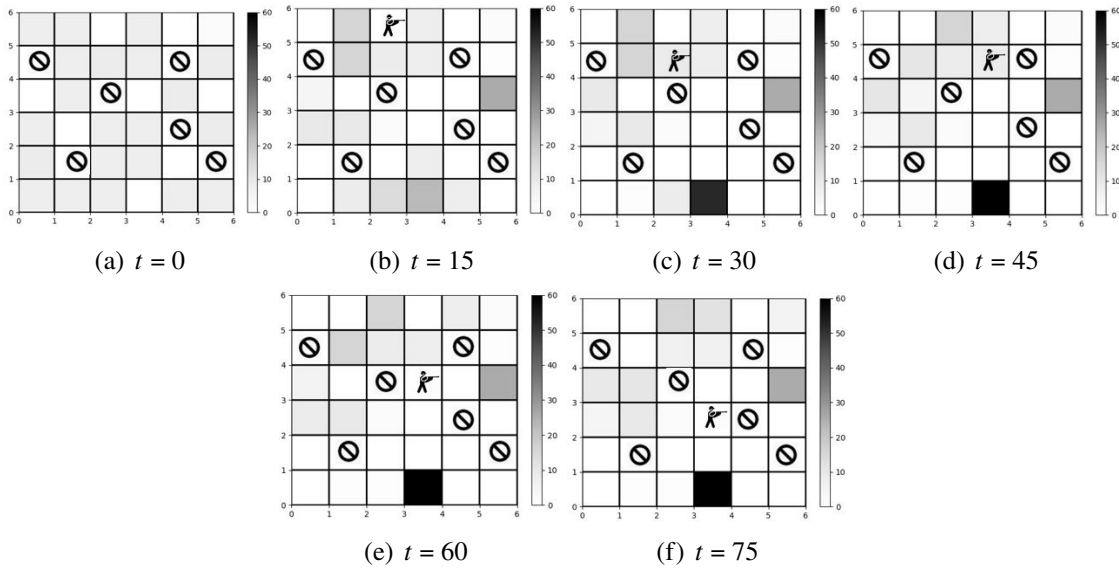


Figure 2.6

Movement of civilians over time: base case

The base case experimental results indicate that the system performance may be highly sensitive to the input parameters. Hence, we now experiment with different input parameters, such as the number of hidden grids $|\mathcal{G}^h|$, entrances/exits $|\mathcal{G}^e|$, cognitive delay of a civilian $\{\pi_n\}_{n \in \mathcal{N}}$, and initial distribution of the civilians, and summarizes the following lessons which are learned from our experiments.

Lesson 1: *Building configurations (e.g., location and number of entrances/exits, hiding places) play a significant role in the safety of civilians under an AS incident.*

The results in Figs. 3.5 and 3.6 support this observation. The graphs present the impact of V_H , V_E , and V_{RISK} under different hiding and entrance/exit configurations. Appendix A5 illustrates different hiding and entrance/exit configurations (locations and numbers) for the tested facility where $|\mathcal{G}^h|$ and $|\mathcal{G}^e|$ are set as $|\mathcal{G}^h| = \{1, 2, 3, 4\}$ and $|\mathcal{G}^e| = \{1, 2, 3, 4\}$. Note that, for the base case, we set $|\mathcal{G}^h| = 1$ and $|\mathcal{G}^e| = 3$. We summarize a few of our key observations below:

- Given capacity restrictions for the hiding grids (e.g., $\{\bar{v}_g\}_{g \in \mathcal{G}^h} = 10$ civilians for our base case experimentations), we realize that the location and number of entrance/exit configurations are more sensitive to an AS situation over the hiding configurations. For instance, when $|\mathcal{G}^e|$ increases from 1 to 4, then V_E increases from 5.1% to 65.1%. Resultantly, we observe that V_{RISK} drops down to 29.1% from 89.1%. On the other hand, when $|\mathcal{G}^h|$ increases from 1 to 4, V_H increases from 5.7% to 19.4%, but both V_E and V_{RISK} drops from 54.3% to 50.3% and 38.3% to 29.7%, respectively. The rate of dropping for V_E and V_{RISK} clearly indicates that the entrance/exit configurations are more sensitive to an AS situation over the hiding configurations.

- It is interesting to note that for $|\mathcal{G}^h| = 4$, the civilians utilized only 85% of the hiding capacity after 75 seconds. This number was only 47.5% and 65% after 45 and 60 seconds, respectively, from the onset of the shooting. This indicates that civilians have higher preferences for exiting the threat area rather than hiding into the facility. We believe this insight can help law enforcement officers to better educating the civilians for the case when exiting the threat area may become infeasible.

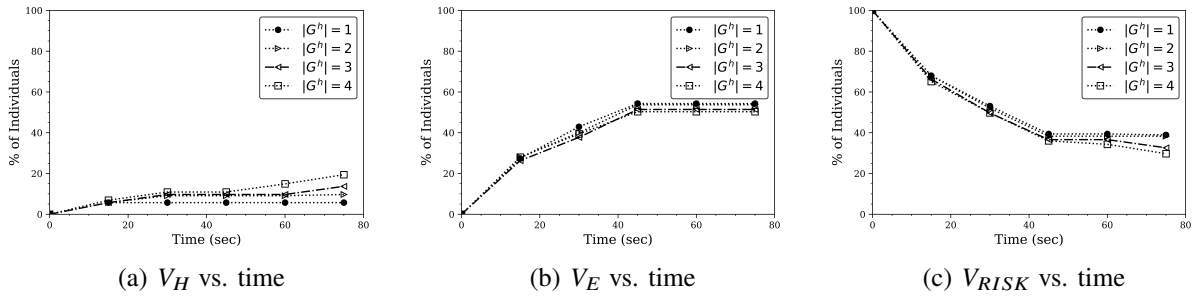


Figure 2.7

Impact of V_H , V_E , and V_{RISK} under different hiding configurations

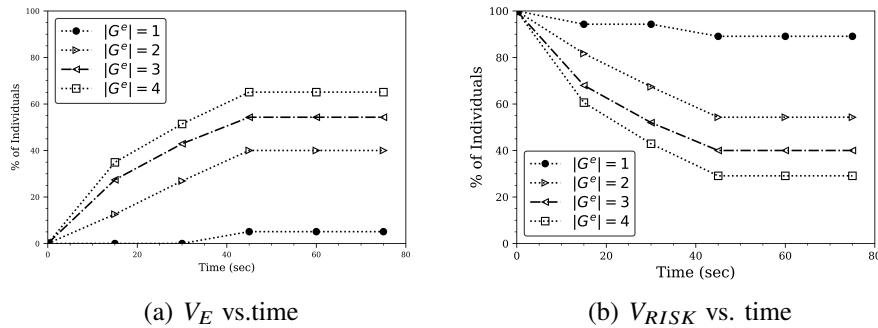


Figure 2.8

Impact of V_E and V_{RISK} under different entrance/exit configurations

Lesson 2: *Initial distribution of civilians has an impact on recovery from an AS incident.*

The results in Fig. 3.7 support this statement where we can see how the initial distribution of civilians impact the performance measures, V_E and V_{RISK} . Let us first introduce Table 3.2 which lists the different initial civilian distribution that we have considered in our test region. Fig. A.6 depicts these initial distributions of the civilians. The first case considered the base distribution where civilians are uniformly distributed over the entire test region (Fig. 1.8(a)). The remaining cases are constructed based on an idea that 70% of the civilians are uniformly distributed in one end of the test region, i.e., left distribution (Fig. 1.8(b)), right distribution (Fig. 1.8(c)), up distribution (Fig. 1.8(d)), and down distribution (Fig. 1.6(e)). Note that, for all the experiments, we set $|\mathcal{G}^h| = 1$ and $|\mathcal{G}^e| = 3$ (Fig. 3.2). We summarize a few of our key observations below:

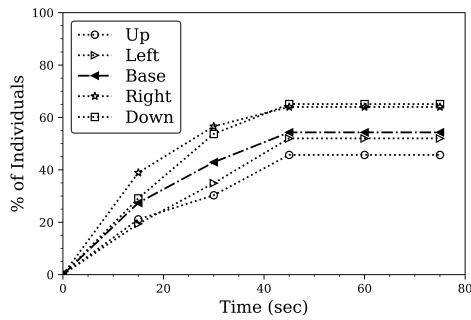
- The results in Fig. 3.7 clearly indicate that the right and down initial distribution of the civilians significantly increases V_E over the other distributions (e.g., base, left, up distributions). For instance, after 75 seconds from the onset of the AS incident, the V_E drops down to approximately 64% and 65.1%, respectively, under the right and down initial distribution of the civilians. Note that at the same time, the V_E only drops down to 45.7% under the up initial distribution case. This is primarily due to the fact the shooter entered into the facility from the upper entrance (see Fig. 3.2), which resulted in the civilians to evade using that exit and using more on the right and downside exits.
- Similar observation can be drawn for the V_{RISK} measure as well which drops significantly for the right and down initial distribution of the civilians over the other distributions. For instance, after 75 seconds from the onset of the AS incident, the V_{RISK} drops down to approximately 30.3% and 29.1%, respectively, under the right and down initial distribution

of the civilians where the number is approximately 49% for the up initial distribution. The results provide several managerial insights to decision-makers. For instance, the rate of the casualty may differ on the different time periods of the day, e.g., the majority of the students are on the left and right side of the facility during the class period which may not be the case under lunch period. Further, the entrance of the shooter and the availability of multiple exits and their locations may help to facilitate the movement of the civilians under an AS situation.

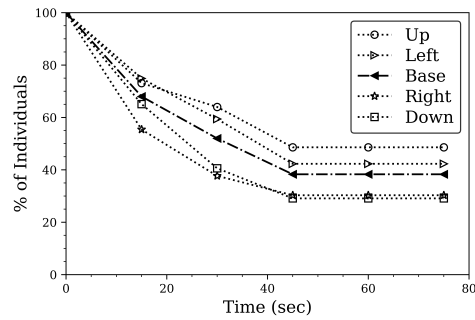
Table 2.2

Initial distribution of civilians over the test region

Item	Description
Base distribution	Civilians are uniformly distributed over the entire region
Left distribution	70% of the civilians are uniformly distributed over the left-side of the region
Right distribution	70% of the civilians are uniformly distributed over the right-side of the region
Up distribution	70% of the civilians are uniformly distributed over the upper-side of the region
Down distribution	70% of the civilians are uniformly distributed over the down-side of the region



(a) V_E vs. time



(b) V_{RISK} vs. time

Figure 2.9

Impact of V_E and V_{RISK} under different civilian distribution configurations

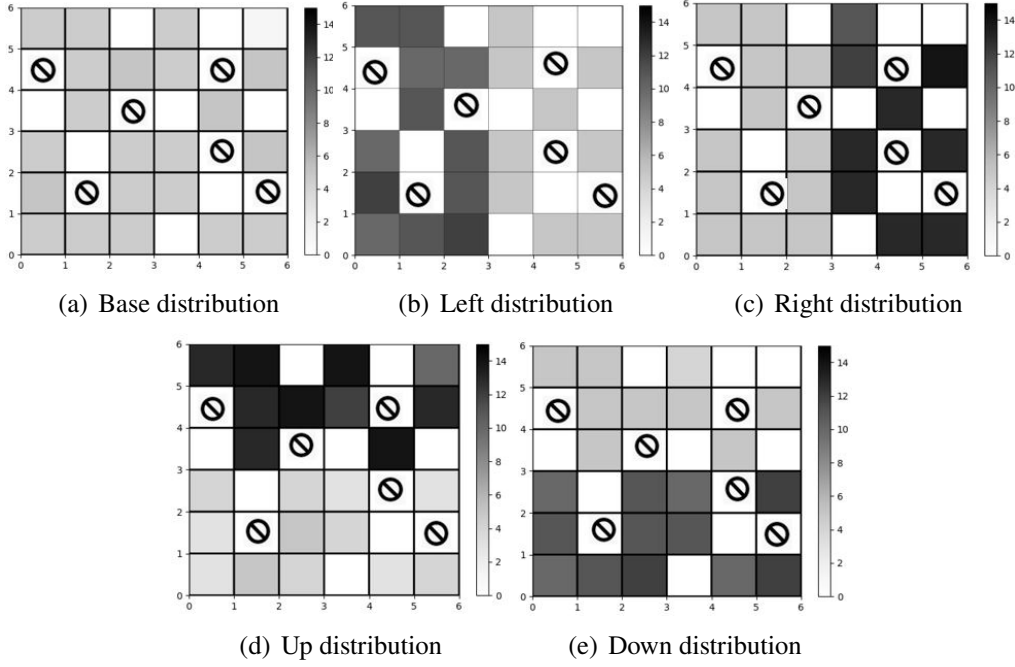


Figure 2.10

Illustration of different civilian distribution configurations

Lesson 3: *Cognitive delay can significantly extend the risk-exposure time for the civilians under an AS incident.*

The results in Fig. 2.11 support this observation. The graphs present the impact of V_E and V_{RISK} under different decision making capabilities of the civilians. We consider six different decision making capabilities of the civilians, namely, base, very slow, slow, average, quick, and very quick, and examine their impact under an AS incident. Note that the base case is constructed using the survey results as demonstrated in Table 2.1. Results clearly indicate that the performance metrics V_E and V_{RISK} are significantly impacted by the different decision making capabilities of the civilians. We summarize a few of our key observations below:

- It is observed that V_E remains 0% and 2.3%, respectively, after 75 seconds when assuming that all the civilians are **very slow** (>8 seconds) and **slow** (6-8 seconds) in responding to an AS situation. The performance improves significantly when the civilians can respond quickly in an AS situation. For instance, V_E reaches to 29.7% when the civilians can take an average time (e.g., 4-6 seconds) in responding to an AS incident. The best situation probably would be the case when the civilians could either take **quick** (2-4 seconds) or **very quick** (<2 seconds) decisions in responding to an AS situation. It is observed that under such cases, the V_E reaches to 59.4% and 60%, respectively. It is important to note that our base case results lie very close to the **quick** or **very quick** decisions results. This is primarily due to the fact that our case sample consists of university students; the majority of their age (98.9%) fall between 16 to 30.
- We observe a similar trend in V_{RISK} calculations as well, where a slow response may lead to a longer risk-exposure time for the civilians in the threat area. We observe that the life of nearly 100% of the civilians remain threatened in the shooting area if they are unable to execute quick decisions (e.g., **very slow** or **slow** responses). However, this number significantly drops down to approximately 34.9% and 34.3%, if the civilians are able to take **quick** or **very quick** decisions, respectively. This signifies the importance of developing a quality training program (e.g., interactive training as opposed to static training) for the civilians that not only introduces them to different possible realistic AS situations but also their possible actions under such a rare but dreadful event.

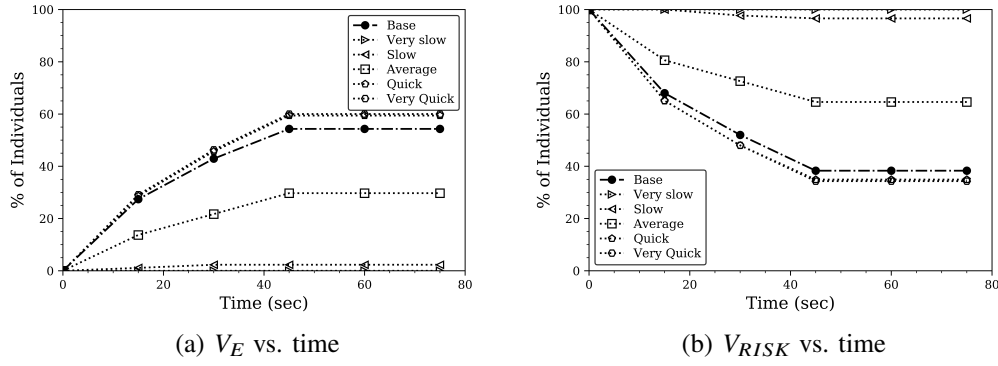


Figure 2.11

Impact of V_E and V_{RISK} under different decision making capabilities of the civilians

2.5 Conclusions and Future Research Directions

This study proposes an innovative mathematical model that accounts explicitly for individual choice behaviors, facility configurations (e.g., location and number of exits/entrances and hiding places), and other related factors (e.g., availability of choices, distribution of the population) to realistically analyze different AS incidents. To capture the time-space movement for both the civilians and the shooter(s), we propose a greedy heuristic that can solve our mathematical model under a rolling horizon framework. We surveyed 175 students (31.4% female) to understand their response behaviors under an AS incidents. The responses are appropriately incorporated into our proposed mathematical model using a choice model. To the end, we summarize the key lessons learned from this study by conducting a series of numerical experiments, such as changing the facility orientations (e.g., location and number of exits/entrances and hiding places), the initial distribution of the population, and cognitive delay of the civilians. We believe the results will cast valuable insights to enhance the reliability and resiliency of various threatening GF facilities (e.g., schools, hospitals, shopping malls).

This study can be extended in several research directions. In this study, we test our model under a uniform sample (i.e., students) in an academic environment. It would be interesting to examine how this model behaves under a large, heterogeneous sample in other environments (e.g., shopping mall, hospital). Next, the model only optimizes individual civilian response strategies and assumed that the shooter would follow a specific trajectory under a given realization. High fidelity models are needed to relax these modeling assumptions and develop a rigorous model and solution approaches (e.g., [87, 95, 94, 7, 4, 6]) for the case when both players (e.g., civilians and shooter) can intelligently optimize their own decisions. These issues will be addressed in future studies.

CHAPTER III

INVERSE REINFORCEMENT LEARNING TO ASSESS SAFETY OF A WORKPLACE UNDER AN ACTIVE SHOOTER INCIDENT

3.1 Introduction

3.1.1 Motivation

Active Shooter events are increasingly becoming more common in the United States. According to the Federal Bureau of Investigation (FBI), a total of 277 active shooter incidents occurred in the United States between 2000 and 2018 [26]. Such incidents resulted in a total of 884 deaths and 1,546 injuries, where 25% of the deaths and 47% of the injuries occurred in 2017 and 2018 alone. In 2019, a total of 417 mass shootings occurred in the United States (31 of those shootings were mass murders), which was the highest number of mass shootings ever recorded in the history of the United States [30]. Despite this increasing trend, another worrisome statistic is that 86% of the past active shooter incidents took place in various built environments (e.g., educational, commercial buildings) where the general public is forbidden to carry firearms [26]. All the statistics clearly indicate that the buildings require a proper methodological assessment to protect civilians against an active shooter incident.

3.1.2 Related Literature

Every active shooter incident is unique with respect to the physical restrictions (open space (e.g., The 2017 Las Vegas shooting) vs. confined space (e.g., The 2018 Stoneman Douglas

High School (Parkland) shooting)), the intent of the shooter (targeted shooting (e.g., The 2000 University of Arkansas shooting) vs. random shooting (e.g., The 2012 Sandy Hook Elementary School shooting)), number of shooters (single (e.g., The 2007 Virginia Tech shooting) vs. multiple (e.g., The 1999 Columbine High School massacre)), type of firearm used (manual (e.g., The 2012 Sandy Hook Elementary School shooting) vs. auto/semiautomatic pistol (e.g., The 2008 Northern Illinois University shooting) or rifle/shotgun), and many others. These incidents are characterized by highly unpredictable, evolve quickly, having (typically) no escape plan for the shooter(s), and with a major goal of mass murdering in a minimal timeframe. Further, unlike many traditional emergency evacuation problems (e.g., hurricane [117], fire [104], football stadium evacuation [42]), the origin of the threat (i.e., shooter(s)) may not be stationary. In fact, the threat actively chases to find the next target to maximize the number of casualties in a given active shooter incident. Finally, realistic active shooter incident data is typically unavailable for the general public and in few instances even a clear description of how the entire incident was conducted is unavailable.

All these unique aspects make much more difficult to fully understand or accurately model an active shooter incident. Even though a large number of reports have been published to date to describe the most recent active shooter incidents (primarily by the Department of Homeland Security (DHS), Texas State University, Purdue Homeland Security Institute and others), very few studies focus on characterizing and determining the optimal action plan for an individual civilian/law enforcement officer, in an attempt to maximize the overall system performance, under an active shooter exposed environment. With the help of an agent-based simulation model (developed in AnyLogic® computer simulation software), a few authors have attempted to cast valuable insights on a number of different possible active shooter situations, such as automatic door locking system

[47], no security/security guard/concealed carry gun scenarios at gun-free zones [40], civilian evacuation time and firearm discharge rate by the shooter and police [48], civilian's cognitive delay [91], the effectiveness of the RUN.HIDE.FIGHT.® (RHF) training program [46], and many others. Even though the existing simulation models provide numerous insights, capturing some vital factors such as individual choice behaviors, making use of learnings from the environment, and the modeling assumptions (e.g., setting one response strategy (move/do not move) for all civilians in a given simulation trial) are missing. We believe such drawbacks can be eliminated in future research by developing more sophisticated simulation models.

A complete understanding of human behavior under crisis conditions is critical for enhancing civilian safety. However, gaining such knowledge is extremely challenging due to the complex interactions with different correlated factors, including social attributes (e.g., herding, leader-following behavior) [55, 89], building attributes (e.g., location and visibility of signage, stairs, exits) [55], and emergency attributes (e.g., firearm, explosions, fires) [43]. Dating back to the early 1950s, numerous innovative theories and models were developed by the researchers in an attempt to better understand these complex interactions under different emergencies (e.g., fires, earthquakes, terrorist attacks). Fortunately, a recent review by [115] broadly categorizes these complex interactions into human-human interactions (i.e., interactions among people or groups of people and their influence on behavior during emergencies), human-building interactions (i.e., how buildings influence human behavior and how human behavior impacts the building performance during emergencies), human-emergency interactions (i.e., how emergency situations impact human behavior and people's coping strategies with emergencies), and the second-order interactions among humans, buildings, and emergencies. It is important to note that the necessity for research in these

areas really fueled after the 2001 World Trade Center (WTC) attack, letting the policy-makers rethink about the protection of civilians in buildings against terrorism-related risks.

Human-human interactions (e.g., herding, grouping, avoiding, leader-following, helping and competing, information sharing) are widely studied in the literature, given they are the crucial determinants of human behaviors during building emergencies [55, 89]. Understanding these complex interactions allow decision-makers to unfold the barriers and patterns that slow down the evacuation process (e.g., disabled occupants [13]). Given 86 % of the past AS incidents took place in various building environments where the general public is forbidden to carry firearms [26] (educational/commercial buildings), human-building interactions are extremely important to enhance human safety during emergencies. Past studies also attempted to understand the interactions between occupants and various building attributes, such as signage [103, 29], corridors [85, 22], exits [73, 15], stairs/elevators [74, 34], and alarms [76, 11], under different human-emergency situations (e.g., fire [20], earthquake [86, 56], and extreme violence (mass shootings, terrorist attacks) [58, 49]).

All the abovementioned interactions are pivotal in understanding the human behaviors mostly observed in different building environments, including pre-evacuation behavior (e.g., pre-event and information-seeking behavior) [57, 39], wayfinding behavior [24, 102], interaction behavior with others (e.g., grouping, competing, helping, queuing, waiting) [17, 90], and interaction behavior with the environment (e.g., risk-taking, property-protecting, and hazard-fighting behavior) [34, 56]. Probably due to ease in modeling or experimenting with an agent to move towards finding a safer destination, wayfinding behavior is widely studied in the literature. Specifically, the researchers aim to study the impact of various factors, such as building attributes (e.g., location and visibility

of signage, stairs, exits [55, 64, 5, 63], personal factors [112, 19], and social factors (e.g., herding, leader-following behavior) [55, 89] that could impact the wayfinding behavior during emergencies. Rather than restricting on observing the aforementioned behaviors, researchers further attempted to develop different social, psychological, and behavioral theories that could explain human behavior in building emergencies, such as panic theory [79, 98], heightened emotional theory [35], social attachment/affiliative theory [65], self-categorized/social identity theory [93], role rule theory [18], organizational breakdown theory [36], social proof theory [23], and the most-recently developed social influence theory [71]. A comprehensive review of these theories can be found in [55]. Apart from the aforementioned studies, researchers recently started to use virtual reality framework to assess the interactions between humans and buildings under an active shooter incident [115, 114]. The aim is to create a safe, non-evasive environment where the impact of safety during active shooter incidents and the corresponding human-building interactions that influence the response performance is studied. Though not directly related to the active shooter incidents, another stream of research attempted to locate detectors to minimize casualties under an intentional attack [62, 105, 70]. These approaches paid attention to quick detection of weapons (e.g., guns, bombs) to reduce casualties in a given threat area. Finally, rather than adopting a methodological framework, a few studies qualitatively discusses human behavior and possible mitigation strategies following an active shooter incident [37, 83].

In most of the real-life problems, researchers are interested in coming up with a policy using which they can efficiently optimize the decision-making process of the agents in interacting with an environment. Hence, discovering the fact of how expert people make sequential decisions and extracting the process and functions that result in these decisions is of high importance. By doing

so, we can retrieve the expert's preference in dealing with an environment, although we do not fully understand what is important and guides his or her actions. A more closely related example of this would be the situation as the trapped civilians experience under an active shooter incident. To tackle this challenge, researchers have been utilizing different topics in machine learning to create a system that can mimic human decisions and behaviors, and based on real-world data, accomplish tasks as efficiently as possible. For example, in some studies [3, 2], it can be observed that scientists are trying to create a complex set of activities that are consisted of simpler and smaller actions taken sequentially. Thus, the question is whether we can explain the decision-making process based on the available data gathered from expert behaviors? The application of extracting knowledge from available behavior data can be found in some studies [50, 100]. These studies try to characterize urban passengers or taxi drivers based on their mobility patterns. Also, they explore the way these agents weigh factors such as travel time, travel cost, or travel time variance. Discovering a reward function or cost function associated with human behaviors plays a crucial role in understanding what we observe and how to mimic this observation.

One of the techniques that have widely been used among researchers to explore human behaviors and its motivational factors is the *inverse reinforcement learning* (IRL) [82]. The IRL problem, also known as an *inverse planning problem*, can be considered as a problem within the *reinforcement learning* framework based on the Markov decision processes (MDPs). In an IRL problem, the goal is to identify an MDP that is consistent with the observed behavior of the rational agent. In other words, all the mentioned factors for an MDP are assumed to be known except the reward function, and the solution of this problem is a reward function that can describe an observed trajectory. Until now, a number of approaches have been proposed such as linear optimal reward [69], maximum

reward margins [3, 81], and maximum reward likelihood [80, 118] to address wide varieties of application areas, including autonomous helicopter control [1], airplane pilot objective inference [110], measuring cultural preferences in negotiation [72], and predicting human behavior [106, 59].

3.1.3 Summary of Major Contributions

This study extends the existing literature by proposing a learning technique that can be used to model the behavior of the shooter and the trapped civilians under an active shooter situation. Our developed decision tool, for the first time in the literature, will provide a methodological basis to enhance our understanding of the complicated interactions that exist between civilians and the shooters, shooter-specific characteristics (e.g., prior shooting experiences, type of firearm carried, the timing of the incident), and building configurations (e.g., number/location of exits, hiding places) with the expected number of casualties in an active shooter incident. Knowledge gained from creating such experiments will allow decision-makers to assess the ongoing safety measures of a workplace (e.g., school, commercial buildings) against an active shooter incident. To summarize, the major contributions of this study to the existing literature are as follows: (i) capturing the dynamic nature of the active shooter incidence by introducing a new framework; (ii) inferring dynamic emergency action plans based upon the observed behavior of expert agents; and (iii) evaluating the performance of the proposed framework in reassessing the safety of a workplace under an active shooter incident by a simplistic and hypothetical environment.

3.2 Problem Formulation

The problem of modeling an active shooter situation can be defined as a traumatized situation with unpredicted movements of the active shooter and ambiguity in the real-time path selection

policies, which leads to a higher rate of fatality and serious injury. To resolve this ambiguity, this study first proposes a Markov Decision Process (MDP) to model the behavior of the attacker and the trapped civilians under an active shooter incident. Then, adapted from [118], we propose a Dynamic Maximum Entropy Inverse Reinforcement Learning (IRL) to achieve the desired behavior escaping behavior.

3.2.1 Markov Decision Process

From robotics to economics and healthcare, MDP is widely used in a variety of applications, particularly when uncertainty is interwoven with system performance procedures. An MDP process is a probabilistic framework that models the interaction of each agent with the environment [92]. Through the interaction procedure, the agent takes action in each time step and transitions from the current state to another state. Moving from one state to another in each time step, the agent receives *(i)* a representation of the environment in the new state, *(ii)* a reward that could be positive, negative, or zero, and *(iii)* the feasible set of actions the agent can take in the new state. Throughout time, the agent learns to enhance its performance simply by taking the actions that result not only in higher rewards, but they also guarantee higher accumulated reward at the end of the time horizon. The typical agent-environment interaction is shown in Figure 3.1.

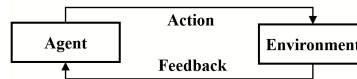


Figure 3.1

Agent-environment interaction

An MDP consists of six tuples (S, A, T, γ, D, R) , where S is the set of feasible states in the environment, A is the set of possible actions that can be taken in each state, T is the transition matrix that provides the probability of an agent ending up in a particular state knowing its current state and the action it would take, $0 < \gamma \leq 1$ is a parameter, referred to as *discount rate*, which guarantees the convergence of the accumulated rewards, D is the initial state distribution, and R is a reward function that specifies the reward an agent receives knowing its current state, and the possible action it takes. The goal of an MDP problem is to find a policy function, π , that maps a series of actions from the state space, $S \rightarrow A$, that results in maximum accumulated rewards as shown in equation (3.1) below.

$$\pi^* = \operatorname{argmax}_{\pi} (\mathbf{E} [\sum_{t \in T} \gamma^t R(s_t, \pi(s_t))]) \quad (3.1)$$

Here, $R(s_t, \pi(s_t))$ is the reward the agent receives if it is in the state s_t , and take action aligned with policy π . Having a set of feasible policy functions, the space of MDP is reduced to a procedure with transition matrices T^π where,

$$T^\pi(s_t, a_t, s_{t+1}) = T^\pi(s_t, \pi(s_t)) \quad (3.2)$$

3.2.2 Incident Modeling

The active shooter incident can be modeled under a MDP framework with a dynamic and moving object environment. We assume that the action of the shooter will be unpredictable within the environment, i.e., the shooter might choose an action from the action set {shoot,

move-towards, move-away, move-left, move-right}, randomly. The agent (civilian) has no control over the behavior of the shooter. Therefore, it accepts the behavior as a part of the dynamics of the environment. Trapped in the environment, each civilian represents an agent who takes a sequence of actions against the shooter to obtain the maximum reward (i.e., to survive or stop the shooter). The feasible set of actions for each agent is given by $A = \{\text{move-left, move-right, move-up, move-down}\}$. We assume that each agent does not interact with others, and in each time step, chooses a move that shortens their distance from the nearest exit door or hiding place, i.e., picking the shortest paths. The choice of paths might change depending on the location of the shooter. What an agent knows is: (i) reaching to exit doors and hiding places has the highest reward among all possible states and (ii) the nearer the agent is to the active shooter, the lower the reward accumulates by the agent. As for the active shooter, we model her/his movement behavior by assigning higher probabilities to the choices of directions towards more populated spots.

3.2.2.1 State definition

The target indoor environment represents a rectangular $n \times n$ grid world, where a subset of the grids to represent entrance/exit doors, blocks, and hiding places, respectively. We assume an active shooter to enter the environment from one of the entrances, carrying a gun with specific point-blank range, r_g , and level of accuracy, l_g . The active shooter's location, and consequently the point-blank range's diameter, change dynamically as the person moves across the environment. The total number of states for each agent is $n \times n$, as each agent can end up in each block of the environment. Considering the initial state, D , civilians are distributed randomly throughout the entire environment.

3.2.2.2 State transitions

To model the state transition process for each agent, we first make the following assumptions: (i) the preference of each agent is to approach hiding and exit blocks in a minimum number of time steps, (ii) the capacity of exit blocks are infinity, (iii) the actions an agent takes do not affect the set of feasible actions for others, (iv) only one movement is allowed per time step, (v) affected by choice distribution and obstacle location, each agent might choose a different path to reach to a hiding or exit block, (vi) each agent has an estimation of the shooting point-blank range. During the state transition process, $s_t \rightarrow s_{(t+1)}$, each agent observes its current state, s_t , and its distance from the location of the obstacle and selects action $\pi(s_t)$ aligned with its current policy. The obstacle responds to the action of the agent(s) and the new positions of obstacle and agent(s) form the new state $s_{(t+1)}$. In each time steps, a subset of blocks, A'_t , (i.e., the location of the obstacle, and the area inside the shooting-blank range), are infeasible for the transition. However, not knowing the response of the obstacle, the agent might take an action which ends up in a new state, $s_{(t+1)}$, which is not in the shooting range at time t and becomes infeasible to move towards in time $t + 1$.

3.2.2.3 Value function

To evaluate the performance of a policy function, the agent needs to define performance metrics (i.e., $S \times A \rightarrow R$). This function stands for the immediate reward received after taking action, $a_t \in A$, in state, $s_t \in S$, and is one of the key elements in identifying the desirability of a chain of events during the learning process, $R_t(s_t, a_t)$. However, to obtain the maximum cumulative reward, the agent must consider the possible rewards in future time step (i.e., $\sum_{k=0}^N R_{(t+k)}$), as a

consequence of taking an action in the present state. To do so, the learner uses the *value function* to estimate the consequent future reward.

$$V^\pi(s) = \mathbf{E}_\pi \left[\sum_{k=0}^{\infty} \gamma^k R_{t+s} | (s_t, a_t) \right] \quad (3.3)$$

which can be shown in the following recursive format:

$$\mathbf{E}_\pi [R_t + \gamma V(s_{t+1}) | (s_t, a_t)] = \sum_{a_t \in A} \pi(s_t, a_t) \sum_{s_{t+1} \in S} P(s_{t+1} | (s_t, a_t)) \left(R_{s_{t+1}, s_t, a_t} + \gamma V^\pi(s_{t+1}) \right) \quad (3.4)$$

Here, $\pi(s_t, a_t) : S \rightarrow A$ is the probability of taking an action, a_t , in the state, s_t . $R_{s_{t+1}, s_t, \pi(s_t)}$ is the reward of taking the action, a_t , in the state, s_t , with probability $\pi(s_t)$ and ending up in the new state $s_{(t+1)}$, $P(s_{t+1} | (s_t, a_t))$ as the probability of ending up in the new state $s_{(t+1)}$, knowing that the agent is in the state, s_t , and would take action, a_t [113]. From the Bellman equation, (3.3), we desire to derive the optimal policy that maximized the cumulative reward in each time step as follows:

$$V^*(s_t) = \max_a \sum_{s_{t+1} \in S} P(s_{t+1} | (s_t, a_t)) \left(R_{s_{t+1}, s_t, a_t} + \gamma V^\pi(s_{t+1}) \right) \quad (3.5)$$

Compared to V^π , there is another value function, $Q^\pi(s_t, a_t)$, which focuses on maximizing the cumulative rewards by considering the choice of action in the present state, s_t :

$$\sum_{s_{t+1} \in S} P(s_{t+1} | (s_t, a_t)) \left(R_{s_{t+1}, s_t, a_t} + \gamma \sum_{a_{t+1} \in A} \pi(s_{t+1}, a_{t+1}) Q^\pi(s_{t+1}, a_{t+1}) \right)$$

Again, the optimal policy is the one that maximizes the value function as follow:

$$Q^*(s_t, a_t) = \sum_{s_{t+1} \in S} P(s_{t+1} | (s_t, a_t)) \left(R_{s_{t+1}, s_t, a_t} + \gamma \max_{a_{t+1} \in A} Q^\pi(s_{t+1}, a_{t+1}) \right) \quad (3.6)$$

We summarize the value function iteration, Q -learning iteration, in **Algorithm 1**. This algorithm will be used in Sections 3.2.2.1 and 3.2.2.2 to obtain the agent's choices of actions and states, by (i) finding the maximum value function in each trajectory of choices and (ii) the optimal choice policy that illustrates the agent's behavior.

3.2.3 Maximum Entropy Inverse Reinforcement Learning (IRL)

During the learning process, what complicates the active shooter problem is the ambiguities in determining the reward function. In other words, the uncertainties in the movement of obstacle and the point-blank range form a dynamically changing environment with stochastic reward function distribution. Despite uncertainties about the reward function, R^* , what is certain is the optimal policy, π^* , which is reaching to survival states in the minimum number of time steps. Therefore, by reversing the process of reinforcement learning, we can form a new learning process that learns the unknown reward using the optimal policy π^* . Several studies propose reversing methodologies to derive the optimal reward function [69], [3], [81]. However, it was not until Zeibart et al. [118] that a solid approach was proposed, referred to as Maximum Entropy (IRL), to match the observed policy and the agent's behavior. In this paper, we use a tailored Maximum Entropy technique to model the distribution of the behavior of civilians in the active shooter problem and match them with the optimal survival policy.

Algorithm 1: Value Function Iteration

Input: $\pi(s, a)$, $|S|$, $P(s_{t+1}|(s_t, a_t))$, R , γ
Function Optimal Value Deterministic
 $V \leftarrow 0$
 $Threshold \leftarrow \epsilon$
 $diff \leftarrow \infty$
while $diff > Threshold$ **do**
 for $s = 1, \dots, |S|$ **do**
 $V^* \leftarrow -\infty$
 for $a = 1, \dots, |A|$ **do**
 $V^* \leftarrow \max \left(V^*, \sum_{s' \in S} P(s'|s, a) (R_{s,a,s'} + \gamma V(s')) \right)$
 $diff^* \leftarrow \max \left(diff, |V(s) - V^*| \right)$
 end
 if $(diff^* > diff)$ **then**
 $diff^* \leftarrow diff$
 end
 $V(s) \leftarrow V^*$
 end
end
for $s = 1, \dots, |S|$ **do**
 $\pi^* \leftarrow \underset{\pi}{\operatorname{argmax}} \left(\sum_{s' \in S} P(s'|s, a) (R_{s,a,s'} + \gamma V(s')) \right)$
end

Function Find Policy
 $V^* \leftarrow$ Function Optimal Value
if *non-deterministic* **then**
 for $s = 1, \dots, |S|$ & $a = 1, \dots, |A|$ **do**
 $Q(a, s) \leftarrow \sum_{s' \in S} P(s'|s, a) (R_{s,a,s'} + \gamma Q(a', s'))$
 end
 $Q^*(a, s) \leftarrow \frac{Q(a, s)}{\sum_{s \in S} Q(a, s)}$
 for $s = 1, \dots, |S|$ **do**
 $\pi^* \leftarrow \underset{a}{\operatorname{argmax}} (Q(a, s))$
 end
end
Output:
 $\pi^*, V^*(s)$
 $\pi^*, Q^*(a, s)$

3.2.3.1 Maximum Entropy

The *Maximum Entropy* approach includes an agent who interacts with the environment and gets feedback in the form of rewards and a learner who tries to model and imitate the behavior of the

agent. From learner's perspective, each agent's behavior is modeled as a set of states and actions $\zeta = \{(s, a)\}$. By entering each state, s_j , the agent is assumed to activate a feature function, f_s , and maps the vector of features of that state into the reward value, $\theta^T f_s$, where θ is the reward weight vector. The reward value of a trajectory ζ is simply the summation of the reward value vectors of each state in the trajectory, and the probability of a trajectory chosen by the agent is:

$$\mathbf{R}(f_\zeta) = \sum_{s \in \zeta} \theta^T f_s \rightarrow \mathbf{P}(\zeta) = e^{\mathbf{R}(f_\zeta)} \quad (3.7)$$

To implement the maximum entropy technique, we need to have an estimation of the agent's behavior and how it chooses the next steps starting from different positions in the grid environment. To do so, adapted from [111], we propose a Generate Demonstration algorithm (**Algorithm 2**) to produce a set of movement trajectories that start from a variety of positions and assimilates agent's choice distribution. In **Algorithm 2**, $St_{x,y}$, and $\bar{S}t_{x,y}$ are the position of trapped agents and the position of the active shooter, respectively. At the beginning of the algorithm, these positions are assigned randomly ($Rand_{St}$). Later, it updates the next positions at the end of each iteration as a result of the movement policy they choose. During the state transition process, $s_t \rightarrow s_{(t+1)}$, each agent observes its current state, s_t , and its distance from the location of the obstacle \bar{s}_t and selects action $\pi(s_t)$ aligned with its current policy.

Algorithm 2: Generate Demonstration

Input: $\pi, |\zeta|, St_{x,y}, \bar{St}_{x,y}, Rand_{St}$ (Random start or not), p_d (probability of deviating optimal policy)
 $\zeta \leftarrow 0$
 $\xi \leftarrow [0]$
for $i = 1, \dots, |\zeta|$ **do**
 if $Rand_{St}$ **then**
 $St_{x,y} \leftarrow random([0, 0], [N, N])$
 end
 $S_{i,1}, S_{i,0}, a_{i,0}, r_{i,0} = \underset{s' \in S}{\operatorname{argmax}} \pi(St_{x,y}, a), St_{x,y}, \underset{a \in A}{\operatorname{argmax}} \pi(St_{x,y}), \mathbf{R}(St_{x,y}, \pi(St_{x,y}))$
 for $j = 1, \dots, |\zeta|$ **do**
 $S_{i,j+1}, S_{i,j}, a_{i,j}, r_{i,j} = \underset{s' \in S}{\operatorname{argmax}} \pi(S_{i,j}, a), S_{i,j}, \underset{a \in A}{\operatorname{argmax}} \pi(S_{i,j}), \mathbf{R}(S_{i,j}, \pi(S_{i,j}))$
 $\xi_{i,j} \leftarrow (S_{i,j+1}, S_{i,j}, a_{i,j}, r_{i,j})$
 end
 $\zeta_i \leftarrow \xi_i$
end
Output: ζ

As an input for Maximum Entropy Imitation algorithm, we need to know about the *State Visitation Frequency* (SVF). Therefore, the learner computes the SVF vector using equation (3.8),

$$\mathbf{P}(s) = \sum_t \mu_t(s) \quad (3.8)$$

where $\mu_t(s)$ is the probability of visiting state s at time t , and $\mathbf{P}(s)$ is the visitation frequency of state s . In each time step, the learner calculates $\mu_t(s)$ by solving the value iteration problem under the non-deterministic space.

$$\mu_{t+1}(s) = \sum_{s_{t+1} \in S} \sum_{a_t \in A} \mu_t(s) \pi(s, a) \mathbf{P}(s_{t+1} | (s_t, a_t)) \quad (3.9)$$

where the learner calculates the optimal policy, $\pi(s, a)$, and transition probability $\mathbf{P}(s_{t+1} | (s_t, a_t))$ by solving MDP and DP. In **Algorithm 3**, we illustrate the SVF computation procedure using MDP.

The output of this algorithm is a vector, $\mathbf{P}_{(|S| \times 1)}$, with the elements showing the expected frequency of visiting each state, $s \in S$.

Algorithm 3: State Visitation Frequency

Input: $\zeta \leftarrow \text{Algorithm 2}$, $|S|$, $|A|$, $\mathbf{P}(s_{t+1}|(s_t, a_t))$, γ
 $\mu \leftarrow 0$
for ξ *in* ζ **do**
 $\zeta_{\xi 0,0} \leftarrow \zeta_{\xi 0,0} + 1$
end
 $\zeta_{\xi 0,0} = \frac{\zeta_{\xi 0,0}}{\zeta}$
for $s = 1, \dots, |S|$ **do**
 for $\xi = 1, \dots, (\zeta - 1)$ **do**
 if *deterministic* **then**
 $\mu_{\zeta_{s'}, [\xi+1]} = \sum_{s \in S} \mu_{\zeta_{s'}, [\xi]} \mathbf{P}(s|(s, \pi(s)))$
 end
 else
 $\mu_{\zeta_{s'}, [\xi+1]} = \sum_{a \in A} \sum_{s \in S} \mu_{\zeta_{s'}, [\xi]} \mathbf{P}(s|(s, a)) \pi(a, s)$
 end
 end
end
 $p = \sum_{s \in S} \mu_{\zeta_s}$
Output: P

To imitate the agent's behavior, the learner uses an estimation of reward weight, which maximizes the likelihood of its behavior to the agent's state-action trajectory. That is:

$$\theta^* = \underset{\theta}{\operatorname{argmax}} \mathbf{L}(\theta) = \underset{\theta}{\operatorname{argmax}} \frac{1}{|\zeta|} \mathbf{P}(\zeta|\theta) = \underset{\theta}{\operatorname{argmax}} \frac{1}{|\zeta|} \sum_{\zeta} \mathbf{R}(\zeta) - \log \sum_{\zeta} e^{\mathbf{R}(\zeta)} \quad (3.10)$$

Finally, finding the gradients, the learner assimilates its behavior to the agent's by differentiating equation (3.10) on $\mathbf{R}(\zeta)$:

$$\nabla_{\theta} L = \frac{1}{|\zeta|} \sum_{s \in \zeta} f_s - \sum_{s \in \zeta} \mathbf{P}(s|\theta) f_s \quad (3.11)$$

where $\mathbf{P}(s|\theta)$ is the frequency of visiting state, s . **Algorithm 4** represents the application of the maximum entropy technique in the agent's behavior imitation. The output of the algorithm is a reward weights matrix most similar to the one aligned with the performance of the agent.

Algorithm 4: Maximum Entropy Imitation

Input: $\zeta \leftarrow \text{Algorithm 2}$, f_ζ , $|S|$, $|A|$, $\mathbf{P}(s_{t+1}|(s_t, a_t))$, γ , α

$N = |H| \times |W|$

$$f_{n,n} = \begin{pmatrix} 0 & \cdots & 0 \\ \vdots & \ddots & \vdots \\ 0 & \cdots & 0 \end{pmatrix}$$

for $k = 1, \dots, N$ **do**

for $i = 1, \dots, |H|$ **do**

for $j = 1, \dots, |W|$ **do**

$kx, ky \leftarrow \text{position}(k)$

$f_{k, \text{position}[i,j]} = |ky - j| + |kx - i|$

end

end

end

$\theta \leftarrow \text{randomUniform}(|f_\zeta|)$

$\text{iteration} \leftarrow 0$

$f_{exp} \leftarrow 0$

for ξ in ζ **do**

for i in ξ **do**

$f_{exp} = f_{exp} + f_{\xi,i}$

end

end

$f_{exp} \leftarrow \frac{f_{exp}}{|\zeta|}$

for t in iteration **do**

$R \leftarrow \sum_{s \in \zeta} \theta^T f_s$

$\pi \leftarrow \text{Algorithm 1}$

$SVF \leftarrow \text{Algorithm 3}$

$\nabla \leftarrow f_{exp} - f \times SVF$

$\theta \leftarrow \theta + \alpha \nabla$

$R \leftarrow \theta^T f$

end

Output: $\theta^T f$

3.2.3.2 Inverse Reinforcement Learning (IRL): A Case in Active Shooting Incidents

Building upon **Algorithms 1-4**, we propose a tailored *maximum entropy inverse reinforcement learning* (IRL) algorithm (shown in **Algorithm 5**) to identify the optimal reward weight for each block in the grid world environment considering the uncertainties in the moves of the obstacle, the point-blank range, and each agent's choice distribution. We assume that each person will pick the shortest path from her current position to the nearest exit/hiding place, if not interfered with by the active shooter. In each time-step, we convert the two-dimension position of each individual to an equivalent integer number, which represents their current states, and we accumulate them to track the length of their escape paths. Further, the algorithm converts the coordinates of the hiding places and entrances/exits into equivalent integers to track the number of civilians currently locating to that cell. The model assumes that at most one block movement is possible in each time step, and each individual has notions of the position of the shooter, the estimation of point-blank range, and the like. Note that we define a set of *danger* states, in size to the point-blank range, in which an agent might shot with a high probability.

The Algorithm starts with forming a grid environment and distributing the agents and obstacles randomly. The initial reward weight matrix, θ , will be chosen randomly. For each agent and active shooter, a set of neighboring locations, on the left, right, bottom, and top of the present location is defined. Let us now define a set of parameters to assess the model performance:

- V_H : to denote the percentage of civilians who are able to reach into the hiding cells, i.e.,

$$V_H = \frac{\sum_{i=1}^{MaxTrial} V_H^i}{MaxTrial}$$

- V_E : to denote the percentage of civilians who are able to exit the threat area via the exit cells,

$$\text{i.e., } V_E = \frac{\sum_{i=1}^{MaxTrial} V_E^i}{MaxTrial}$$

Algorithm 5: Maximum Entropy Inverse Reinforcement Learning

Input: grid environment, $\mathbf{P}(s_{t+1}|(s_t, a_t))$
 $St_{x,y}(\forall Agents), \bar{St}_{x,y}(obstacle)$
 $N_{x,y} \leftarrow$ array 1×4 four blocks neighboring the block with the coordinate $(x, y)(\forall agents)$
 $N_{\bar{x},\bar{y}} \leftarrow$ array 1×4 four blocks neighboring the block with the coordinate $(x, y)(obstacle)$
 $\theta^0 \leftarrow Random(\theta)$
 $\theta^* \leftarrow \theta^0$
 $V^0, \pi^0 \leftarrow \text{Algorithm 1}, \theta^*$
 $\mathbf{V}^*, \pi^* \leftarrow V^0, \pi^0$
 $V_H, V_E, V_{RISK} \leftarrow 0, 0, 0$
 $t \leftarrow 0$
for $i = 1, \dots, MaxTrial$ **do**
 while $t < maxTime$ **do**
 for $k = 1, \dots, |neighboring|$ **do**
 $location_{agent}[1, k] =$ neighboring location in the i th side of $St_{x,y}$
 $location_{obstacle}[1, k] =$ neighboring location in the i th side of $\bar{St}_{x,y}$
 end
 $\zeta_{obstacle} \leftarrow$ Random with more weight toward more occupied blocks
 $\zeta_{Agent} \leftarrow$ Shortest path to hiding places and exit blocks, while keeping distance from obstacle ($\forall agents$)
 Algorithm 3 \leftarrow **Algorithm 4**, ζ
 $\theta^* \leftarrow$ **Algorithm 3**
 $\mathbf{V}^*, \pi^* \leftarrow$ **Algorithm 1**, θ^*
 $St_{x,y}, \bar{St}_{x,y} \leftarrow$ **Algorithm 2**, \mathbf{V}^*, π^*
 for $k = 1, \dots, |neighboring|$ **do**
 if $location_{\forall Agent}[1, k] = St_{x,y}$ **then**
 $N_{x,y}[1, k] \leftarrow St_{x,y}$
 end
 if $location_{obstacle}[1, k] = \bar{St}_{x,y}$ **then**
 $N_{\bar{x},\bar{y}}[1, k] \leftarrow \bar{St}_{x,y}$
 end
 end
 $t \leftarrow t + 1$
 end
 $St_{x,y} \leftarrow argmax_{x,y}(N_{x,y})$
 $\bar{St}_{x,y} \leftarrow argmax_{\bar{x},\bar{y}}(N_{\bar{x},\bar{y}})$
 $V_H^i, V_E^i, V_{RISK}^i \leftarrow St_{x,y}(\forall agent)$
end
Output: $V_H = \frac{\sum_{i=1}^{MaxTrial} V_H^i}{MaxTrial}$, $V_E = \frac{\sum_{i=1}^{MaxTrial} V_E^i}{MaxTrial}$, $V_{RISK} = \frac{\sum_{i=1}^{MaxTrial} V_{RISK}^i}{MaxTrial}$

- V_{RISK} : to denote the percentage of civilians who are still freely floating within the threat area (i.e., the ones who are unable to reach the hiding/exit cells), i.e., $V_{RISK} = \frac{\sum_{i=1}^{MaxTrial} V_{RISK}^i}{MaxTrial}$

where, i and `MaxTrial` stand for individual trial and maximum number of the trials used in our experiments, respectively. To be specific, the **Algorithm 5** generates a number of trials, `MaxTrial`, in which the active shooter chooses a random trajectory across the environment. In each trial, the algorithm (i) builds a set of movement trajectories, ζ , aligned with the shortest paths to hiding and exit blocks and considering the longest possible distance from the active shooter, (ii) calculates the state visitation frequency aligned with the optimal policy π^* , (iii) obtain the gradient $\nabla_{\theta} L$ and update the reward weight matrix of θ for the next time step, (iv) finds the optimal value function, V^* , and policy, π^* , for the corresponding reward, θ , obtained from step (ii), (v) aligned with the given policy, π^* and updated the position of civilians and shooter(s), and consequently, the number of civilians who are endangered, have exited, hidden, and are still inside the threat area. After experiencing all the number of trials, the model calculates the overall performance metrics given the ones computed for the individual trials. The output of **Algorithm 5** is the overall safety metrics for the threat area.

3.3 Experimental Results

This section first presents a test grid to visualize and validate the experimental results. We then summarize the key lessons learned from running the experiments under different simulated active shooter situations. All the solution algorithms are coded in Python 3.7.6 on a desktop computer with Intel Core i7 3.6 GHz processor and 32.0 GB RAM.

3.3.1 Input Parameters

Figure 3.2 shows a 10×10 test grid facility that we have considered as a test-bed to visualize and validate our modeling results. The facility has three *entrances/exits* (grid 6, 51, and 96), four

blocked grids (grid 23, 28, 73 and 77), and a *hiding* grid (grid 47). Later, we test this base facility with varying entrance/exit and hidden grid configurations. We assume that the shooter will enter the facility from one of the entrances and reach to her/his destination by visiting different grids during this active shooting period. Note that approximately 70 % of the past active shooter incidents ended in less than 5 minutes (11 % among them ended in less than 2 minutes [84]). As such, we designed our experiments such that they could include even extreme cases of active shooter incidents. Fixing the duration of the experiments to T seconds, we assumed that the attacker would have at least T seconds to move across the environment before law enforcement intervenes in his or her action. The agents will have 15 seconds in each time period to follow their assigned policy. In our experiments, the base configuration and input parameters are evaluated under four different simulation scenarios, i.e., $T = \{75, 90, 105, 120\}$ seconds.

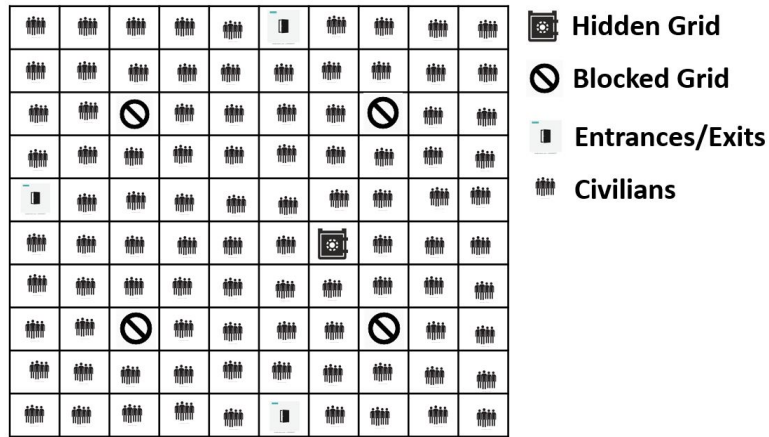


Figure 3.2

10×10 test grid facility

3.3.2 Lessons Learned

In this section, first, we evaluate the performance of the proposed approach using the base case. Afterward, we will vary some of the key input parameters, such as the number of hidden grids $|G_h|$, entrances/exits $|G_e|$, shooting range of the attacker, and the initial distribution of civilians in our 10×10 test grid facility (shown in Figure 3.2), to derive important lessons for the decision-makers. We believe that the metrics developed in this study provides a customized tool for decision-makers to design a safe and reliable facility and assess the safety of the existing facility. Since our experiments are subject to stochasticity, 50 trials are conducted to validate and denote the safety metrics' value throughout the experiments. Moreover, for base input parameters as discussed in Section 3.3.1, to represent the impact of simulation time on the safety metrics, four different simulation times, i.e., 75, 90, 105, 120 seconds, are evaluated (See Table 3.1). Table 3.1 represents the average, standard deviation, maximum, and minimum value of the metrics over 50 trial in each simulation time scenario (The detailed information of trial-specific metrics are presented in Appendix A5). It can be observed that when the simulation time increases from 75 seconds to 120 seconds, percentage of individuals (175 in our experiments) who could exit the threat area increases from 52.89 % to 67.03 %. To further visualize the individuals' overall behavior over time, we use the information related to the first trial and simulation time equal to 75 seconds. Figure 3.3 represents the values of performance metrics, V_E^1 , V_H^1 , and V_{RISK}^1 , over five consecutive time periods $t = \{0, 15, 30, 45, 60, 75\}$. The results corresponding to the first trial indicates that the curve V_H^1 stabilizes after 45 seconds. On the other hand, we notice that the values or performance measures V_E^1 and V_{RISK}^1 increase and decrease till the end of simulation time (45 seconds), respectively. This might be due to the availability of the current entrance/exit

configurations ($|Ge| = 3$), the initial and updated positions of the civilians and shooter, and the attacker's shooting range or a combination thereof. Moreover, using Maximum Entropy IRL, we derive the corresponding reward values for all unblocked grids, $R(s)$, in different time periods, which describe the best optimal policy that could be undertaken dynamically in different grids in our test facility under an active shooting situation. Figure 3.4 demonstrates how the reward, $R(s)$, from the majority of the individuals are changing in different grids concerning the shooter's position on different time periods (when the simulation time is fixed to $t = 75$ seconds under the first trial).

Table 3.1

The summary of performance metrics over 50 trials (in %)

statistics	T=75			T=90			T=105			T=120		
	V_H	V_E	V_{RISK}	V_H	V_E	V_{RISK}	V_H	V_E	V_{RISK}	V_H	V_E	V_{RISK}
Average	8.48	52.89	38.54	8.5	59.76	31.69	8.54	64.43	27.02	8.58	67.03	24.42
Standard Deviation	0.24	3.71	3.74	0.22	3.69	3.71	0.18	3.78	3.79	0.12	3.71	3.71
Max	8.6	58.3	43.4	8.6	65.1	37.1	8.6	70.3	32.6	8.6	73.1	30.3
Min	8	48	33.1	8	54.3	26.3	8	58.9	21.1	8	61.1	18.3

The base case experimental results indicate that the system performance may be susceptible to the input parameters. Note that the explored environment in this study is hypothetical and all the calculated results are based on limited numerical simulations. Nevertheless, running several experiments and doing sensitivity analysis, we are to evaluate the fact that if the proposed framework can successfully function following the embedded environmental characteristics. The following

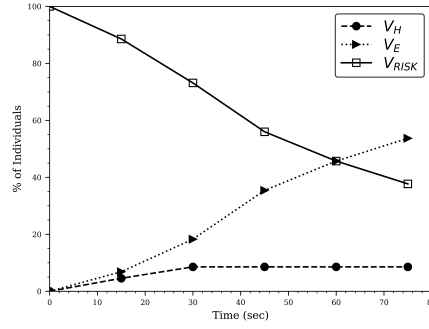


Figure 3.3

Impact of V_H^1 , V_E^1 , and V_{RISK}^1 under base input parameters when simulation time is 75 seconds.

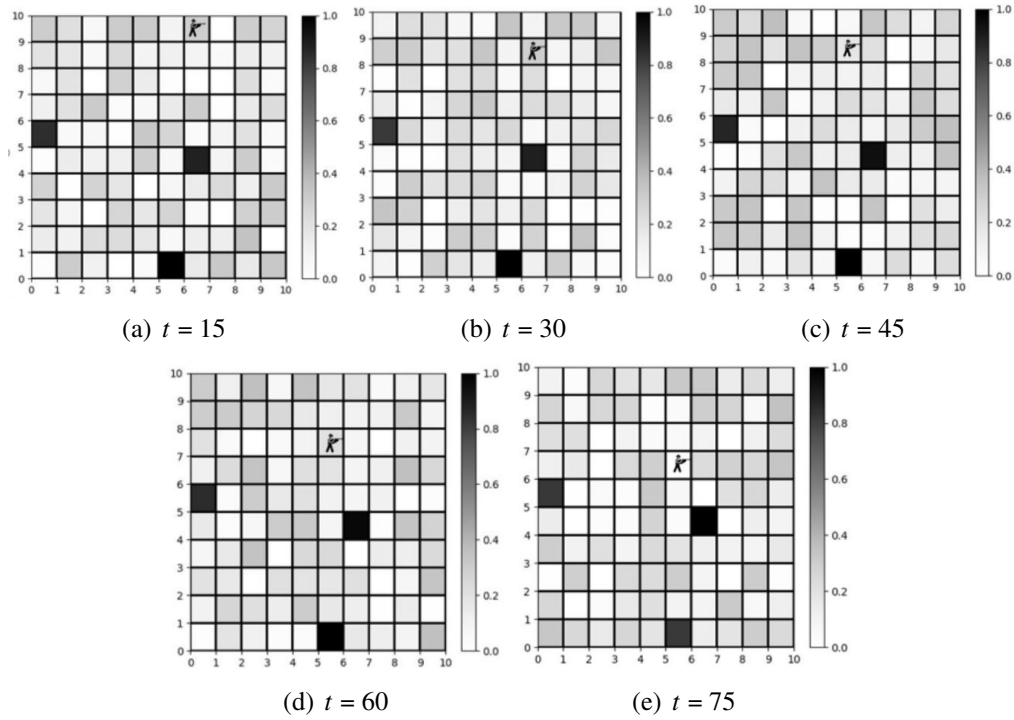


Figure 3.4

Reward illustration for first trial when simulation time is 75 seconds

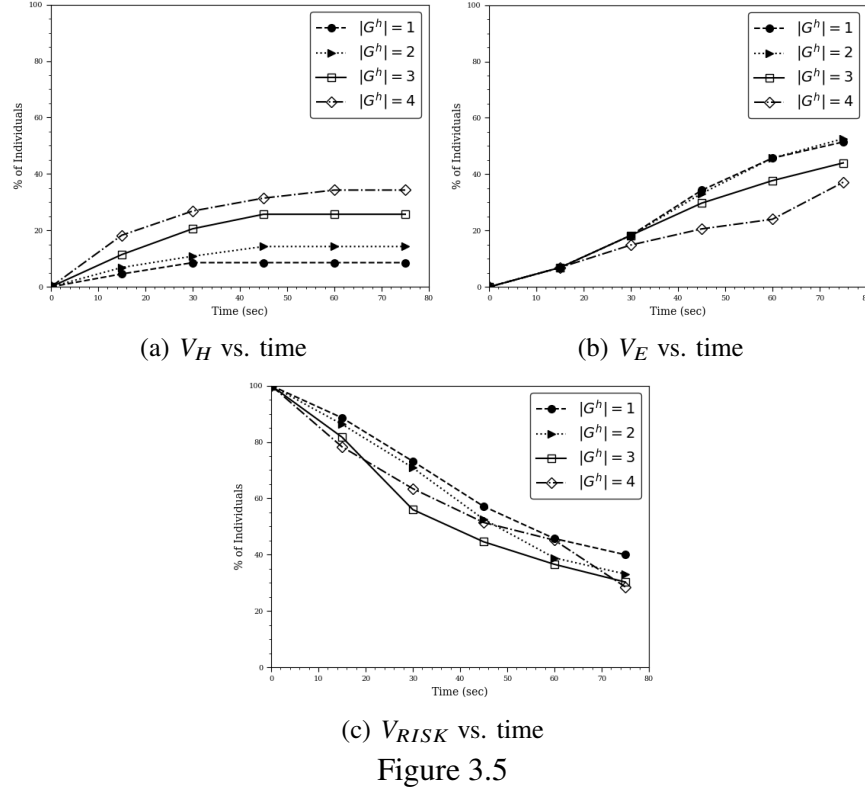
lessons summarize our observation of the numerical simulations for the case where the simulation time is fixed to 75 seconds.

Lesson 1: *Building configurations (e.g., location and number of entrances/exits, hiding places) play a significant role in the safety of civilians under an active shooter incident.*

The results in Figures 3.5 and 3.6 support this observation. The graphs demonstrate the impact of V_H , V_E , and V_{RISK} under different hiding and entrance/exit configurations. Appendix A6 shows different hiding and entrance/exit configurations (locations and numbers) for the tested facility, where $|\mathcal{G}^h|$ and $|\mathcal{G}^e|$ are set as $|\mathcal{G}^h| = \{1, 2, 3, 4\}$ and $|\mathcal{G}^e| = \{1, 2, 3, 4\}$, respectively. Note that, for the base case, we set $|\mathcal{G}^h| = 1$ and $|\mathcal{G}^e| = 3$. We summarize a few of our key observations below:

- Given capacity restrictions for the hiding grids (e.g., $\{\bar{v}_g\}_{g \in \mathcal{G}^h} = 10$ civilians for our base case experimentations), we realize that the location and number of entrance/exit configurations are more sensitive to an active shooter situation over the hiding configurations. For instance, when $|\mathcal{G}^e|$ increases from 1 to 4, then V_E increases from 5.7% to 71.4%, respectively, while V_{RISK} drops down to 20.1% from 85.7%. On the other hand, when $|\mathcal{G}^h|$ increases from 1 to 4, V_H increases from 8.5% to 34.2%, but both V_E and V_{RISK} drops from 51.4.3% to 37.14% and 40.3% to 28.5%, respectively. The rate of dropping for V_E and V_{RISK} clearly indicates that the entrance/exit configurations are more sensitive to an active shooter incident over the hiding configurations.
- It is interesting to note that for $|\mathcal{G}^h| = 4$, the civilians utilized 100% of the hiding capacity after 75 seconds. This number was only 53.3% and 78.3% after 15 and 30 seconds, respectively, from the onset of the shooting. Based on our experimental study (under pre-specified

modeling assumptions and experimental conditions), we observe that civilians have higher preferences for exiting the threat area rather than hiding into the facility.



Impact of V_H , V_E , and V_{RISK} under different hiding configurations.

Lesson 2: *Initial distribution of civilians has an impact on recovery from an active shooter incident.*

The results in Figure 3.7 show the gravity of the initial distribution of civilians on performance measures, V_E and V_{RISK} . Before delving into the details, let us first introduce Table 3.2, which lists different initial civilian distributions for our experiments. These distributions are depicted in Appendix A7. As can be seen, the base distribution is constructed by assuming that the civilians

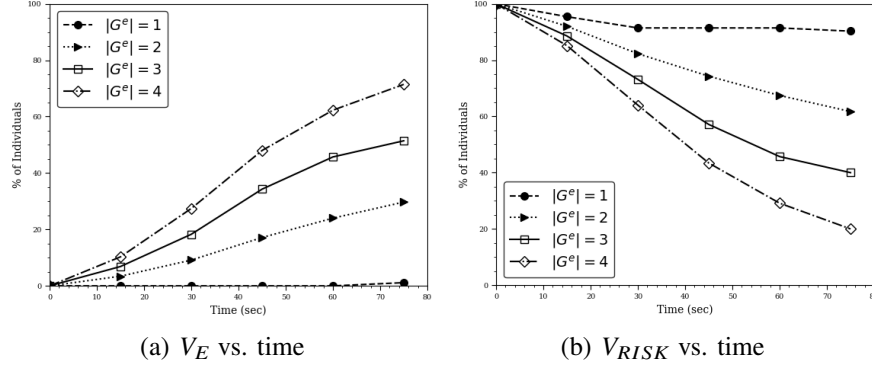


Figure 3.6

Impact of V_E and V_{RISK} under different entrance/exit configurations.

are uniformly distributed over the entire test region, while the remaining cases are constructed based on an idea that 70% of the civilians are uniformly distributed in one end of the test region, i.e., left distribution, right distribution, up distribution, and down distribution. Further, to run the experiments, we kept the base values for $|\mathcal{G}^h|$ and $|\mathcal{G}^e|$, i.e., $|\mathcal{G}^h| = 1$ and $|\mathcal{G}^e| = 3$ (see Figure 3.2). We summarize a few of our key observations below:

- Results in Figure 3.7(a) indicate that the left and down initial distribution of the civilians significantly increases V_E over the other distributions (e.g., base, right, and up distributions). For instance, after 75 seconds from the onset of the active shooter incident, the V_E drops down for the left and down initial distribution of the civilians to approximately 67.4% and 57.1%, respectively, while in the same time, the V_E only drops down to 44% under the up initial distribution case. This is primarily due to the fact the shooter entered into the facility from the upper entrance (see Figure 3.2), which resulted in the civilians to evade using that exit and instead utilizing more on the right and downside exits.

- We observe similar observations for the V_{RISK} measure, which drops significantly for the **left** and **down** initial distribution of the civilians over the other distributions (See Figure 3.7(b)). For instance, after 75 seconds from the onset of the active shooter incident, the V_{RISK} drops down for the **left** and **down** initial distribution of the civilians to approximately 24.3% and 34.1%, respectively, while the number is approximately 47.5% for the **up** initial distribution. The results provide several managerial insights to decision-makers, such as, the rate of the casualty may differ on the different time periods of the day, e.g., the majority of the students are on the **left** and **right** side of the facility during the class period which may not be the case under lunch period. Further, the entrance of the shooter and the availability of multiple exits and their locations may help to facilitate the movement of the civilians under an active shooter situation.
- The results in Figure 3.7(c) demonstrate the utilization of the hidden place under different civilian distribution configurations. As can be seen in Figure 3.7(c) that after 75 seconds from the onset of the active shooter incident, only 26.6% of the hidden place is utilized for the **left** distribution, while the number is nearly 93.3% for the **right** initial civilian distribution. Further, after 45 seconds, the hidden place is entirely utilized irrespective of the civilian distribution. Though a different configuration and number of hidden places may end up with different results, it can be generally stated that their positions and numbers shall have an impact on dropping the V_{RISK} measure under an active shooter incident.

Table 3.2

Initial distribution of civilians over the test region	
Item	Description
Base distribution	Civilians are uniformly distributed over the entire region
Left distribution	70% of the civilians are uniformly distributed over the left-side of the region
Right distribution	70% of the civilians are uniformly distributed over the right-side of the region
Up distribution	70% of the civilians are uniformly distributed over the upper-side of the region
Down distribution	70% of the civilians are uniformly distributed over the down-side of the region

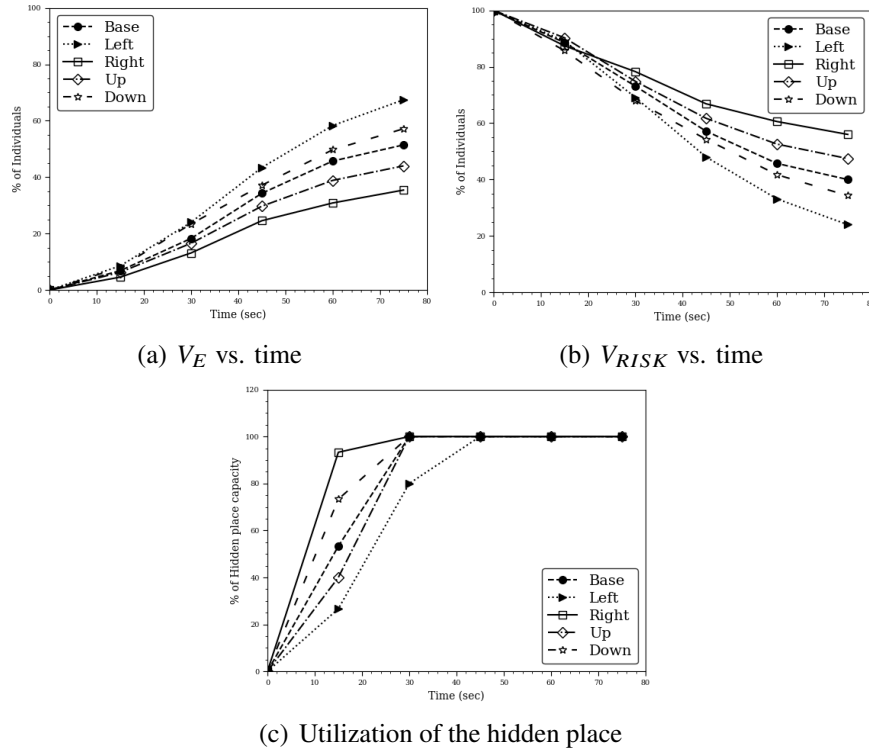


Figure 3.7

Impact of V_E , V_{RISK} , and hidden place utilization under different civilian distribution.

Lesson 3: *Shooting range and accuracy has an impact on recovery from an active shooter incident.*

The results in Figure 3.8 support this observation. It can be observed that the shooting range and the accuracy of the gun, carried by the shooter, has an impact on the performance measure V_{RISK} . We assume that the shooter will enter into the facility with a fully-loaded pistol. Before delving into the details of our results, let us first introduce different possible shooting ranges (range 1 to 4) and accuracy levels (45%, 60%, 75%, and 90%) that we use in our experimental setup (shown in Appendix A4). First figure in Appendix A4 demonstrates different possible shooting ranges of the gun, which may be carried by the shooter. As can be seen that depending on the type of firearm being used, more civilians may fall under the shooting range of the shooter, which greatly increases the security concerns (assuming no obstacles are in between). On the other hand, for a given shooting range, the accuracy of the shooter will also significantly increase the security concerns for the civilians (assuming again that no obstacles are in between). This cumbersome relationship is depicted in a three-dimensional plot in Figure 3.8. The results essentially convey two major findings.

- First, for a given shooting range, the V_{RISK} increases with an increase in shooter's shooting accuracy. For instance, in *range 1*, V_{RISK} increases from 6% to 14%, when the shooting accuracy increases from 45% to 90%, respectively (see Figure 3.8). For *range 4*, this performance metric increases from 42% to 68%, when the shooting accuracy again increases from 45% to 90%, respectively. The above results indicate that the shooter's prior shooting experiences can prove to be deadly, which can greatly increase the security concern in an active shooter situation.

- Second, for a given shooting accuracy, the V_{RISK} increases with an increase in shooting range. For instance, for a shooting accuracy of 45%, V_{RISK} increases from 6% to 42%, when the shooting range increases from range 1 to 4, respectively (see Figure 3.8). We also observe the similar increasing trend for shooting ranges, given the shooting accuracy remains fixed for that experiment. The above results indicate that the quality of the firearm carried by the shooter may pose serious security concerns to the civilians under an active shooter incident.

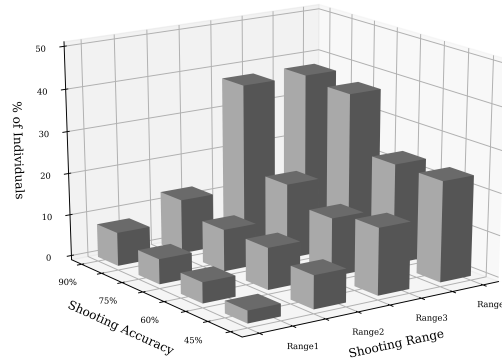


Figure 3.8

V_{RISK} vs. shooting range and accuracy. Note that V_{RISK} denotes the percentage of civilians who are still freely floating within the threat area.

3.4 Conclusions and Future Work

This study proposes a dynamic maximum entropy inverse reinforcement learning technique to model the behavior of the shooter and the trapped civilians under an active shooter incident. We derive a number of insights by demonstrating the proposed technique in a testing facility.

We methodologically demonstrate that building configurations (e.g., location and number of entrances/exits, hiding places) can play a significant role in the safety of civilians under an active shooter situation. We further demonstrate that the casualty rate may differ in the different periods of the day (e.g., lunchtime vs. class time in a school setting) when the civilians may initially locate in different locations (e.g., classroom, cafeteria). Finally, we demonstrate that the shooter's prior shooting experiences or the firearm carried may pose serious security concerns to the civilians under an active shooter incident. We believe our proposed technique holds promise to assess the safety and security of various vulnerable facilities (e.g., schools, hospitals, shopping malls) against a possible active shooter incident.

This study can be extended in several research directions. First, all the insights generated in this study are based on pure numerical simulation without any validation or comprehensive incorporation of realistic human behavior in the simulation model. Therefore, such insights may not be applicable to realistic situations. To alleviate such challenges and to generate reliable insights, future studies will focus on collecting human evacuation behavioral data via various existing research methods (e.g., virtual reality [54, 116], hypothetical surveys [90, 61], and controlled experiments [68, 31]) and incorporate such behavioral data into our proposed modeling framework. Second, we aim to integrate advanced choice theory models in our proposed framework in an attempt to explain human behavior and the possible trajectories that resulted from the behaviors under an active shooter incident. Finally, this study considers a hypothetical test facility to demonstrate the performance of the proposed learning algorithm. Efforts will be paid in future studies to demonstrate the performance of the learning algorithm in assessing the safety and security

of different realistic environments under an active shooter situation, such as school buildings, hospitals, shopping malls, and related facilities.

REFERENCES

- [1] P. Abbeel, A. Coates, and A. Y. Ng, “Autonomous helicopter aerobatics through apprenticeship learning,” *The International Journal of Robotics Research*, vol. 29, no. 13, 2010, pp. 1608–1639.
- [2] P. Abbeel, A. Coates, M. Quigley, and A. Y. Ng, “An application of reinforcement learning to aerobatic helicopter flight,” *Proceedings of the Twentieth Annual Conference on Neural Information Processing Systems*, 2007.
- [3] P. Abbeel and A. Y. Ng, “Apprenticeship learning via inverse reinforcement learning,” *Proceedings of the Twenty-First International Conference on Machine Learning*, 2004, pp. 1–8.
- [4] A. Aghalari, M. Marufuzzaman, B. S. Aladwan, S. Tanger, and B. K. Da Silva, “A bilevel model formulation for solving a post-hurricane damaged timber management problem,” *Computers & Industrial Engineering*, vol. 162, 2021, p. 107726.
- [5] A. Aghalari, N. Morshedlou, M. Marufuzzaman, and D. Carruth, “Inverse reinforcement learning to assess safety of a workplace under an active shooter incident,” *IIE Transactions*, vol. 53, no. 12, 2021, pp. 1337–1350.
- [6] A. Aghalari, D. E. Salamah, C. Marino, and M. Marufuzzaman, “Electric vehicles fast charger location-routing problem under ambient temperature,” *Annals of Operations Research*, 2021, pp. 1–39.
- [7] Aghalari, A., Nur, F. and Marufuzzaman, M. , “A Bender’s based nested decomposition algorithm to solve a stochastic inland waterway port management problem considering perishable product,” *International Journal of Production Economics*, vol. 229, 2020, p. 107863.
- [8] Akgun I., Kandakoglu A., Ozok A.F., “Fuzzy integrated vulnerability assessment model for critical facilities in combating the terrorism,” *Expert Systems with Applications*, vol. 37, 2010, pp. 3561–3573.
- [9] Anklam C., Kirby A., Sharevski F., Dietz J.E., “Mitigating active shooter impact: analysis for policy options based on agent/computer-based modeling,” *Journal of Emergency Management*, vol. 13, no. 3, 2015, pp. 201–216.

- [10] Apostolakis G.E., Lemon D.M., “A screening methodology for the identification and ranking of infrastructure vulnerabilities due to the terrorism,” *Risk Analysis*, vol. 25, 2005, pp. 361–376.
- [11] J. D. Averill, R. D. Peacock, and E. D. Kuligowski, “Analysis of the evacuation of the World Trade Center towers on September 11, 2001,” *Fire Technology*, vol. 49, no. 1, 2013, pp. 37–63.
- [12] Bard J.F., Feinberg A., “A two-phase methodology for technology selection and system design,” *IEEE Transactions on Engineering Management*, vol. 36, no. 1, 1989, pp. 28–36.
- [13] G. Bernardini, E. Quagliarini, and M. D’Orazio, “Towards creating a combined database for earthquake pedestrians’ evacuation models,” *Safety Science*, vol. 82, 2016, pp. 77–94.
- [14] Bierlaire M., “Incorporating behavioral model into transport optimization.,” Available from: <http://transp-or.epfl.ch/documents/talks/delft2018.pdf>, 2018.
- [15] N. W. Bode and E. A. Codling, “Human exit route choice in virtual crowd evacuations,” *Animal Behaviour*, vol. 86, no. 2, 2013, pp. 347–358.
- [16] Briggs T., Kennedy W., “Active shooter: an agent-base model of unarmed resistance.,” Proceedings of the 2016 Winter Simulation Conference, , 5090-4486, edited by T.M.K Roeder et al., Piscataway: New Jersey: IEEE., 2016.
- [17] M. Burroughs and E. R. Galea, “Real time, real fire, real response: An analysis of response behaviour in housing for vulnerable people,” *Proceedings of the 6th International Symposium on Human Behaviour in Fire*, 2015, pp. 477–488.
- [18] D. Canter, “Fires and human behaviour: Emerging issues,” *Fire Safety Journal*, vol. 3, no. 1, 1980, pp. 41–46.
- [19] L. Cao, J. Lin, and N. Li, “A virtual reality based study of indoor fire evacuation after active or passive spatial exploration,” *Computers in Human Behavior*, vol. 90, 2019, pp. 37–45.
- [20] S. Cao, L. Fu, P. Wang, G. Zeng, and W. Song, “Experimental and modeling study on evacuation under good and limited visibility in a supermarket,” *Fire Safety Journal*, vol. 102, 2018, pp. 27–36.
- [21] Castillo P., Castro P.M., Mahalec V., “Global optimization algorithm for large-scale refinery planning models with bilinear terms,” *Industrial & Engineering Chemistry Research*, vol. 56, 2007, pp. 530–548.
- [22] M. L. Chu, P. Parigi, K. H. Law, and J.-C. Latombe, “Simulating individual, group, and crowd behaviors in building egress,” *Simulation*, vol. 91, no. 9, 2015, pp. 825–845.
- [23] R. B. Cialdini and R. B. Cialdini, *Influence: The Psychology of Persuasion*, HarperCollins, New York, NY, 2007.

- [24] R. P. Darken and B. Peterson, “Spatial orientation, wayfinding, and representation.,” *Handbook of Virtual Environment Technology*, Erlbaum, Mahwah, NJ, 2002, pp. 493–518.
- [25] Dijkstra E.W., “A note on two problems in connexion with graphs,” *Numerische Nathematik*, vol. 1, no. 1, 1959, pp. 269–271.
- [26] Federal Bureau of Investigation (FBI), “Active shooter incidents in the United States from 2000-2018.,” Available from: <https://www.fbi.gov/file-repository/active-shooter-incidents-2000-2018.pdf/view>, 2018.
- [27] Federal Bureau of Investigation (FBI), “Quick Look: 250 active shooter incidents in the United States from 2000 to 2017.,” Available from: <https://www.fbi.gov/about/partnerships/office-of-partner-engagement/active-shooter-incidents-graphics>, 2018.
- [28] Fox W.P., Binstock J., Minutas M., “Modeling and methodology for incorporating existing technologies to produce higher probabilities of detecting suicide bombers,” *International Journal of Operations Research and Information Systems*, vol. 4, no. 3, 2013, pp. 1–18.
- [29] E. R. Galea, H. Xie, and P. J. Lawrence, “Experimental and survey studies on the effectiveness of dynamic signage systems,” *Fire Safety Science*, vol. 11, 2014, pp. 1129–1143.
- [30] Gun Violence Archive (GVA), “Mass shootings in 2019.,” Available from: <https://www.gunviolencearchive.org/reports>, 2020.
- [31] R.-Y. Guo, H.-J. Huang, and S. Wong, “Route choice in pedestrian evacuation under conditions of good and zero visibility: Experimental and simulation results,” *Transportation Research Part B: Methodological*, vol. 46, no. 6, 2012, pp. 669–686.
- [32] Hausken K., Zhuang J., “The timing and deterrence of terrorist attacks due to exogenous dynamics,” *Journal of the Operational Research Society*, vol. 63, no. 6, 2012, pp. 726–735.
- [33] Hayes R., Hayes R., “Agent-based simulation of mass shootings: determining how to limit the scale of a tragedy,” *Journal of Artificial Societies and Social Simulation*, 17(2):5. Available from: <<http://jasss.soc.surrey.ac.uk/17/2/5.html>>, 2014.
- [34] G. Hofinger, R. Zinke, and L. Künzer, “Human factors in evacuation simulation, planning, and guidance,” *Transportation Research Procedia*, vol. 2, 2014, pp. 603–611.
- [35] I. L. Janis, “Problems of theory in the analysis of stress behavior.,” *Journal of Social Issues*, vol. 10, no. 3, 1954, pp. 12–25.
- [36] N. R. Johnson, “Panic and the breakdown of social order: Popular myth, social theory, empirical evidence,” *Sociological Focus*, vol. 20, no. 3, 1987, pp. 171–183.

- [37] Jones J., Kue R., Mitchell P., Eblan G., Dyer K.S., “Emergency medical services response to active shooter incidents: provider comfort level and attitudes before and after participation in a focused response training program.,” *Prehospital and Disaster Medicine*, vol. 29, no. 4, 2014, pp. 350–357.
- [38] Kaplan E.H., Kress M., “Operational effectiveness of suicide-bomber-detector schemes: A best-case analysis,” *Proceedings of National Academy of Sciences of the USA*, vol. 102, no. 29, 2005, pp. 10399–10404.
- [39] M. T. Kinatader, E. D. Kuligowski, P. A. Reneke, and R. D. Peacock, *A review of risk perception in building fire evacuation*, NIST.T.N.1840, National Institute of Standards and Technology, 2014.
- [40] Kirby A., Anklam C.E., Dietz J.E., “Active shooter mitigation for gun-free zones.,” IEEE Symposium on Technologies for Homeland Security (HST), Waltham, MA, USA., 2016.
- [41] Klassen A.B., Marshall M., Dai M., Mann N.C., Sztajnkrzyer M.D., “Emergency medical services response to mass shooting and active shooter incidents, United States, 2014-2015.,” *Prehospital Emergency Care*, vol. 23, no. 2, 2019, pp. 159–166.
- [42] H. Klüpfel and T. Meyer-König, “Simulation of the Evacuation of a football stadium using the CA Model PedGo,” *Traffic and Granular Flow’03*, Springer, 2005, pp. 423–428.
- [43] M. Kobes, I. Helsloot, B. De Vries, and J. G. Post, “Building safety and human behaviour in fire: A literature review,” *Fire Safety Journal*, vol. 45, no. 1, 2010, pp. 1–11.
- [44] Kotora J.G., Clancy T., Manzon L., Malik V., Loudon R.J., Merlin M.A., “Active shooter in the emergency department: a scenario-based training approach for healthcare workers.,” *American Journal of Disaster Medicine*, vol. 9, no. 1, 2014, pp. 39–51.
- [45] Lakats L.M., Pate-Cornell M.E., “Organizational warning systems: a probabilistic approach to optimal design,” *IEEE Transactions on Engineering Management*, vol. 51, no. 2, 2004, pp. 183–196.
- [46] Lee J.Y., “Agent-based modeling to assess the effectiveness of run hide fight.,” Master’s Thesis. Purdue University., 2019.
- [47] Lee J.Y., Dietz J.E., “Assessing the effectiveness of automatic door lock system by discharge detection to lower casualty during an academic active shooting incident.,” *Proceedings of The 2018 International Association of Journals & Conferences*, ISBN 978-1-60643-379-9, 2018.
- [48] Lee J.Y., Ostrowski K., “Agent-based modeling for casualty rate assessment of large event active shooter incidents.,” *Proceedings of the 2018 Winter Simulation Conference*, Gothenburg, Sweden., 2018.

- [49] S. Li, J. Zhuang, and S. Shen, "A three-stage evacuation decision-making and behavior model for the onset of an attack," *Transportation Research Part C: Emerging Technologies*, vol. 79, 2017, pp. 119–135.
- [50] X. Li, H. Cao, E. Chen, H. Xiong, and J. Tian, "BP-growth: Searching strategies for efficient behavior pattern mining," *2012 IEEE 13th International Conference on Mobile Data Management*, 2012, pp. 238–247.
- [51] Li D., Han B., "Behavioral effect on pedestrian evacuation simulation using cellular automata.," *Safety Science*, vol. 80, 2015, pp. 41–45.
- [52] Li S., Zhuang J., Shen S., "A three-stage evacuation decision-making and behavior model for the onset of an attack.," *Transportation Research Part C*, vol. 79, 2017, pp. 119–135.
- [53] Li X., Li Q., Claramunt C., "A time-extended network model for staged evacuation planning.," *Safety Science*, vol. 108, 2018, pp. 225–236.
- [54] J. Lin, L. Cao, and N. Li, "Assessing the influence of repeated exposures and mental stress on human wayfinding performance in indoor environments using virtual reality technology," *Advanced Engineering Informatics*, vol. 39, 2019, pp. 53–61.
- [55] J. Lin, R. Zhu, N. Li, and B. Becerik-Gerber, "How occupants respond to building emergencies: A systematic review of behavioral characteristics and behavioral theories," *Safety Science*, vol. 122, 2020, p. 104540.
- [56] M. K. Lindell, C. S. Prater, H. C. Wu, S.-K. Huang, D. M. Johnston, J. S. Becker, and H. Shiroshita, "Immediate behavioural responses to earthquakes in Christchurch, New Zealand, and Hitachi, Japan," *Disasters*, vol. 40, no. 1, 2016, pp. 85–111.
- [57] M. Liu and S. M. Lo, "The quantitative investigation on people's pre-evacuation behavior under fire," *Automation in Construction*, vol. 20, no. 5, 2011, pp. 620–628.
- [58] Q. Liu, "A social force model for the crowd evacuation in a terrorist attack," *Physica A: Statistical Mechanics and its Applications*, vol. 502, 2018, pp. 315–330.
- [59] S. Liu, M. Araujo, E. Brunskill, R. Rossetti, J. Barros, and R. Krishnan, "Understanding sequential decisions via inverse reinforcement learning," *2013 IEEE 14th International Conference on Mobile Data Management*. IEEE, 2013, pp. 177–186.
- [60] Lo S.M., Huang H.C., Wang P., Yuen K.K., "A game theory based exit selection model for evacuation.," *Fire Safety Journal*, vol. 41, 2006, pp. 364–369.
- [61] R. Lovreglio, A. Fonzone, L. Dell'Olio, D. Borri, and A. Ibeas, "The role of herding behaviour in exit choice during evacuation," *Procedia-Social and Behavioral Sciences*, vol. 160, 2014, pp. 390–399.

- [62] M. Marufuzamman, A. Aghalari, R. K. Buchanan, C. H. Rinaudo, K. M. Houte, and J. H. Ranta, "Optimal Placement of Detectors to Minimize Casualties in an Intentional Attack," *IEEE Transactions on Engineering Management*, vol. in press and online available, 2020.
- [63] M. Marufuzzaman, A. Aghalari, R. Buchanan, C. H. Rinaudo, K. M. Houte, and J. H. Ranta, "Optimal Placement of Detectors to Minimize Casualties on a Manmade Attack," *arXiv preprint arXiv:2101.10184*, 2021.
- [64] M. Marufuzzaman, A. Aghalari, J. H. Ranta, and R. Jaradat, "Optimizing civilian response strategy under an active shooting incident," *IEEE Systems Journal*, vol. 15, no. 4, 2021, pp. 4804–4815.
- [65] A. Mawson, "Panic behavior: A review and a new hypothesis," *9th World Congress of Sociology, Uppsala, Sweden*, 1978.
- [66] McFadden D., Train K., "Mixed MNL models for discrete choice response.," *Journal of Applied Econometrics*, vol. 15, no. 5, 2000, pp. 447–470.
- [67] Mechem C.C., Bossert R., Baldini C., "Rapid assessment medical support (RAMS) for active shooter incidents.," *Prehospital Emergency Care*, vol. 19, no. 2, 2015, pp. 213–217.
- [68] R. Nagai, M. Fukamachi, and T. Nagatani, "Evacuation of crawlers and walkers from corridor through an exit," *Physica A: Statistical Mechanics and its Applications*, vol. 367, 2006, pp. 449–460.
- [69] A. Y. Ng and S. J. Russell, "Algorithms for inverse reinforcement learning.," *Proceedings of the Seventeenth International Conference on Machine Learning*, 2000, pp. 663–670.
- [70] Nie X., Batta R., Drury C., Lin L., "Optimal placement of suicide bomber detectors," *Military Operations Research*, vol. 12, no. 2, 2007, pp. 65–78.
- [71] D. Nilsson and A. Johansson, "Social influence during the initial phase of a fire evacuation—Analysis of evacuation experiments in a cinema theatre," *Fire Safety Journal*, vol. 44, no. 1, 2009, pp. 71–79.
- [72] E. Nouri, K. Georgila, and D. Traum, "A cultural decision-making model for negotiation based on inverse reinforcement learning," *Proceedings of 34th Annual Meeting of the Cognitive Science Society*, 2012, pp. 2097–2103.
- [73] V. Oven and N. Cakici, "Modelling the evacuation of a high-rise office building in Istanbul," *Fire Safety Journal*, vol. 44, no. 1, 2009, pp. 1–15.
- [74] R. D. Peacock, P. A. Reneke, E. D. Kuligowski, and C. Hagwood, "Movement on stairs during building evacuations," *Fire Technology*, vol. 53, no. 2, 2017, pp. 845–871.

- [75] Pirani M., Nekouei E., Sandberg H., Johansson K.H., “A game-theoretic framework for security-aware sensor placement problem in networked control systems.,” 2019 American Control Conference (ACC), Philadelphia, PA, USA., 2019.
- [76] G. Proulx, “Occupant behaviour and evacuation,” *Proceedings of the 9th International Fire Protection Symposium*, 2001, pp. 219–232.
- [77] Przemieniecki J.S., *Mathematical methods in defense analyses*, American Institute of Aeronautics and Astronautics, Reston, VA, 2000.
- [78] Qu Y., Gao Z., Xiao Y., Li X., “Modeling the pedestrian’s movement and simulating evacuation dynamics on stairs.,” *Safety Science*, vol. 70, 2014, pp. 189–201.
- [79] E. L. Quarantelli, “The nature and conditions of panic,” *American Journal of Sociology*, vol. 60, no. 3, 1954, pp. 267–275.
- [80] D. Ramachandran and E. Amir, “Bayesian Inverse Reinforcement Learning.,” *Proceedings of the Twentieth International Joint Conference on Artificial Intelligence*, 2007, pp. 2586–2591.
- [81] N. D. Ratliff, J. A. Bagnell, and M. A. Zinkevich, “Maximum margin planning,” *Proceedings of the 23rd International Conference on Machine Learning*, 2006, pp. 729–736.
- [82] S. Russell, “Learning agents for uncertain environments,” *Proceedings of the Eleventh Annual Conference on Computational Learning Theory*, 1998, pp. 101–103.
- [83] Sanchez L., Young V.B., Baker M., “Active shooter training in the emergency department: a safety initiative.,” *Journal of Emergency Nursing*, vol. 44, no. 6, 2018, pp. 598–604.
- [84] Schweit K.W., “Active Shooter Incidents in the United States in 2014 and 2015,” Federal Bureau of Investigation, U.S. Department of Justice, Washington, D.C., 2016.
- [85] Z. Shahhoseini and M. Sarvi, “Pedestrian crowd flows in shared spaces: Investigating the impact of geometry based on micro and macro scale measures,” *Transportation Research Part B: Methodological*, vol. 122, 2019, pp. 57–87.
- [86] S. Shapira, L. Aharonson-Daniel, and Y. Bar-Dayana, “Anticipated behavioral response patterns to an earthquake: The role of personal and household characteristics, risk perception, previous experience and preparedness,” *International Journal of Disaster Risk Reduction*, vol. 31, 2018, pp. 1–8.
- [87] Sheng G., Min M., Xiao L., Liu S., “Reinforcement learning-based control for unmanned aerial vehicle,” *Journal of Communications and Information Networks*, vol. 3, no. 3, 2018, pp. 39–48.

- [88] Sherali H.D., Desai J., Glickman T.S., “Allocating emergency response resources to minimize risk with equity considerations,” *American Journal of Mathematical and Management Sciences*, vol. 24, no. 3–4, 2004, pp. 367–410.
- [89] A. Shipman and A. Majumdar, “Fear in humans: A glimpse into the crowd-modeling perspective,” *Transportation Research Record*, vol. 2672, no. 1, 2018, pp. 183–197.
- [90] N. Shiwakoti, R. Tay, P. Stasinopoulos, and P. J. Woolley, “Likely behaviours of passengers under emergency evacuation in train station,” *Safety Science*, vol. 91, 2017, pp. 40–48.
- [91] Stewart A., “Active shooter simulations: An agent-based model of civilian response strategy,” Master’s Thesis. Iowa State University, 2017.
- [92] R. S. Sutton and A. G. Barto, *Reinforcement Learning: An Introduction*, MIT press, Cambridge, MA, 2018.
- [93] H. Tajfel, J. C. Turner, W. G. Austin, and S. Worchel, “An integrative theory of intergroup conflict,” *Organizational Identity: A Reader*, Oxford University Press, Oxford, United Kingdom, 1979, pp. 56–65.
- [94] Tang J., Wang Y., Hao W., Liu F., Huang H., Wang Y. , “A mixed path size logit based taxi customer-search model considering spatio-temporal factors in route choice,” *IEEE Transactions on Intelligent Transportation Systems*, vol. 21, no. 4, 2020, pp. 1347–1358.
- [95] Tang J., Zheng L., Han C., Yin W., Zhang Y., Zou Y., Huang H., “Statistical and machine-learning methods for clearance time prediction of road incidents: A methodology review,” *Analytic Methods in Accident Research*, vol. 27, 2020, p. 100123.
- [96] Telesca L., Lovullo M., “Are global terrorist attacks time-correlated?,” *Physica A: Statistical Mechanics and its Applications*, vol. 362, 2006, pp. 480–484.
- [97] The New York Times, “Serious case of shooting-navigation,” Available from: https://en.wikipedia.org/wiki/List_of_school_shootings_in_the_United_States, 1853.
- [98] A. Trivedi and S. Rao, “Agent-based modeling of emergency evacuations considering human panic behavior,” *IEEE Transactions on Computational Social Systems*, vol. 5, no. 1, 2018, pp. 277–288.
- [99] Tutun S., Khasawneh M.T., Zhuang J., “New framework that uses patterns and relations to understand terrorist behaviors,” *Expert Systems with Applications*, vol. 78, 2017, pp. 358–375.
- [100] M. R. Uddin, C. Ravishankar, and V. J. Tsotras, “Finding regions of interest from trajectory data,” *2011 IEEE 12th International Conference on Mobile Data Management*. IEEE, 2011, pp. 39–48.

- [101] United States Department of Homeland Security, “Active Shooter: How to respond,” Available from: http://www.dhs.gov/xlibrary/assets/active_shooter_booklet.pdf, 2019.
- [102] E. Vilar, F. Rebelo, and P. Noriega, “Smart Systems in Emergency Wayfinding: A Literature Review,” *International Conference of Design, User Experience, and Usability*, 2018, pp. 379–388.
- [103] H. Xie, L. Filippidis, E. R. Galea, D. Blackshields, and P. J. Lawrence, “Experimental analysis of the effectiveness of emergency signage and its implementation in evacuation simulation,” *Fire and Materials*, vol. 36, no. 5-6, 2012, pp. 367–382.
- [104] Xie X., Ren A., Zhou X., “Determination of the best evacuation route in high-rise building fire,” *Journal of Natural Disasters*, vol. 12, 2003, p. 75.
- [105] Yan X., Nie X., “Optimal placement of multiple types of detectors under a small vessel attack threat to port security,” *Transportation Research Part E*, vol. 93, 2016, pp. 71–94.
- [106] S. Y. Yang, Q. Qiao, P. A. Beling, W. T. Scherer, and A. A. Kirilenko, “Gaussian process-based algorithmic trading strategy identification,” *Quantitative Finance*, vol. 15, no. 10, 2015, pp. 1683–1703.
- [107] Yang T.P., Asirvadam V.S., “Optimizing detector placement and mapping using imaging techniques,” 2011 National Postgraduate Conference, Kuala Lumpur, Malaysia., 2011.
- [108] Yang T.P., Asirvadam V.S., Saad N.B., “Optimal placement of fire detector using dual-view,” 4th International Conference on Intelligent and Advanced Systems (ICIAS2012), Kuala Lumpur, Malaysia., 2012.
- [109] Yang X., Dong H., Wang Q., Chen Y., Hu X., “Guided crowd dynamics via modified social force model,” *Physica A: Statistical Mechanics and its Applications*, vol. 411, 2014, pp. 63–73.
- [110] N. Yokoyama, “Inference of aircraft intent via inverse optimal control including second-order optimality condition,” *Journal of Guidance, Control, and Dynamics*, vol. 41, no. 2, 2018, pp. 349–359.
- [111] C. You, J. Lu, D. Filev, and P. Tsiotras, “Advanced planning for autonomous vehicles using reinforcement learning and deep inverse reinforcement learning,” *Robotics and Autonomous Systems*, vol. 114, 2019, pp. 1–18.
- [112] Y. Zhang, W. Xie, S. Chen, and T. Li, “Experimental study on descent speed on stairs of individuals and small groups under different visibility conditions,” *Fire Technology*, vol. 54, no. 3, 2018, pp. 781–796.
- [113] S. Zhifei and E. M. Joo, “A survey of inverse reinforcement learning techniques,” *International Journal of Intelligent Computing and Cybernetics*, vol. 5, no. 3, 2012, pp. 293–311.

- [114] R. Zhu, B. Becerik-Gerber, G. Lucas, E. Southers, and D. V. Pynadath, “Information Requirements for Virtual Environments to Study Human-Building Interactions during Active Shooter Incidents,” *ASCE International Conference on Computing in Civil Engineering 2019*. ASCE, 2019, pp. 188–195.
- [115] R. Zhu, J. Lin, B. Becerik-Gerber, and N. Li, “Human-building-emergency interactions and their impact on emergency response performance: A review of the state of the art,” *Safety Science*, vol. 127, 2020, p. 104691.
- [116] R. Zhu, G. M. Lucas, B. Becerik-Gerber, and E. G. Southers, “Building preparedness in response to active shooter incidents: Results of focus group interviews,” *International Journal of Disaster Risk Reduction*, vol. 48, 2020, p. 101617.
- [117] Zhu Y., Xie K., Ozbay K., Yang H., “Hurricane evacuation modeling using behavior models and scenario-driven agent-based simulations.,” *Procedia Computer Science*, vol. 130, 2018, pp. 836–843.
- [118] B. D. Ziebart, A. L. Maas, J. A. Bagnell, and A. K. Dey, “Maximum entropy inverse reinforcement learning.,” *Proceedings of the Twenty-Third AAAI Conference on Artificial Intelligence*, 2008, pp. 1433–1438.

APPENDIX A
ILLUSTRATION OF INPUT DATA

A.1 Summary of sets, parameters, and decision variables for chapter 2

- \mathcal{I} : set of alternatives
- \mathcal{N} : set of civilian
- \mathcal{G}^b : set of blocked grids
- \mathcal{G}^u : set of unblocked grids
- \mathcal{G}^e : set of entrance/exit grids
- \mathcal{G}^a : set of threat grids
- \mathcal{G}^h : set of hiding grids
- \mathcal{G} : set of grids where $\mathcal{G} = \mathcal{G}^b \cup \mathcal{G}^u$ and $\mathcal{G}^b \cap \mathcal{G}^u = \emptyset$
- \mathcal{G}^g : subset of neighboring cells for grid $g \in \mathcal{G}^u$
- $\mathcal{G}_{g,i}$: subset of neighboring cells for grid $g \in \mathcal{G}^u$ given action $i \in \mathcal{I}$ is undertaken
- \mathcal{I}_g : subset of alternatives that can end up in $g \in \mathcal{G}^h$
- $\mathcal{G}'_{g,i}$: subset of neighboring cells for grid $g \in \mathcal{G}^h$ given action $i \in \mathcal{I}_g$ is undertaken

Parameters:

- π_n : cognitive delay of civilian $n \in \mathcal{N}$
- \bar{v}_g : hiding capacity for the civilians in grid $g \in \mathcal{G}^h$
- $\tilde{t}_{gg'}$: standard average travel time for a civilian to run from grid $g \in \mathcal{G}^u$ to $g' \in \mathcal{G}^g$
- $t_{ngg'}$: realized running time for civilian $n \in \mathcal{N}$ located in grid $g \in \mathcal{G}^u$ to $g' \in \mathcal{G}^g$
- ζ_g : a 0/1 indicator which refers the proximity of shooter to grid $g \in \mathcal{G}^u$

Decision Variables:

- Y_{ing} : 1 if alternative $i \in \mathcal{I}$ is available to civilian $n \in \mathcal{N}$ located in grid $g \in \mathcal{G}^u$; 0 otherwise

- Y_{ngr} : 1 if alternative $i \in \mathcal{I}$ is available to civilian $n \in \mathcal{N}$ located in grid $g \in \mathcal{G}^u$ under scenario $r = 1, 2, \dots, R$; 0 otherwise
- Z_{ngr} : 1 if alternative $i \in \mathcal{I}$ is chosen by civilian $n \in \mathcal{N}$ located in grid $g \in \mathcal{G}^u$ under scenario $r = 1, 2, \dots, R$; 0 otherwise
- $Z_{ingg'r}$: 1 if choosing alternative $i \in \mathcal{I}$ let the civilian $n \in \mathcal{N}$ move from grid $g \in \mathcal{G}^u$ to grid $g' \in \mathcal{G}_{g,i}$ under scenario $r = 1, 2, \dots, R$; 0 otherwise
- X_{ngr} : to representing the discounted utility associated with alternative $i \in \mathcal{I}$ chosen by civilian $n \in \mathcal{N}$ located in grid $g \in \mathcal{G}^u$ under scenario $r = 1, 2, \dots, R$
- U_{ngr} : the utility associated with choosing alternative $i \in \mathcal{I}$ by civilian $n \in \mathcal{N}$ located in grid $g \in \mathcal{G}^u$ under realization $r = 1, 2, \dots, R$
- U_{ngr} : the highest discounted utility associated with choosing an alternative by civilian $n \in \mathcal{N}$ located in grid $g \in \mathcal{G}^u$ under realization $r = 1, 2, \dots, R$

A.2 Proof of Proposition 1

Proof. We prove this by constructing two cases as shown below:

Case 1: For the first case, we assume that $Y_{ngr} = 1$. With this, $\forall i \in \mathcal{I}, n \in \mathcal{N}, g \in \mathcal{G}^u, r = 1, 2, \dots, R$ constraints (3.4)-(3.7) become:

$$l_{ngr} \leq X_{ngr} \tag{A.1a}$$

$$X_{ngr} \leq l_{ngr} + \bar{\phi}_{ngr} \tag{A.1b}$$

$$U_{ngr} \leq X_{ngr} \tag{A.1c}$$

$$X_{ngr} \leq U_{ngr} \tag{A.1d}$$

Constraints (A.1c) and (A.1d) ensure that $X_{ingr} = U_{ingr}; \forall i \in \mathcal{I}, n \in \mathcal{N}, g \in \mathcal{G}^u, r = 1, 2, \dots, R$.

We plug this enforcement into equations (A.1a) and (A.1b) for each $i \in \mathcal{I}, n \in \mathcal{N}, g \in \mathcal{G}^u$, and $r = 1, 2, \dots, R$ and obtain the following:

$$l_{ngr} \leq U_{ingr} \quad (\text{A.2a})$$

$$U_{ingr} \leq l_{ngr} + \bar{\phi}_{ingr} = l_{ngr} + (\phi_{ingr} - l_{ngr}) = \phi_{ingr} \quad (\text{A.2b})$$

The validity of constraints (A.2a) and (A.2b) are ensured via constraint (3.8).

Case 2: For the second case, we assume that $Y_{ingr} = 0$. With this, $\forall i \in \mathcal{I}, n \in \mathcal{N}, g \in \mathcal{G}^u, r = 1, 2, \dots, R$ constraints (3.4)-(3.7) become:

$$l_{ngr} \leq X_{ingr} \quad (\text{A.3a})$$

$$X_{ingr} \leq l_{ngr} \quad (\text{A.3b})$$

$$U_{ingr} - \bar{\phi}_{ingr} \leq X_{ingr} \quad (\text{A.3c})$$

$$X_{ingr} \leq U_{ingr} \quad (\text{A.3d})$$

Constraints (A.3a) and (A.3b) ensure that $X_{ingr} = l_{ngr}; \forall i \in \mathcal{I}, n \in \mathcal{N}, g \in \mathcal{G}^u, r = 1, 2, \dots, R$.

We plug this enforcement into equations (A.3c) and (A.3d) for each $i \in \mathcal{I}, n \in \mathcal{N}, g \in \mathcal{G}^u$, and $r = 1, 2, \dots, R$ and obtain the following:

$$U_{ingr} - \bar{\phi}_{ingr} = U_{ingr} - (\phi_{ingr} - l_{ngr}) \leq l_{ngr} \quad (\text{A.4a})$$

$$l_{ngr} \leq U_{ingr} \quad (\text{A.4b})$$

Again, the validity of constraints (A.4a) and (A.4b) are ensured via constraint (3.8). This completes the proof.

A.3 Proof of Proposition 2

Proof. To prove this proposition, we again construct two cases as shown below:

Case 1: For the first case, we assume that $Z_{ingr} = 1$. With this, $\forall i \in \mathcal{I}, n \in \mathcal{N}, g \in \mathcal{G}^u, r = 1, 2, \dots, R$ constraints (2.15)-(2.16) become:

$$X_{ingr} \leq U_{ngr} \quad (\text{A.5a})$$

$$U_{ngr} \leq X_{ingr} \quad (\text{A.5b})$$

Constraints (A.5a) and (A.5b) ensure that $X_{ingr} = U_{ngr}; \forall i \in \mathcal{I}, n \in \mathcal{N}, g \in \mathcal{G}^u, r = 1, 2, \dots, R$. This indicates that the highest discounted utility is assigned to alternative i .

Case 2: For the second case, we assume that $Z_{ingr} = 0$. With this, $\forall i \in \mathcal{I}, n \in \mathcal{N}, g \in \mathcal{G}^u, r = 1, 2, \dots, R$ constraints (2.15)-(2.16) become:

$$X_{ingr} \leq U_{ngr} \quad (\text{A.6a})$$

$$U_{ngr} \leq X_{ingr} + \bar{\phi}_{ngr} \quad (\text{A.6b})$$

We plug the values of $\bar{\phi}_{ngr} = (\phi_{ngr} - l_{ngr})$ into constraints (A.6b) to obtain the following for each $i \in \mathcal{I}, n \in \mathcal{N}, g \in \mathcal{G}^u$, and $r = 1, 2, \dots, R$:

$$U_{ngr} \leq X_{ingr} + \phi_{ngr} - l_{ngr}$$

This is always guaranteed since $(X_{ingr} - l_{ngr}) \geq 0$. This completes the proof.

A.4 Sample Utility Calculation

In our study, the MMNL model is adopted to study the choice of individuals under an AS incident. Both the attributes of the alternatives and socio-economic characteristics of the individuals are collected using a survey among 175 respondents (see Table 2.1). In this survey, based on the current and possible next position of the shooter, the individuals with their hypothetical current location were asked to select one of the five alternatives, namely, staying in the same location, running to the right grid, running to the left grid, running to the up grid, and running to the down grid. Different scenarios (current location and possible move of the shooter in the 6x6 grid facility (Figure 3.2)) are provided to the participants, and their behavioral decisions (i.e., alternative selected) are recorded. The socio-economic attributes, i.e., individual-specific attributes, considered in this study are gender (binary), age (categorical), ethnicity (categorical), disability status (binary), education status (categorical), active shooting related training status (binary), the gaming experience of the respondents (binary). Moreover, the alternative-specific attributes considered in this study are distance to the attacker (DA), distance to the closest hiding place (DH), distance to the closest entrance while avoiding the shooting range (DE), taking out of shooting range (TOS). The position of the attacker in the upcoming time periods in an AS incident is random; hence, two of the alternative-specific attributes, namely, DA and TOS , are considered as a random variable enabling us to capture the presence of preference heterogeneity in the sampled population. For instance, Figure A.1 represents the utility of the majority of the individuals along with the position of the attacker at time $t = 30$ seconds. From this figure,

it could be inferred that most people in the grid 21 ($g=21$) prefer to go to the right grid. Let $d(g_1, g_2)$ to represent the Euclidean distance between grids g_1 and g_2 . Given Figure A.1, which represents the number of grids, the alternative-specific attributes related to this alternative is calculated as follows: $DH = d(22, 21) + d(21, 15) + d(15, 14) + d(14, 13)$; $DE = d(22, 23)$; $DA = d(22, 21) + d(21, 27) + d(27, 26)$; $TOS = 1$, where DH , DE , and DA represents, respectively, the Euclidean distance of the individual to the hiding place, closest entrance, attacker after taking the running-right action, i.e., going from grid 21 to grid 22. Further, as can be seen, taking this alternative, the individual could manage to leave the shooting range of the attacker; hence, the value of the TOS attribute for this alternative is fixed to 1.

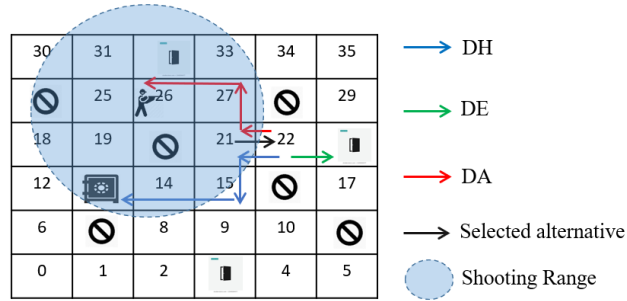


Figure A.1

A sample utility calculation for grid 21

A.5 Illustration of different hiding and entrances/exits configurations in chapter 2

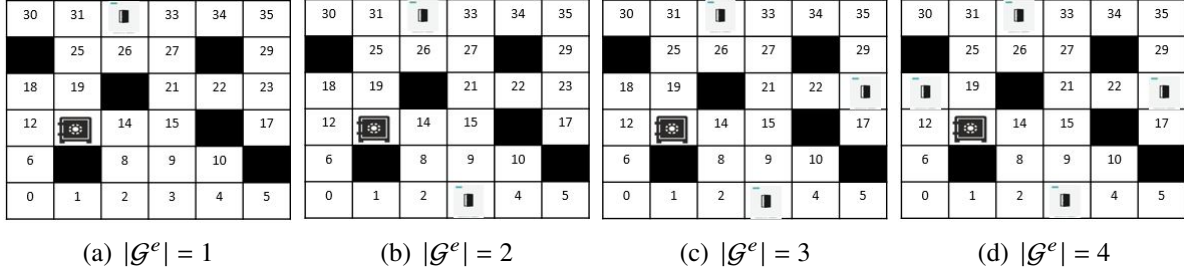


Figure A.2

Illustration of different exit/entrance configurations

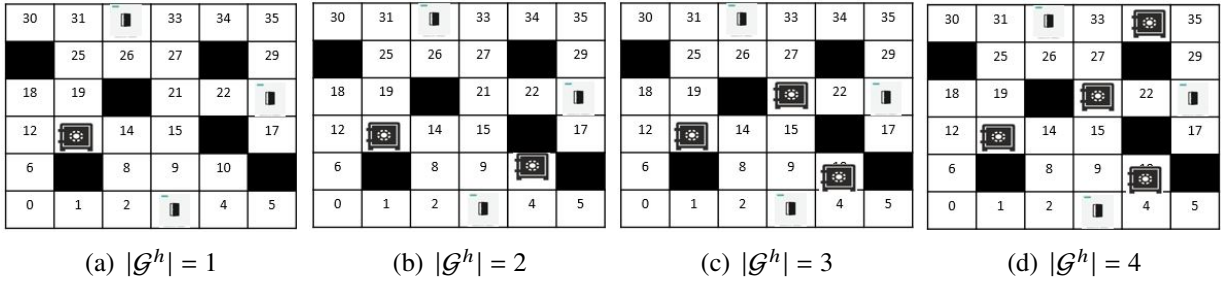


Figure A.3

Illustration of different hiding configurations

A.6 Illustration of different hiding and entrances/exits configurations in chapter 3

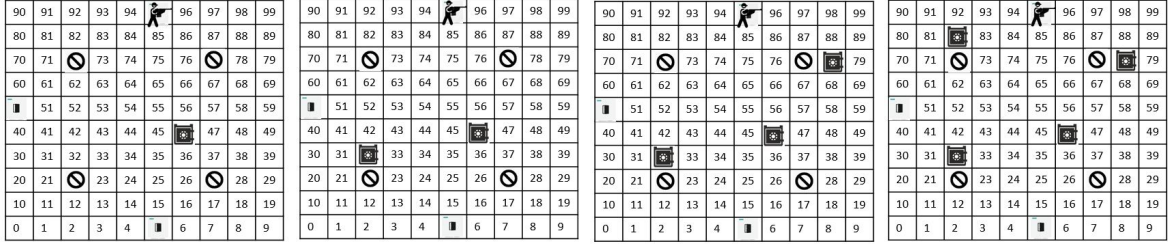


Figure A.4

Illustration of different hiding configurations. $|G^h|$ represents the number of the available hidden places in the threat area.

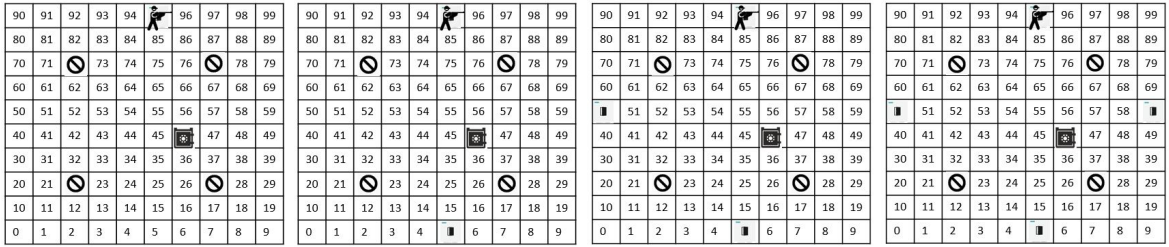


Figure A.5

Illustration of different exit/entrance configurations. $|G^e|$ represents the number of the exit/entrance cells in the threat area.

A.7 Illustration of different civilian distribution configurations in chapter3

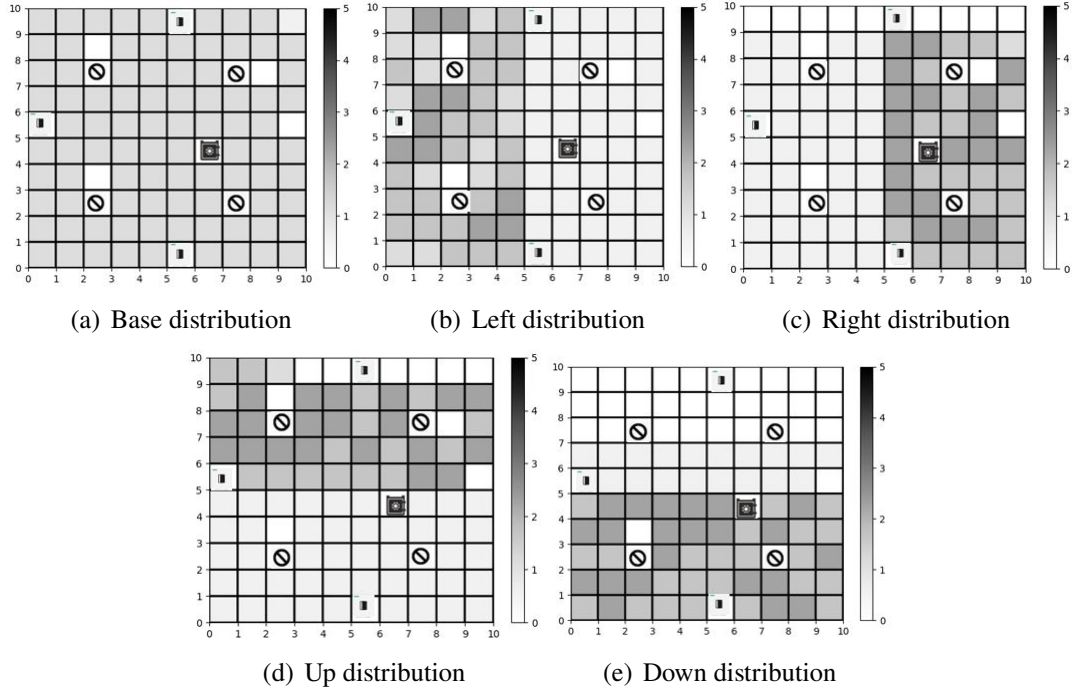


Figure A.6

Illustration of different civilian distribution configurations

A.8 Illustration of different shooting ranges and accuracy in chapter3

To capture different characteristics of the used weapon by the shooter, four different shooting ranges ranging from 1 to 4 were considered. To be more clear, assume that all the grids in the environment are 1 by 1, and the attacker is positioned in the center of one of the grids. Then the ranges 1, 2, 3, and 4 stand for a circle with a radius of 1.5, 2.5, 3.5, and 4.5 around the shooter (see Figure A.8), respectively. Moreover, Figure A.7 illustrates different accuracy scenarios used in this study. With an increase in the shooting accuracy, the respective probability of casualties in the attacker's shooting range increases accordingly.

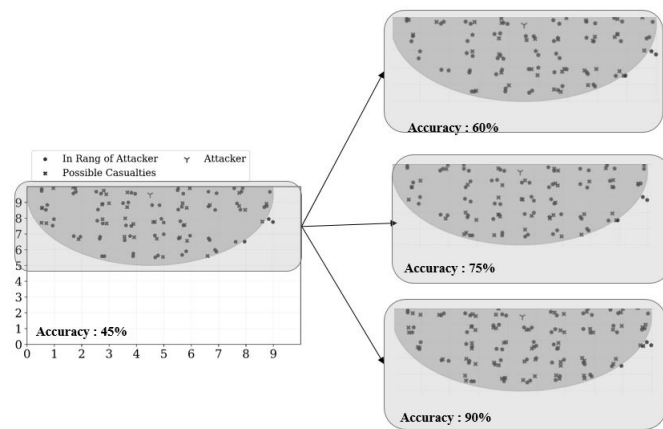


Figure A.7

Illustration of different shooting accuracy

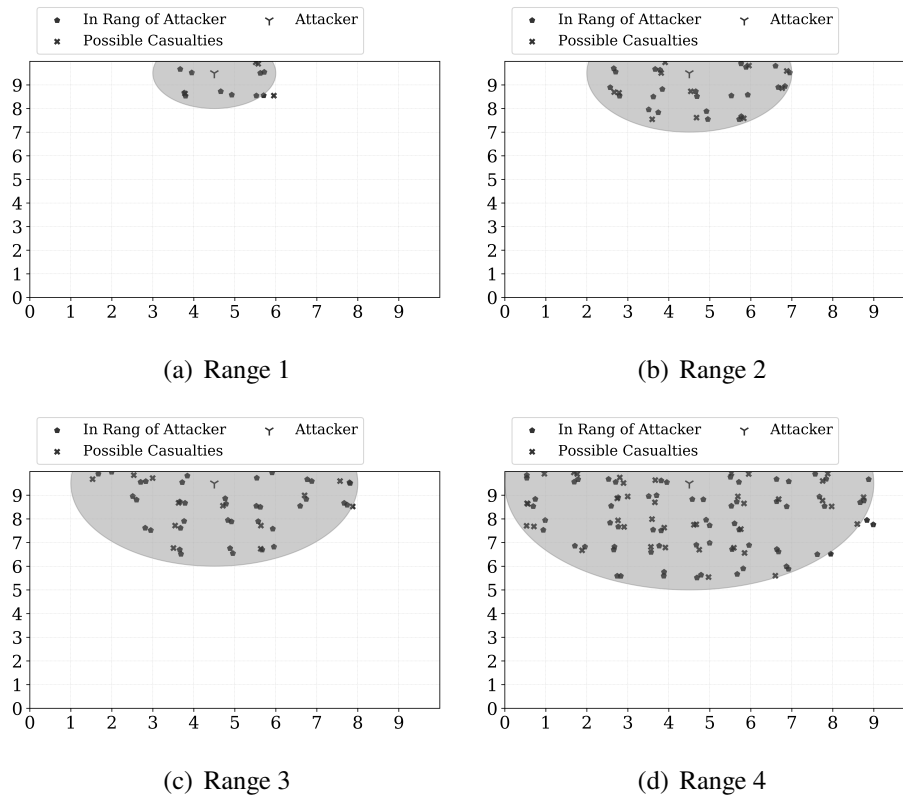


Figure A.8

Illustration of different shooting ranges

A.9 Performance metrics over trials in chapter3

Table A.1

The detailed information of the performance metrics based upon individual trials (in %)

Trial	T=75			T=90			T=105			T=120		
	V_H^I	V_E^I	V_{RISK}^I	V_H^I	V_E^I	V_{RISK}^I	V_H^I	V_E^I	V_{RISK}^I	V_H^I	V_E^I	V_{RISK}^I
1	8.6	49.1	42.3	8.6	55.4	36	8.6	60	31.4	8.6	62.9	28.6
2	8.6	49.7	41.7	8.6	56	35.4	8.6	60	31.4	8.6	62.3	29.1
3	8	50.3	41.1	8	56.6	34.9	8.6	61.1	30.3	8.6	64	27.4
4	8	58.3	33.1	8	65.1	26.3	8.6	69.7	21.7	8.6	72.6	18.9
5	8.6	48.6	42.9	8.6	55.4	36	8.6	60	31.4	8.6	62.9	28.6
6	8	51.4	40.6	8	58.9	33.1	8	64	28	8	66.9	25.1
7	8	48	43.4	8	54.9	36.6	8	60	31.4	8.6	62.9	28.6
8	8.6	57.7	33.7	8.6	65.1	26.3	8.6	70.3	21.1	8.6	73.1	18.3
9	8.6	57.1	34.3	8.6	64.6	26.9	8.6	69.1	22.3	8.6	72	19.4
10	8.6	57.1	34.3	8.6	63.4	28	8.6	68.6	22.9	8.6	70.9	20.6
11	8.6	49.1	42.3	8.6	56	35.4	8.6	61.1	30.3	8.6	64	27.4
12	8.6	50.9	40.6	8.6	57.7	33.7	8.6	62.3	29.1	8.6	65.1	26.3
13	8.6	49.1	42.3	8.6	56.6	34.9	8.6	61.1	30.3	8.6	64	27.4
14	8.6	58.3	33.1	8.6	65.1	26.3	8.6	69.1	22.3	8.6	71.4	20
15	8.6	58.3	33.1	8.6	64.6	26.9	8.6	69.7	21.7	8.6	72.6	18.9
16	8.6	48	43.4	8.6	54.9	36.6	8.6	58.9	32.6	8.6	61.7	29.7
17	8.6	57.7	33.7	8.6	65.1	26.3	8.6	70.3	21.1	8.6	72.6	18.9
18	8	53.1	38.3	8	60	31.4	8	65.1	26.3	8.6	67.4	24
19	8.6	57.7	33.7	8.6	64.6	26.9	8.6	68.6	22.9	8.6	70.9	20.6
20	8.6	57.7	33.7	8.6	64.6	26.9	8.6	69.1	22.3	8.6	72	19.4
21	8.6	48.6	42.9	8.6	54.9	36.6	8.6	58.9	32.6	8.6	61.7	29.7
22	8.6	51.4	40	8.6	57.7	33.7	8.6	62.3	29.1	8.6	65.1	26.3
23	8.6	52.6	38.9	8.6	59.4	32	8.6	64.6	26.9	8.6	67.4	24
24	8.6	48	43.4	8.6	54.3	37.1	8.6	59.4	32	8.6	61.7	29.7
25	8	57.1	34.3	8.6	64	27.4	8.6	69.1	22.3	8.6	71.4	20
26	8.6	49.1	42.3	8.6	56	35.4	8.6	60	31.4	8.6	62.9	28.6
27	8	49.1	42.9	8	56.6	35.4	8	61.7	30.3	8	64.6	27.4
28	8.6	48	43.4	8.6	54.9	36.6	8.6	59.4	32	8.6	62.3	29.1
29	8.6	48.6	42.9	8.6	56	35.4	8.6	60.6	30.9	8.6	63.4	28
30	8.6	54.3	37.1	8.6	60.6	30.9	8.6	65.7	25.7	8.6	68	23.4
31	8.6	55.4	36	8.6	61.7	29.7	8.6	66.9	24.6	8.6	69.1	22.3
32	8.6	54.3	37.1	8.6	61.7	29.7	8.6	65.7	25.7	8.6	68	23.4
33	8.6	48.6	42.9	8.6	56	35.4	8.6	60.6	30.9	8.6	63.4	28
34	8.6	50.3	41.1	8.6	57.7	33.7	8.6	62.3	29.1	8.6	65.1	26.3
35	8	54.3	37.1	8.6	60.6	30.9	8.6	65.7	25.7	8.6	68.6	22.9
36	8	57.1	34.3	8	63.4	28	8	68.6	22.9	8.6	70.9	20.6
37	8.6	58.3	33.1	8.6	65.1	26.3	8.6	69.7	21.7	8.6	72	19.4
38	8.6	50.3	41.1	8.6	57.1	34.3	8.6	62.3	29.1	8.6	64.6	26.9
39	8.6	54.3	37.1	8.6	61.1	30.3	8.6	66.3	25.1	8.6	69.1	22.3
40	8.6	53.1	38.3	8.6	60	31.4	8.6	64	27.4	8.6	66.3	25.1
41	8.6	57.1	34.3	8.6	64	27.4	8.6	69.1	22.3	8.6	71.4	20
42	8.6	53.7	37.7	8.6	61.1	30.3	8.6	65.1	26.3	8.6	68	23.4
43	8.6	52	39.4	8.6	59.4	32	8.6	64	27.4	8.6	66.3	25.1
44	8.6	52.6	38.9	8.6	60	31.4	8.6	64	27.4	8.6	66.3	25.1
45	8.6	53.7	37.7	8.6	60.6	30.9	8.6	65.1	26.3	8.6	67.4	24
46	8.6	57.1	34.3	8.6	63.4	28	8.6	67.4	24	8.6	69.7	21.7
47	8.6	48	43.4	8.6	54.3	37.1	8.6	58.9	32.6	8.6	61.1	30.3
48	8.6	49.1	42.3	8.6	56.6	34.9	8.6	61.1	30.3	8.6	63.4	28
49	8	53.7	37.7	8	61.1	30.3	8.6	66.3	25.1	8.6	68.6	22.9
50	8.6	57.7	33.7	8.6	64	27.4	8.6	68.6	22.9	8.6	71.4	20

A.10 A summary of the characteristics in chapter 3

A summary of the agents' characteristics and capabilities, the environment, and the agent interactions are provided below. The code used for this study could be provided upon request.

Environment characteristics:

- The environment designed in this study is $m \times m$ rectangular with equal-sized grids.
- Each one of the grids represents a specific state in the Markov Decision Process model.
- The grids (states) in the environment are categorized into 4 groups: 1-Blocked grids, which represent the set of grids that attacker and agents cannot travel or no threatened individuals are present; 2- unblocked grids, which represent the set of grids that an attacker and agent can travel or threatened individuals are present; 3- entrance/exit grids, which represent a set of grids using which the attacker can enter the threat area and the agent can safely exit the threat area; 4- hiding grids, which represent grids that are only available for agents to survive the active shooter incident and has a limited capacity to accommodate individuals.
- Given each grid's configuration, at most four possible actions are available for state transition in the designed environment, i.e., the neighboring grids of each grid are the ones on the left-side, right-side, up-side, and down-side of that grid.
- Exit and hiding grids (states) have the highest reward among all possible states for agents.
- The grid (state) where the attacker is located and its neighboring grids have the lowest reward among all possible states for agents.

Agents characteristics:

- N agents are present in the environment and randomly distributed in the grids.
- Given each agent's location, he or she can select one of the feasible actions to survive the incident. For instance, when the left neighboring grid to an agent is blocked grid, then the respective feasible action set does not have move-left action.
- We assume that each agent does not interact with others, and in each time step.

- We assume all agents need equal time to move from a specific grid to all its neighboring grids.
- Only one movement is allowed per time for each agent
- The agents choose a move that shortens their distance from the nearest exit door or hiding place, i.e., picking the shortest paths to survive the threat area.
- To account for real-life active shooting incidents where even expert agents could show abnormal decisions, we consider a small probability (denoted by parameter p_d in algorithm 2) that let trajectories deviate the shortest path to the target grids.

Active shooter characteristics:

- One active shooter is present in the environment that in each trial, it chooses to randomly enter the environment from one of the entrances.
- We assume that the shooter carries a gun with specific point-blank range, r_l , and level of accuracy, l_g .
- To model the attacker movement behavior, we assign higher probabilities to the choices of directions towards more populated spots.
- Given the attacker's location, he or she can select one of the feasible actions to survive the incident. The action which leads the attacker to the hidden place or the blocked grid is not present in its viable actions in this grid.
- We assume the attacker needs the same time as all agents to move from a specific grid to its neighboring grids.
- Only one movement is allowed per time for the attacker.

- We assume that the active shooter decides to cease the actions after T seconds, and we consider this time as our simulation duration.